PH.D. DISSERTATION

János Kontos

2025.

Neural network-based modeling of vehicle dynamics parameters for safety-critical automotive applications

Az értekezés doktori (PhD) fokozat elnyerése érdekében készült a Pannon Egyetem Informatikai Tudományok Doktori Iskolája keretében

informatikai tudományok tudományágban

Írta: Kontos János

Témavezetők: Dr. Fogarassyné dr. Vathy Ágnes, Dr. Kránicz Balázs

Elfogadásra javaslom: igen / nem.

…….
témavezető

Elfogadásra javaslom: igen / nem.

…….
témavezető

Az értekezés bírálatra bocsátható.

…….
TDHT elnök

A jelölt az értekezés nyilvános vitáján ……. %-ot ért el.

A bíráló Bizottság tagjai:

elnök:…….

bírálók:..……

tagok:…….

Veszprém,

…….
Bíráló Bizottság elnök

A doktori (PhD) oklevél minősítése:.....

Veszprém,

…….
EDHT elnök

University of Pannonia
Faculty of Information Technology
Doctoral School of Information Science and Technology

NEURAL NETWORK-BASED MODELING OF VEHICLE DYNAMICS PARAMETERS FOR SAFETY-CRITICAL AUTOMOTIVE APPLICATIONS

PhD Dissertation

by

János Kontos

DOI:10.18136/PE.2025.943

Head of Doctoral School
Dr. Ferenc Hartung, DSc

Supervisors
Dr. Ágnes Vathy-Fogarassy, PhD
Dr. Balázs Kránicz, PhD

Veszprém
Hungary
2025

Köszönetnyilvánítás

A mentorok szerepe meghatározó minden kutató életében: ők azok, akik gondolataikkal, tanácsaikkal és bátorításukkal irányt mutatnak, akár a tudományos pálya kezdetén, akár annak bármely szakaszában járunk. Az ő segítségük nélkül a tudományos munka olykor megoldhatatlan feladatnak tűnne.

Köszönettel tartozom témavezetőmnek, Dr. Fogarassyné dr. Vathy Ágnesnek, akiknek folyamatos támogatása, szakmai tanácsai és emberi példája nélkül e disszertáció nem készülhetett volna el. Köszönöm a rengeteg türelmet, bizalmat és a kritikai észrevételeket, amelyek segítettek kutatásaim kiteljesedésében. Köszönettel tartozom a Pannon Egyetem Műszaki Informatikai Karának és az Informatikai Tudományok Doktori Iskola minden munkatársának a háttértámogatásért, a szakmai közegért és az inspiráló környezetért, amely nélkül e kutatás nem teljesedhetett volna ki.

Külön köszönetet szeretnék kifejezni a Continental Automotive Hungary Kft. részéről Bódis Lászlónak a folyamatos szakmai mentorálásért, valamint a járműtesztelő csapatnak a mérési adatok gyűjtésében nyújtott segítségért. Hálás vagyok továbbá minden felettesemnek és kollégámnak, akik szakmai inspirációval segítették munkámat és motiváltak a mindennapi kihívások során.

Végül, de korántsem utolsósorban szeretném hálámat és szeretetemet kifejezni családomnak, különösen feleségemnek és szüleimnek, akik állhatatosan mellettem álltak; támogatásuk nélkül elképzelhetetlen lett volna e munka befejezése. Külön szeretnék megemlékezni azokról, akik ma már nem lehetnek velünk, de akik szeretetét és támogatását mindvégig éreztem, és akiknek emléke előtt ezzel a munkával is tisztelegni szeretnék.

Abstract

In the automotive industry, Software-Defined Vehicles are replacing traditional mechanical systems with complex, software-driven architectures, increasing the demand for real-time data processing and predictive capabilities in safety-critical functions. While transformers-based models dominate AI research with outstanding performance, their significant resource requirements make them unsuitable for embedded automotive systems with limited hardware capacity. This dissertation presents neural network-based models specifically designed for such environments, focusing on the prediction of key vehicle dynamics parameters, including longitudinal and lateral acceleration, yaw rate, and roll rate. These predictions enhance the functionality of critical systems such as Electronic Stability Control, Anti-lock Braking System, and Active Rollover Protection, thereby improving vehicle safety and stability. Additionally, the developed models support the plausibility checking of sensor signals and can be applied in autonomous driving functions.

The developed models were trained, validated, and tested using extensive experimental data collected under both urban and off-road conditions, with scenarios executed by certified test drivers. Input signals were obtained from standard vehicle sensors, including wheel speeds, steering wheel angle, lateral and longitudinal accelerations, and yaw and roll rates. Each model underwent a thorough hyperparameter tuning process to optimize network architecture, ensuring high prediction accuracy while maintaining low computational demands.

For lateral acceleration, a compact feedforward neural network was developed, capable of running not only on the brake system but also directly on the sensor. Acting as a virtual sensor, it accurately estimates lateral acceleration based on other sensor inputs. For longitudinal acceleration, yaw rate, and roll rate, LSTM-based forecasting models were created to predict future values from current and past sensor data. The longitudinal acceleration model uses 0.1 seconds of past data to predict 0.1 seconds ahead, while the yaw rate model operates with a 0.2-second window for both input and forecast. Although primarily designed for solid road conditions, a dedicated roll rate model was developed for off-road scenarios, providing reliable predictions up to 0.04 seconds ahead based on 0.04 seconds of historical data.

All forecasting models were benchmarked against approaches found in the literature. Despite significantly lower resource requirements, the developed models achieved superior accuracy. The optimal amount of training data was also investigated, showing that 15 minutes of data may be suffice for non-safety-critical applications. For the yaw rate model, sensitivity analysis was also performed, examining the effects of passenger load, tire pressure, and vehicle body structure. The results confirmed that the model maintains its performance and complies with the highest automotive safety standards, even under varying conditions.

Absztrakt

Az autóiparban egyre inkább szoftver alapú megoldások váltják fel a hagyományos mechanikai rendszereket, amelyet a valós idejű adatfeldolgozás, a prediktív és önvezető képességek iránti megnövekedett igény hajt. Bár napjainkban a transzformer alapú megoldások dominálják a mesterséges intelligencia kutatást, jelentős erőforrásigényük miatt nem alkalmasak korlátozott hardverkapacitású beágyazott járműrendszerekbe.

Doktori kutatásom során olyan mesterséges neurális hálózatokat fejlesztettem, amelyek kiválóan működnek korlátozott hardveres környezetben is, mint az elektromos fékvezérlőkben és szenzorokban. Ezek a modellek pontosan képesek becsülni és előrejelezni a hossz- és oldalirányú gyorsulást, valamint a perdületi és dőlési szögsebességet, jelentősen javítva ezzel a járművek biztonsági rendszereinek működését, mint az elektronikus stabilitásszabályozó, blokkolásgátló és aktív borulásvédelem. A modelleket városi és terepi körülmények között, szakképzett tesztvezetők segítségével gyűjtött adatokkal fejlesztettem és validáltam, biztosítva valós közlekedési helyzetekben való megbízhatóságukat.

A bemeneti jelek között a modern gépjárművekben megtalálható szenzoradatokat használtam, mint a keréksebesség, kormánykerék-szög, gyorsulások, valamint perdületi és dőlési szögsebességek. A hiperparaméter-optimalizált modellek közül az oldalirányú gyorsulás becslésére egy előrecsatolt hálózatot dolgoztam ki, amely virtuális szenzorként is alkalmazható. A hosszirányú gyorsulás, perdületi és dőlési szögsebesség előrejelzésére pedig Long Short-Term Memory (LSTM) hálózatokat használtam, amelyek pontos előrejelzéseket adnak különböző időtávokra (hosszirányú gyorsulás: 0,1 s, perdületi sebesség: 0,2 s, dőlési sebesség terepi körülmények között: 0,04 s.

Az általam kifejlesztett modellek mindegyike felülmúlta a szakirodalomban található megoldásokat: kevesebb erőforrást igényelnek, mégis pontosabb eredményt adnak. Kutatásom során azt is megállapítottam, hogy a nem biztonságkritikus alkalmazásokhoz már 15 percnyi gyűjtött adat is elegendő lehet a modellek tanításához. Az érzékenységi vizsgálatok bebizonyították, hogy a kidolgozott modellek megbízhatóan működnek változó körülmények között is – legyen szó a jármű utasinak számának változásáról, a gumiabroncsok nyomásának ingadozásáról vagy a jármű teljes szerkezetének megváltozásáról. Ezen tulajdonságok miatt kijelenthető, hogy a létrehozott modellek széleskörű járműdinamikai felhasználással bírnak.

Abstrakt

In der Automobilindustrie ersetzen Software-definierte Fahrzeuge zunehmend traditionelle mechanische Systeme durch komplexe softwarebasierte Architekturen, wodurch der Bedarf an Echtzeitdatenverarbeitung und Vorhersagefähigkeiten in sicherheitskritischen Funktionen steigt. Obwohl große Transformer die KI-Forschung dominieren, macht ihr hoher Ressourcenbedarf sie ungeeignet für eingebettete Automobilsysteme mit begrenzter Hardware.

Diese Dissertation präsentiert neuronale Netzwerkmodelle, die speziell für solche Umgebungen entwickelt wurden und die Vorhersage wichtiger Fahrzeugparameter wie Längs- und Querbeschleunigung sowie Gier- und Wankrate ermöglichen. Diese Vorhersagen verbessern kritische Systeme wie elektronische Stabilitätskontrolle, Antiblockiersysteme und aktiven Überrollschutz und erhöhen so die Fahrzeugsicherheit. Die Modelle unterstützen zudem die Plausibilitätsprüfung von Sensorsignalen und autonome Fahrfunktionen. Training, Validierung und Tests erfolgten mit umfangreichen experimentellen Daten aus Stadt- und Offroad-Fahrten zertifizierter Fahrer.

Die Eingangssignale umfassten Standard-Fahrzeugsensoren wie Raddrehzahlen, Lenkwinkel, Beschleunigungen sowie Gier- und Wankraten. Jedes Modell wurde durch intensives Hyper-parameter-Tuning optimiert, um eine hohe Genauigkeit bei minimalem Rechenaufwand zu erreichen.

Für die Querbeschleunigung wurde ein kompaktes Feedforward-Netz entwickelt, das sowohl auf Bremssystemen als auch direkt auf Sensoren als virtueller Sensor genutzt werden kann.

Für die Vorhersage von Längsbeschleunigung, Gierrate und Wankrate wurden Long Short-Term Memory (LSTM) Modelle eingesetzt. Das Längsbeschleunigungsmodell prognostiziert mit 0,1 Sekunden, das Gierratenmodell mit 0,2 Sekunden und das Wankratenmodell speziell für Offroad-Szenarien mit 0,04 Sekunden Vorhersagehorizont.

Alle Modelle erreichten im Vergleich zur Literatur trotz geringerer Ressourcen überlegene Genauigkeit. Eine Untersuchung zur optimalen Datenmenge zeigte, dass bereits 15 Minuten Daten für nicht sicherheitskritische Anwendungen genügen. Eine Sensitivitätsanalyse bestätigte zudem die Robustheit der Modelle gegenüber variierenden Bedingungen wie Passagierlast, Reifendruck und Fahrzeugstruktur und deren Eignung für höchste Sicherheitsstandards.

Contents

List of Figures

List of Tables

Abbreviations

ABS	Anti-lock Braking System
ACC	Adaptive Cruise Control
ADAS	Advanced Driver-Assistance Systems
AEB	Automatic Emergency Braking
ANN	Artificial Neural Network
ARIMA	Autoregressive Integrated Moving Average
ARP	Active Rollover Protection
ASIL	Automotive Safety Integrity Level
CAN	Controller Area Network
CPU	Central Processing Unit
ECU	Electronic Control Unit
EDA	Exploratory Data Analysis
EH∞KF	Extended H-infinity Kalman Filter
EKF	Extended Kalman Filter
ESC	Electronic Stability Control
EV	Electric Vehicle
FL	Front Left (Wheel Speed)
FR	Front Right (Wheel Speed)
GNSS	Global Navigation Satellite System
GPS	Global Positioning System
GPU	Graphics Processing Unit
GRU	Gated Recurrent Unit
HSA	Hill Start Assist
IMU	Integrated Measurement Unit
INS	Inertial Navigation System
IQR	Inter-quartile Range
LSTM	Long Short-Term Memory
MAE	Mean Absolute Error

MHMM	Finite Mixture of Hidden Markov Models
MLOps	Machine Learning Operation
MSE	Mean Squared Error
NARX	Nonlinear AutoRegressive with eXogenous
RL	Rear Left (Wheel Speed)
RLS	Recursive Least Squares
RMSE	Root Mean Squared Error
RR	Rear Right (Wheel Speed)
SDV	Software-Defined Vehicle
SUV	Sport Utility Vehicle
TCS	Traction Control System
TPMS	Tire Pressure Monitoring System
YOLO	You Only Look Once

Formulas

α	Significance level for statistical tests
a_{lat}	Lateral acceleration
a_{long}	Longitudinal acceleration
b_C	Bias vector for the candidate cell state calculation
b_f	Bias vector for the forget gate
b_i	Bias vector for the input gate
b_o	Bias vector for the output gate
C_{t-1}	Cell state at previous time step $t-1$
C_t	Cell state at time step t
C'_t	Candidate cell state at time step t
d	distinct driving scenarios (*aggressive*, *calm*, *city*, and *combined* driving)
δ	Steering angle of front axle
f_t	Forget gate activation at time step t
g	analysis condition (variations in tire pressure, passenger load, or vehicle type)
h_{t-1}	Hidden state at previous time step $t-1$
H_0	Null hypothesis for statistical tests
H_1	Alternative hypothesis for statistical tests
h_t	Hidden state at time step t
i_t	Input gate activation at time step t
k	Number of samples
$n_{\text{look\_back}}$	Number of past time steps in input window
$n_{\text{look\_future}}$	Number of future time steps in prediction horizon
o_t	Output gate activation at time step t
$\dot{\Phi}$	Yaw rate
$\dot{\Psi}$	Roll rate
σ	Sigmoid activation function
$\tanh$	Hyperbolic tangent activation function

v_{FL}	Wheel speed (Front left)
v_{FR}	Wheel speed, (Front right)
v_{RL}	Wheel speed, (Rear left)
v_{RR}	Wheel speed, (Rear right)
W_C	Weight matrix for the candidate cell state calculation; transforms $[h_{t-1}, x_t]$
W_f	Weight matrix for the forget gate; transforms $[h_{t-1}, x_t]$
W_i	Weight matrix for the input gate; transforms $[h_{t-1}, x_t]$
W_o	Weight matrix for the output gate; transforms $[h_{t-1}, x_t]$
x_t	Input vector at time step t
y_i	Actual measured value for sample i
$\hat{y}_i$	Predicted value for sample i
$\overline{y}$	Mean of actual measured values

Chapter 1

Introduction

1.1 Motivation

Software-driven solutions dominate today's automotive industry, which has moved from mechanical engineering traditions to embrace the technological pioneer of Software-Defined Vehicles (SDVs). Modern vehicles primarily operate through software-driven systems that provide driver assistance, entertainment capabilities, and advanced safety features, establishing the basis for interconnected autonomous driving systems [1].

Key trends also underline this transformation. The auto markets experience a structural evolution due to electrification because it supports emission reduction and fulfils sustainability criteria. Electric Vehicle (EV) technology gains market dominance because of improvements in battery systems and charging station networks [2].

Vehicle dynamics are progressing through substantial changes as technology advances. New advanced powertrain solutions combined with adaptive suspension features in conjunction with improved chassis control systems are providing better stability and increased safety while boosting vehicle performance. The current technological progress enables improved vehicle handling alongside superior comfort features and better energy utilization, which fulfil modern consumer requirements and comply with government regulations. The integration of essential safety mechanisms, including braking technology, stands as a fundamental element for advancing vehicle performance and system dependability [3, 4, 5].

Electric brake systems continue to demonstrate critical importance to car manufacturers as the automotive industry progresses. They provide precise, reliable braking performance, which enhances vehicle dynamics and advancements. The independence of electric brake systems from the drivetrain configuration makes them essential for both conventional vehicles and electric models. Their capability to operate across different vehicle models enhance safety and performance while facilitating the transition to automated and electrified trans-

portation. The consistent verification of sensor outputs and anomaly detection capabilities are critical for electric brake systems, which rely on precise real-time data to ensure safe and responsive braking performance [6, 7, 8].

Current brake systems contain embedded advanced features which enhance driving attributes with safety improvements. Anti-lock Braking System (ABS) and Electronic Stability Control (ESC) represent mandatory safety features which must be present in newly sold vehicles throughout the European Union territory and in the United States. Braking performance grows better through ABS because it stops wheel lock-up in emergency stops which helps drivers keep control of their vehicle. ESC is the basic safety framework that automatically prevent skidding incidents and regain control during vehicle instability. Vehicle stabilization becomes possible during sharp turns and slippery conditions because ESC applies specific brake pressure on individual wheels while matching engine power output. The systems work together to enhance safety on vehicles through their effectiveness in reducing accident risks as well as preserving driver control during emergency situations [9, 10, 11, 12]. Advanced automotive safety innovations are increasingly mandated by law in many countries, as legislators prioritize reducing traffic collisions and enhancing road safety worldwide. Alongside these regulatory-driven advancements, modern braking systems now address nuanced driving challenges through other features. Vehicle rollback can be prevented when starting uphill surfaces through Hill Start Assist (HSA) which gives added brake power control. Advanced Driver-Assistance Systems (ADAS) technologies provide the brake system with superior capabilities since they implement Automatic Emergency Braking (AEB) and Adaptive Cruise Control (ACC) and lane-keeping assistance through precise braking control to enhance safety and usability. The regenerative braking systems in electric and hybrid vehicles transform kinetic energy from slowing down into electrical energy to boost energy efficiency. As we can see, vehicle brakes now feature multiple essential functions after transitioning from basic mechanical components into highly advanced systems that reshape safety and performance capabilities [13, 14, 15].

Electric brake systems exemplify the modern approach to braking technology. These systems use electronically controlled hydraulic circuits to generate and regulate braking forces, relying on multiple input signals to achieve optimal and adaptive performance. Signals such as accelerations, yaw rate, roll rate, wheel speed, steering wheel angle, and brake pedal position provide critical information about the vehicle's dynamics and the driver's intentions. By processing these inputs in real-time, the system ensures precise and reliable braking, enhancing safety and improving the driving experience [16, 12].

Modern brake systems require absolute priority when designing and implementing safety measures. The mentioned signals require valid assessment as plausibility monitoring fulfils this essential function. The brake controller maintains vehicle safety because it detects anomalies between expected values and actual measurements, which point to sensor mal-

functions and data errors through continuous comparison processes. The use of virtual sensors has become essential for improving system reliability. Advanced algorithm-powered virtual sensors complement physical sensors by estimating principal parameters and providing backup functionalities for essential safety applications [17].

Given these challenges, the primary objective of this work was to develop neural network-based models capable of accurately estimating and forecasting key vehicle dynamics parameters, specifically tailored for embedded automotive systems with limited hardware capacity. A further goal was to ensure that the developed models operate independently of any vehicle-specific calibration parameters, enabling broad applicability across different vehicle types. Where feasible, the models were also designed to provide not only real-time estimations but short-term forecasts of future values, supporting proactive safety mechanisms and more intelligent control strategies.

To meet these requirements, lightweight artificial neural network architectures were applied, optimized for real-time operation within Electronic Control Units (ECUs) or directly on sensor-level hardware. These models can be utilized as virtual sensors or in sensor plausibility monitoring frameworks. Compared to existing approaches in the literature, the developed models demonstrated higher prediction accuracy while maintaining significantly lower computational demands. Importantly, they were shown to be robust across a wide range of operational conditions, including variations in tire pressure, passenger load distribution, and structural configurations. Based on these results, the original goals of the research have been successfully achieved.

Reliable safety systems depend heavily on accurate and trusted input signals, making their prediction and calculation essential for achieving high levels of operational integrity. Generating accurate acceleration or rate signals becomes difficult because the methods needed present complex hurdles which demand numerous precise parameters. The development of these signals through empirical mathematical models and estimations requires meticulous calibration to match a specific vehicle configuration. Accurate results require comprehensive information about vehicle specifications, including mass distribution alongside suspension geometry and dynamic behavior [18, 19, 20]. Early-stage development does not provide complete design and assembly information because vehicle body parameters remain undefined until these processes are finalized. The calibration model requires approximations or assumptions to compensate for the unavailable detailed data, which endangers signal precision. The process of vehicle development becomes more intricate due to the requirement for adjusting numerous parameters. The recurrent calibration cycles combined with continuously changing vehicle prototypes expose creators to complicated challenges when generating dependable acceleration and rate signals during initial development stages [21, 22].

1.2 Research Topics

In my PhD thesis, I have developed artificial neural network-based models to predict the most critical input signals for electric brake systems, including lateral and longitudinal acceleration, yaw rate, and roll rate. I have designed these models not only to estimate the current sensor signals with high accuracy but also, in certain cases, to predict their future values. This capability allows the models to assess the potential effects of a given intervention and supports the selection of optimal intervention strategies, such as determining the appropriate braking pressure for each tire. Importantly, one of the models has been specifically optimized to operate on hardware with extremely limited computational capacity, ensuring its applicability in resource-constrained environments. Furthermore, all of the models have been designed to function on hardware commonly available in modern vehicles, leveraging signals that are already accessible through standard vehicle sensors. Additionally, specific models have been tailored for distinct driving environments, including urban, off-road conditions, and highway scenarios, ensuring adaptability to varying operational contexts. To achieve this, extensive experimental data was collected under diverse driving conditions, carefully preprocessed and structured into training, validation, and test sets to ensure the robustness and accuracy of the models. I would like to highlight that these models do not require any vehicle-dependent adjustable parameters as input, making them robust and broadly applicable across different vehicle configurations.

A key objective of this research was to develop models that are not only accurate and computationally efficient but also transferable across different vehicle platforms without the need for complex vehicle-specific calibration procedures. This contrasts with traditional physics-based approaches, such as single-track and double-track models, which require detailed parameter identification through highly controlled maneuvers and often depend on experienced test drivers. In contrast, the proposed neural network models were trained on a wide variety of real-world driving conditions and demonstrated robust performance even under changes in tire pressure, vehicle load and structural configuration.

Considering the state-of-the-art predictive models, transformer—initially introduced in 2017 for natural language processing—has significantly advanced sequential data modeling through their sophisticated self-attention mechanisms, effectively capturing complex, long-range temporal dependencies [23]. Architectures such as TimesNet exemplify their effectiveness, making transformer models highly suitable for intricate forecasting tasks, including vehicle dynamics parameter prediction [24, 25]. Nevertheless, transformer models inherently demand substantially greater computational resources compared to LSTM (Long Short-Term Memory) networks and standard feedforward neural networks [26, 27]. This elevated computational cost primarily arises from the extensive matrix operations associated with self-attention, which scale quadratically with sequence length [28]. Consequently,

while LSTM and feedforward networks remain preferable in embedded systems with limited hardware capabilities, transformer typically necessitates advanced processors and expanded memory capacities. Given these hardware constraints, transformer is challenging to directly integrate into automotive control units, especially within sensor hardware or brake control systems [29]. Therefore, in my dissertation, lightweight feedforward neural networks were selected for estimating signals directly at the sensor level due to their efficiency and capability for accurate current-value predictions, while LSTM networks were employed in the brake control ECU to leverage historical data for accurate short-term future predictions.

My PhD thesis focuses on two primary research directions: predicting vehicle acceleration (longitudinal and lateral) and predicting vehicle rates (yaw and roll rates). A feedforward neural network is employed for lateral acceleration estimation, designed to be lightweight for direct integration into sensor hardware without significant computational demands. Meanwhile, a LSTM network is used to predict longitudinal acceleration, capturing temporal dependencies in vehicle dynamics. This model was optimized for incorporation into electric brake systems. In both cases, hyperparameter tuning is performed to enhance model performance. Where feasible, the accuracy of these models is compared to alternative approaches in the literature. For vehicle rate prediction, an LSTM-based model was developed to forecast yaw rate leveraging historical sensor data. A detailed sensitivity analysis was conducted to assess the impact of external conditions such as tire pressure, passenger load, and vehicle body dynamics on prediction accuracy. Hyperparameter tuning was performed to refine the model's predictive performance. Another LSTM model was designed for roll rate prediction, specifically developed for off-road environments, providing reliable forecasts under challenging driving conditions and supporting Active Rollover Protection (ARP) systems to enhance vehicle stability and safety. The models were implemented using architectures optimized for low hardware consuption, making them suitable for real-time applications such as virtual sensors and sensor plausibility monitoring. Their vehicle-agnostic design and low parameter count further reduce integration complexity in production systems.

A crucial component of the thesis is the data that underpins the model development. The datasets used for training and validation were collected from extensive experimental measurements. During my work, I have thoroughly investigated the characteristics of the signals collected and developed a systematic preprocessing workflow to preprocess these data for model development.

The proposed models significantly enhance the precision and reliability of brake system input signal predictions, even under challenging conditions. By utilizing existing signals, such as wheel speed, steering angle of the front axle, longitudinal and lateral acceleration, and yaw and roll rate, the models can provide a comprehensive and accurate representation

of the vehicle's dynamic state. The ability to generate accurate predictions enables improved decision-making for safety-critical interventions, ensuring optimal performance and reducing risks. This approach not only addresses current challenges in signal estimation but also paves the way for more advanced and adaptive braking strategies in future vehicle systems. In my thesis, I will also highlight that the developed models demonstrate superior predictive performance compared to existing models in the literature, which not only validates their effectiveness but also lays the foundation for their real-world applicability in modern vehicle systems.

Figure 1.1 illustrates the visualization of my PhD research topics. Before delving into the detailed results of each area, the following three subchapters offer a brief overview.

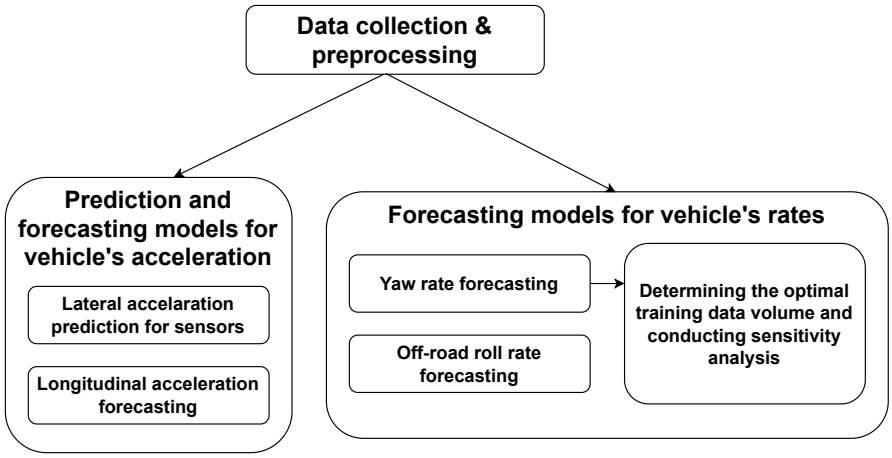

Figure 1.1. The research topic structure of my PhD study.

1.2.1 Modeling and Predicting of Acceleration in Vehicle Dynamics

Longitudinal and lateral accelerations are essential in vehicle dynamics, simply due to the fact that these two parameters play a crucial role in the quest for safety, performance, and comfort. Longitudinal acceleration reflects the capacity of the vehicle to accelerate or decelerate in the forward or rearward direction, which has important implications for systems like ABS, Traction Control Systems (TCS), and collision avoidance systems. On the other hand, lateral acceleration is essential for handling and stability control, especially during cornering maneuvers or lane changes. Together, these accelerations are required for control and stability during dynamic driving maneuvers, and their accurate monitoring and prediction are crucial.

Within this topic, I have developed two alternative neural network models to surpass main prerequisites in acceleration prediction for constrained hardware environments. The

first model is a neural network-based lateral acceleration predictor. The model was trained particularly to predict current longitudinal acceleration values from a minimum number of input signals: four wheel speeds, longitudinal acceleration, and the front axle steering angle. The structure has one hidden layer with five neurons, making it very concise for implementation on sensors with very limited computational capabilities. These sensors have internal plausibility checks for signal integrity, and this model enhances their capability by providing strong predictive outputs. The simplicity of the architecture ensures compliance with hardware constraints, while delivering high reliability for safety-critical systems.

The second model employs LSTM architecture to forecast future longitudinal acceleration values. This advanced framework receives historical and real-time inputs of the four wheel speeds, longitudinal and lateral accelerations, front axle steering angle, and yaw rate. The optimized network architecture, consisting of one hidden layer with five LSTM neurons, was carefully tuned to predict future states with low computational complexity. The developed model is capable of providing future predictions for a time horizon of 100 milliseconds by processing 100 milliseconds of past sensor data and was designed for integration into electric brake systems, optimally balancing the depth of historical data utilized with the extent of future predictions to maintain accuracy and efficiency. By carefully selecting the length of past observations and the prediction horizon, it ensures reliable performance while adhering to stringent safety constraints.

To optimize the performance of the two models, a hybrid approach to hyperparameter optimization was employed. It initiated with random search within the stochastic parameter space and followed up with grid search for deterministic optimization. The models were discovered to be extremely trustworthy, with compliance in strict safety demands, and can be used as supporting tools for sensor plausibility checks. They are capable of operating reliably across a variety of driving conditions. The procedures for training, validation, and testing of both neural networks are included in subsequent parts of this work, ensuring openness and reproducibility of the methodologies involved. The models demonstrate the potential of neural networks for real-time, resource-constrained problem-solving in the automotive industry, while introducing opportunities for future enhancement of vehicle dynamics modeling.

1.2.2 Predictive Modeling of Yaw and Roll Rates in Vehicle Dynamics

Yaw rate and roll rate are fundamental vehicle dynamics parameters that influence stability, handling, and safety, especially in complex driving maneuvers. Yaw rate, which represents the rotational speed of the vehicle around the vertical axis, is a vital input for ESC systems. The roll rate is a quantification of a vehicle's angular velocity around its longitudinal axis.

Accurate prediction of these parameters is highly desirable for ADAS and stability control systems. In my work, I developed two LSTM-based neural network models to predict yaw rate and roll rate for a specified driving situation.

The first model predicts yaw rate across various driving styles, including urban, aggressive, and calm conditions. The model relies on historical and current information, including longitudinal and lateral acceleration, yaw rate, front axle steering angle, and wheel speeds. The optimized LSTM model, featuring a single hidden layer with five neurons, predicts yaw rate values 200 milliseconds into the future while leveraging data from the previous 200 milliseconds, ensuring minimal computational demands.

The robustness of the yaw rate prediction model was confirmed by performing a sensitivity test to see the effects of tire pressure, passenger configuration and vehicle load distribution prediction accuracy. The results indicated that alterations in tire pressure, passenger load distribution and vehicle's body result in minimal deviations in prediction accuracy, maintaining the model within the critical safety limits. This kind of reliability justifies its implementation in real-world scenarios.

The second model was developed for roll rate prediction. Roll rate prediction is particularly critical for Sport Utility Vehicles (SUVs) and off-road vehicles, where the higher center of mass makes rollover more susceptible. The developed LSTM roll rate predictor receives as inputs features such as longitudinal and lateral accelerations, yaw and roll rates, front axle steering angle, and wheel speeds. I have trained and validated this model on extensive experimental data, which was specifically collected in off-road scenarios. The final structure consists of a single hidden layer with seven LSTM neurons, enabling accurate short-term roll rate prediction up to 40 milliseconds in advance.

The LSTM-based models' performance was also compared to existing methods, with superior predictive capability at low computational complexity. Compared to traditional estimation techniques that require sensor fusion or vehicle-specific parameters, the proposed LSTM approach yields a more generalized system without sacrificing accuracy for diverse driving conditions.

1.2.3 Data collecting and processing

Data plays a central role in the development of neural network-based methods, particularly in areas like vehicle dynamics, where precision, reliability, and adaptability across diverse scenarios are critical. Therefore, in safety-critical systems, developing neural networks requires gathering large amounts of data that reflect real-world scenarios. Preparing and processing the real-world collected data is particularly important, as it ensures compatibility with computational models while preserving its original integrity, thereby enhancing the accuracy and reliability of neural network-based predictions.

The experimental data utilized in my PhD study were collected under various driving conditions, including off-road tests conducted in Brimley, Michigan (USA), urban driving scenarios within the city of Veszprém, and additional vehicle dynamics assessments performed at the Veszprém Continental test track. These tracks provided a controlled environment for comprehensive vehicle dynamics research, ensuring the reliability and accuracy of the gathered data. The data collection captured core vehicle dynamics signals such as the speeds of all four wheels (front left, front right, rear left, and rear right), longitudinal and lateral acceleration, yaw rate, front axle steering angle, and, in some cases, roll rate. These signals were sampled at a high resolution of 0.01 seconds to maintain the temporal dynamics critical for training and testing neural networks.

The experimental setup primarily utilized a commercial 2022 SUV. This choice was strategic, as SUVs exhibit unique dynamics due to their specialized suspension systems and higher center of mass, making them ideal candidates for studying and predicting vehicle behavior under various conditions. These vehicles present significant challenges from a dynamics perspective, highlighting the importance of accurately capturing their behavior through robust data.

1.3 Outline of the Subsequent Chapters of the Dissertation

The foundation of this PhD thesis is rooted in the essential role of data in black-box modeling, particularly in the context of vehicle dynamics. Black-box models, such as neural networks, rely heavily on vast amounts of high-quality data to identify patterns and relationships without predefined mathematical structures. Since the accuracy and reliability of these models depend on the quality of the input data, the first major section (Section 2) of this thesis focuses on data collection, preprocessing, and transformation. The involved sensor signals are described in Section 2.2, while the detailed data collection methodology is provided in Section 2.3. Section 2.4 presents the preprocessing steps applied to the raw data to ensure consistency and quality. Additionally, the characteristics and statistical properties of the individual datasets used in the predictive tasks are summarized in Section 2.5. These datasets serve as the foundation for the development and validation of the neural network models introduced in the following chapters.

Building upon the prepared datasets, the next section (Section 3) focuses on the development and evaluation of neural network models for vehicle acceleration prediction. Specifically, it details the creation of a feedforward neural network aimed at predicting lateral acceleration and a LSTM based model for estimating features related to longitudinal acceleration. Section 3.2 establishes the theoretical foundation by reviewing relevant

literature concerning these predictive methodologies. The core development process, including model architecture design, hyperparameter tuning strategies, the datasets utilized for training and validation, and the performance metrics employed, is thoroughly described in Section 3.3. Finally, Section 3.4 summarizes and analyzes the predictive performance achieved by the proposed models.

The next section (Section 4) extends the investigation into vehicle state prediction using LSTM networks, specifically targeting yaw and roll rate estimation. Section 4.2 provides the theoretical context by reviewing existing literature pertinent to yaw and roll rate prediction methodologies. Subsequently, Section 4.3 outlines the specific datasets utilized for the development and validation of the models presented in this chapter. The core development of the yaw rate forecasting model, including its architecture, hyperparameter tuning, and predictive performance evaluation, is detailed in Section 4.4. Furthermore, Section 4.5 delves into analyses for the yaw rate estimation model, focusing on identifying the optimal volume of training data and conducting a sensitivity analysis regarding the effects of tire pressure, passenger configuration and whole vehicle body. Finally, Section 4.6 describes the architectural design, hyperparameter optimization, and performance assessment of the LSTM-based roll rate estimation model tailored for off-road scenarios.

Chapter 2

Data Used for Model Development

2.1 Introduction

Data is a fundamental element in black-box modeling, particularly in neural networks, where the accuracy and reliability of predictions are directly influenced by the quality of the input data [30]. Selecting the appropriate sensors for data collection is critical, as they must provide signals that have a direct and meaningful impact on the predicted output. Modern vehicles are equipped with hundreds of sensors, making the selection process complex [31]. Fortunately, from the perspective of vehicle stability within an electric brake system, only a limited number of sensors play a crucial role [32]. These key sensors, which will be discussed in this chapter, provide essential signals for stability control and predictive modeling.

Beyond sensor selection, the origin of the data significantly affects the model's predictive capabilities. When using simulation data, it is crucial to ensure that both the precision of the signals and the behavior of the system closely align with experimental measurements. At the same time, generating data through simulations can be considerably more efficient and cost-effective. However, the most accurate models can only be achieved with real experimental data, despite the higher costs and logistical challenges associated with data collection. Therefore, throughout my PhD study, all models were exclusively developed using experimental data.

Another key aspect of working with data is preprocessing, which is essential to ensure that the dataset used for training, validation, and testing contains a high variety of experimental conditions while maximizing information content. Proper preprocessing enhances the consistency and reliability of the dataset, ultimately improving the performance and generalization ability of the developed models.

In this part of my thesis, I will present the sensor signals used as input and output in

the developed models, detailing the exact steps and conditions under which the data was collected. The preprocessing techniques applied to the raw data will be discussed, along with the structure and composition of the datasets created for model development.

2.2 Sensor Signals

Modern vehicles are equipped with numerous ECUs that communicate with each other through an internal network to manage various aspects of vehicle performance, safety, and efficiency. These ECUs exchange data in real-time, enabling coordinated operation across subsystems such as the powertrain, braking, steering, and driver assistance systems. The most commonly used communication protocol is the Controller Area Network (CAN), which allows for reliable data transmission with minimal latency. In more complex applications, FlexRay or Automotive Ethernet is used to support higher data transfer rates and deterministic communication. The growing complexity of modern vehicles, particularly with the integration of advanced driver assistance systems, has made efficient and reliable communication between ECUs a fundamental requirement for ensuring both performance and safety. However, the primary signals received by the brake control ECU from other ECUs are primarily related to deceleration. As a result, the critical inputs necessary for vehicle dynamics are not sourced from other ECUs but sensors.

One of the most critical ECUs within this system is the Brake Control ECU, which is responsible for executing key braking and stability functions. This ECU receives input signals from multiple sensors and processes them in real-time to manage braking interventions and maintain vehicle stability. Its primary role is to regulate braking pressure at each wheel based on sensor feedback, preventing excessive slip and ensuring optimal traction. The Brake Control ECU is connected to other ECUs, such as those governing engine control, steering, and chassis dynamics, allowing for coordinated control actions across different vehicle subsystems. Given its safety-critical nature, the Brake Control ECU operates with high redundancy and fail-safe mechanisms to guarantee reliability.

The most important vehicle functions managed by the Brake Control ECU include ABS, ESC, and TCS. ABS prevents the wheels from locking up during emergency braking by continuously monitoring wheel speeds and modulating brake pressure at each wheel to maintain traction. ESC builds upon ABS functionality by detecting and mitigating oversteer and understeer conditions. It selectively applies braking force to individual wheels and adjusts engine torque to help keep the vehicle on its intended path. TCS is designed to prevent excessive wheel slip during acceleration by reducing engine power or applying braking force to slipping wheels. All three of these functions rely on precise sensor inputs to operate effectively.

The operation of these functions is dependent on several key vehicle dynamics param-

eters. Longitudinal acceleration, denoted as a_{long}, represents the rate of change in velocity along the vehicle's forward or backward direction. It is measured in meters per second squared $[\mathrm{m/s^2}]$ or in gravitational acceleration units [g], where $1\,\mathrm{g}$ corresponds $9.81\,\mathrm{m/s^2}$. Longitudinal acceleration is a crucial input for functions such as traction control and emergency braking interventions. Lateral acceleration, a_{lat}, describes the acceleration perpendicular to the vehicle's longitudinal axis, occurring mainly during cornering maneuvers. Like longitudinal acceleration, it is measured in $[\mathrm{m/s^2}]$ or [g]-units and is fundamental for stability control, as it helps detect excessive lateral forces that could lead to loss of traction.

Yaw rate, ($\dot{\Phi}$), describes the rotational velocity of the vehicle around its vertical axis. It is measured in degrees per second $[^\circ/\mathrm{s}]$ and is a key input for ESC, as it helps determine whether the vehicle is following the intended trajectory set by the driver. Roll rate, ($\dot{\Psi}$), represents the rotational velocity around the vehicle's longitudinal axis, which is particularly relevant in roll stability control applications. It is also measured in $[^\circ/\mathrm{s}]$ and plays a role in detecting potential rollover situations, especially in vehicles with a high center of gravity.

Figure 2.1 provides a visual representation of the mentioned sensor signals.

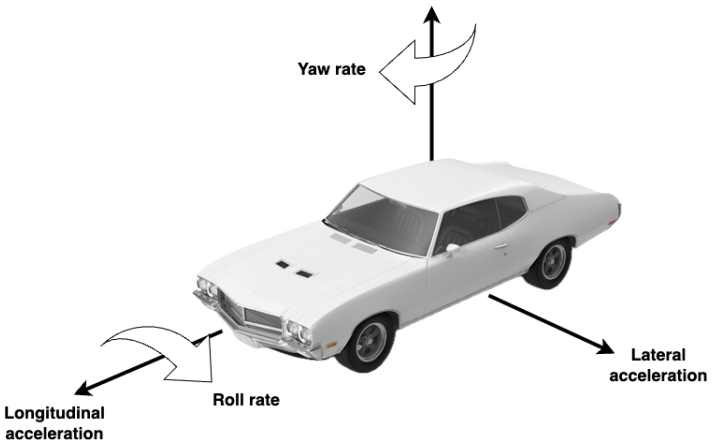

Figure 2.1. A visual representation showing longitudinal acceleration, lateral acceleration, yaw rate, and roll rate is provided.

The steering angle of the front axle (δ) represents the deviation of the front wheels from the straight-ahead position. It is measured in degrees [°] and determines the direction in which the vehicle is intended to move. The steering angle is a fundamental input for ESC and other stability functions, as it allows the system to compare the driver's intended direction with the actual movement of the vehicle. Discrepancies between these values can indicate potential loss of control, triggering corrective braking interventions. I used the steering angle of the front axle rather than the steering wheel angle because it is independent of the vehicle's steering system. Nevertheless, these two variables are strongly correlated. The relationship between them is characterized by the steering gain, which quantifies how much steering wheel angle change is needed for a one-degree change in the steering angle of the front axle. Steering gains may differ for left and right steering directions.

The four wheel speeds, denoted as v_{FL} , v_{FR}, v_{RR} ,v_{RL}, correspond to the rotational velocities of the front-left (FL), front-right (FR), rear-left (RL), and rear-right (RR) wheels, respectively. These values are typically measured in kilometers per hour $[\mathrm{km/h}]$. The differences between individual wheel speeds provide essential information for detecting wheel slip, determining yaw motion, and identifying traction loss. These signals are used as primary inputs for ABS, ESC, and TCS to modulate braking and optimize vehicle stability.

In Figure 2.2, the vehicle's longitudinal dynamics are illustrated, showcasing how the primary source of longitudinal acceleration is the variation in wheel speeds. When the vehicle accelerates, the increase in wheel speed results in a rise in longitudinal acceleration, while deceleration leads to a decrease. Furthermore, in Figure 2.3, the relationship between the steering wheel angle and lateral acceleration is presented. The correlation between these variables is evident; however, for a comprehensive description of lateral acceleration, the vehicle's longitudinal effects must also be considered. When lateral acceleration is negative, it signifies that the vehicle body is experiencing acceleration toward the right direction, and a similar trend applies to the steering wheel angle.

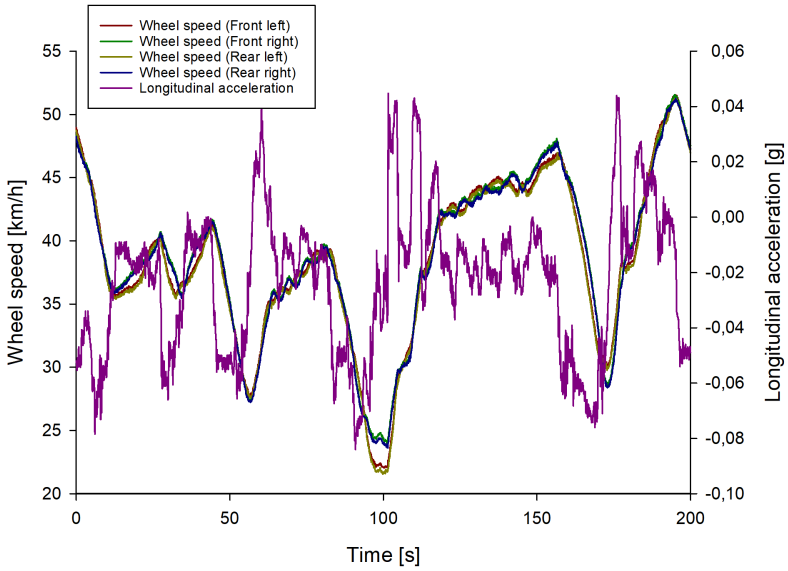

Figure 2.2. Example data from the collected database showing wheel speeds and longitudinal acceleration under standard test track conditions.

Additionally, the wheel speeds of all four wheels generally move in unison; however, during left and right turns, minor differences arise due to the geometric constraints of the vehicle. This variation is dictated by the distinct paths each wheel follows. In left turns, the right-side wheels cover a slightly greater distance than the left-side wheels, and vice versa for right turns. Consequently, the wheel speeds exhibit subtle deviations, though these differences remain within a predictable range dictated by the vehicle's geometry. These effects further reinforce the importance of considering both longitudinal and lateral dynamics when

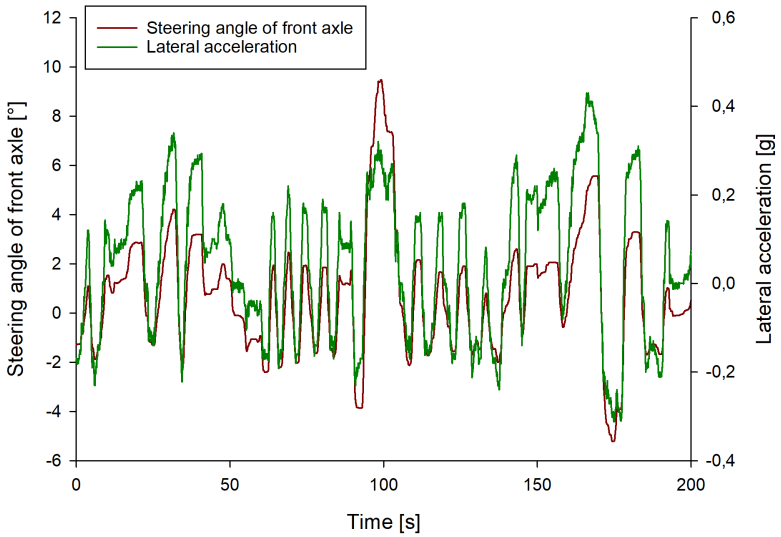

Figure 2.3. Example data from the collected database showing steering wheel angle and lateral acceleration sensors under standard test track conditions.

analyzing vehicle movement.

Figure 2.4 presents the relationship between the steering angle of the front axle, yaw rate, and roll rate over time, offering insight into the vehicle's dynamic behavior under off-road conditions. The changes in the steering angle indicate alternating left and right turns, which directly influence the yaw rate, representing the vehicle's rotational motion. The close correlation between these two variables highlights how the vehicle responds to steering inputs, demonstrating the delay and smooth transitions in direction. The roll rate shows more rapid variations, reflecting the lateral tilting of the vehicle body. This roll movement is particularly significant in off-road conditions, where uneven terrain, varying surface grip, and external disturbances such as bumps and inclines play a major role. Compared to normal road conditions, the effects on the roll rate occur at a much higher frequency, as the irregularities of the terrain cause continuous fluctuations in the vehicle's body movement. The extent of the roll is influenced by the vehicle's weight distribution, suspension characteristics, and center of gravity, with sudden changes amplifying the oscillations. When navigating rough terrain, lateral forces cause the body to lean unpredictably, making roll stability a critical aspect of off-road driving. Overall, the graph effectively illustrates how the interaction between steering, yaw motion, and roll dynamics shapes the vehicle's handling characteristics in an off-road environment. The significantly higher frequency of roll rate variations compared to normal road conditions highlights the increased complexity of vehicle control in such challenging terrains, emphasizing the need for optimized suspension and stability management systems.

These key vehicle dynamics parameters are measured using various sensors, the most critical of which are housed within the Inertial Measurement Unit (IMU). The IMU is re-

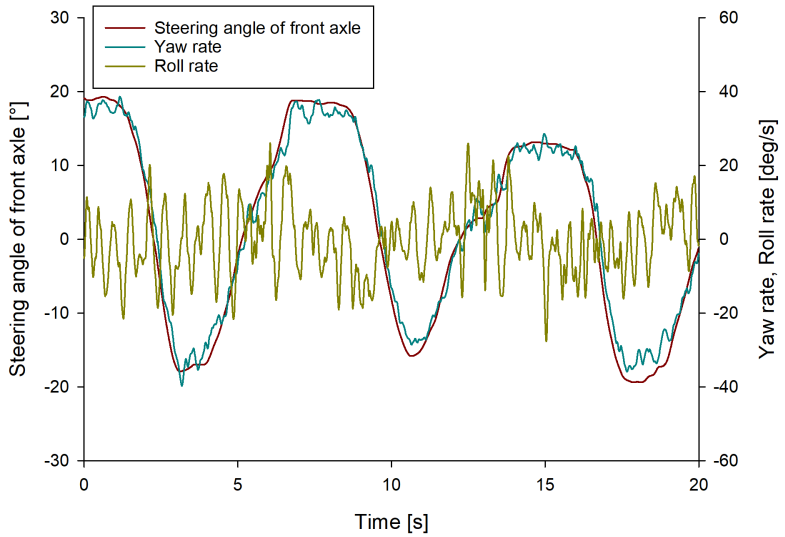

Figure 2.4. Example data from the collected database showing steering angle of the front axle, yaw rate, and roll rate under off-road conditions.

sponsible for capturing acceleration and rotational rate signals in different axes, providing essential data for stability control functions. The IMU can be implemented as a separate sensor module or integrated directly into the Brake Control ECU. In a discrete configuration, the IMU functions as a separate unit, transmitting data over the vehicle network. This allows for flexibility in sensor placement, ensuring optimal positioning for accurate measurements. However, this setup requires additional wiring and introduces potential delays due to network communication. When the IMU is integrated into the Brake Control ECU, sensor signals are processed directly within the unit, reducing latency and eliminating the need for separate connections. While this integration improves reliability, it also limits flexibility in sensor placement and increases dependency on a single hardware component.

The placement of the IMU within the vehicle is crucial for accurate measurements. It should be positioned as close as possible to the vehicle's center of mass to minimize errors caused by body movement and structural flexing. The most common mounting locations for the IMU are behind the airbag module in the steering wheel or beneath the center console near the handbrake. These locations provide a stable reference point while also allowing for easy integration into the vehicle's electronic architecture.

The accuracy and integration of these sensor signals play a crucial role in modern stability control systems. By processing real-time data from accelerometers, gyroscopes, wheel speed sensors, and steering angle sensors, the Brake Control ECU can dynamically adjust braking and traction interventions to enhance vehicle safety and performance. The effectiveness of these functions depends not only on the precision of individual sensor measurements but also on the ability of the system to process and interpret this data in real time. Ensuring reliable signal acquisition and processing is fundamental to the development of robust

vehicle stability control models.

2.3 Data Collection Methodology

The data collection process played a crucial role in ensuring the accuracy and reliability of subsequent analyses, encompassing both experimental and simulation-based methodologies. The aim was to gather high-quality sensor data under controlled conditions to support the development and validation of predictive models for vehicle dynamics. The dataset was structured to reflect real-world driving scenarios while allowing for precise control over the test conditions.

For the experimental data collection, a commercially available SUV was selected as the test vehicle (*Vehicle Original*). Due to disclosure agreements, the exact type and OEM cannot be specified. This vehicle type was particularly suitable due to its unique dynamic properties, including a higher center of mass and a specialized suspension system, which significantly influence its handling characteristics. Given that SUVs pose distinct challenges in terms of stability and maneuverability, studying their behavior under various driving conditions was essential.

The measurements were conducted at several locations: the Continental test track in Veszprém, Hungary; within the city of Veszprém; and for off-road conditions, in Brimley, Michigan. The test track provided a controlled environment where predefined maneuvers could be executed with high precision, while the urban environment offered insights into vehicle behavior in realistic traffic conditions. The data was collected within a limited timeframe, ensuring consistency in ambient conditions. All measurements were performed within days, or at most within a single week, to maintain uniform temperature and weather conditions, minimizing variations due to external environmental factors. It is important to emphasize that no function intervention occurred during the measurements, ensuring that the collected data accurately represents the vehicle's behavior under stable conditions. During the tests, the driver was the sole occupant of the vehicle, and the data collection tool was a laptop with negligible weight compared to the driver. Additionally, all tires were set to 2.3 bar, in accordance with the manufacturer's specifications, ensuring that tire pressure remained consistent throughout the measurements. These conditions contributed to the reliability and reproducibility of the collected data, eliminating potential variations due to changes in vehicle load or tire pressure. To further optimize data collection, the test driver was instructed to stop the vehicle every 5–10 minutes. This procedure allowed for smaller measurement sections that started from standstill and returned to standstill condition. Furthermore, all measurements were conducted under high-friction conditions, ensuring that the recorded data reflects vehicle dynamics without the influence of low-traction surfaces.

A key component of the measurement setup was the modified brake ECU, which served

as the primary data acquisition system. The ECU was specifically configured to log high-frequency vehicle dynamics data with minimal latency, ensuring that critical parameters were captured accurately. The data was recorded in the standardized MF4 file format, a widely used format in the automotive industry that enables efficient storage and retrieval of large datasets. The sampling frequency was set at 100 Hz, allowing for high-resolution time-series analysis of dynamic vehicle behavior.

Each measurement session included more than 2000 simultaneously recorded signals, providing a comprehensive representation of the vehicle's motion and response to different driving scenarios. The key recorded parameters included wheel speeds for all four wheels, the steering angle of front axle, longitudinal and lateral accelerations, yaw rate, and roll rate. During the tests, the vehicle speed varied from a complete stop to approximately 130 $\mathrm{km/h}$ on highways and up to 50 $\mathrm{km/h}$ in city conditions, encompassing a wide range of driving scenarios. The maneuvers executed by the test driver were designed to induce variations in lateral and longitudinal acceleration, ensuring a diverse dataset that captured various aspects of the vehicle's dynamic response.

2.4 Data Preprocessing

The process of data preprocessing plays a crucial role in ensuring the reliability and accuracy of machine learning models, particularly in the domain of vehicle dynamics. The data used for training, validating, and testing neural network-based predictive models were collected through systematic experiments conducted under controlled conditions. These experiments provided raw sensor data that needed to be cleaned, normalized, and divided into appropriate datasets before being used in the model development process.

The dataset used for model development was collected by professional test drivers under real-world driving conditions. As mentioned before, vehicles were equipped with advanced onboard measurement systems that recorded key dynamic variables such as longitudinal acceleration, lateral acceleration, yaw rate, roll rate, steering angle, and wheel speeds. During data collection, the vehicle's motion was continuously monitored, but stationary periods were removed from the dataset. This was necessary because non-moving intervals did not provide relevant dynamic information and could introduce biases into the training process. Consequently, any recorded data where the vehicle speed was below a threshold of $0.11\,\mathrm{km/h}$ was excluded. The $0.11\,\mathrm{km/h}$ value of the wheel speed signals represents the zero reading of the wheel speed sensor. A drop to exactly zero would indicate a sensor failure or wiring disconnection rather than actual vehicle standstill.

To ensure consistent scaling across all input variables, normalization was performed using expert-defined limits. This step was crucial to prevent numerical instability and improve model convergence. The normalization ranges were defined as follows: acceleration data

(longitudinal and lateral) was scaled to the range of $[-1, 1]$ g, based on typical sensor output characteristics. The yaw rate was constrained within $[-75, 75]$ °/s, which aligns with empirical driving conditions. Roll rate was normalized between $[-90, 90]$ °/s, reflecting the range of vehicle roll motion theoretical maximum and minimum values. Wheel speeds were normalized within a range spanning from a minimum of 0.11 $\mathrm{km/h}$ at standstill to a maximum of 70 $\mathrm{km/h}$ for city, up to 40 $\mathrm{km/h}$ for off-road driving and up to 130 $\mathrm{km/h}$ under highway conditions. The steering angle was limited to $[-40, 40]$ ° to reflect realistic driving scenarios. By applying these normalization strategies, the dataset became more robust to variations in driving conditions. Prior to normalization, Exploratory Data Analysis (EDA) was conducted to assess data quality and detect potential outliers. The analysis did not reveal significant outliers or anomalous values that would require removal or additional filtering. As a result, no further data cleaning was necessary, ensuring that the dataset remained representative of real-world driving scenarios. By applying these normalization strategies, the dataset became more robust to variations in driving conditions.

After preprocessing, the dataset was partitioned into three distinct subsets to facilitate the development and evaluation of the models. The training set accounted for around 80% of the total dataset and was used to train the neural networks and optimize the model parameters. A validation set, representing 10% of the training set, was randomly selected to tune hyperparameters and prevent overfitting. The test set, comprising around 20% of the total dataset, was reserved for evaluating the final performance of the trained models on unseen data. This splitting strategy ensured that the models could generalize well to new data while minimizing overfitting.

In the case of the development a standard feedforward neural network, all subsets contained data with the same statistical distribution, ensuring that the training, validation, and test sets were representative of the overall dataset. This approach allows the model to learn patterns effectively without biasing its performance toward specific driving conditions.

For developing LSTM models, a different approach was required due to the temporal nature of the data. Instead of randomly selecting individual samples, the dataset was divided into continuous data chunks, where each chunk represented a complete driving scenario—from a standstill to standstill. This method ensures that temporal consistency is preserved, preventing unnatural discontinuities in the training data that could otherwise affect model learning. Each subset contained randomly assigned data chunks, maintaining the original proportion of training, validation, and test sets. Additionally, the statistical distribution of each subset was verified to ensure that all sets remained representative of the overall dataset, preventing bias in the model's learning process.

2.5 Datasets

In the following subsections, the six collected datasets will be introduced. To comprehensively capture the variability inherent in real-world driving and ensure robust model training, six distinct datasets were established. It's important to note that the creation of these datasets was also an iterative process; as the research topics evolved and the scope of the investigation expanded over time, the need for additional, more specifically targeted data became apparent, ultimately leading to the collection of these six distinct sets. This multi-dataset approach is crucial for covering a wide spectrum of vehicle behaviors. I will outline each dataset's specific purpose and the precise conditions under which the data was recorded. The content of each dataset will be detailed, including the measured signals (such as steering angle, vehicle speed, accelerations, yaw rate, etc.) and their direct relevance to predicting vehicle dynamics. Additionally, fundamental statistical properties – including standard deviation, quartiles, and overall data distribution – will be presented. This statistical overview provides crucial insights into the variability within each specific condition and the representativeness of the collected data overall, offering a clear picture of the phenomena captured in each set.

The reliability and robustness of neural network models in vehicle dynamics prediction are heavily influenced by the quality and, critically, the diversity of the training data. A well-prepared composite dataset, formed from these individual collections, must encompass a wide range of driving conditions. This ensures that the model can generalize effectively across various scenarios encountered in reality while maintaining high predictive accuracy. Special attention must be given to the lower and upper bounds of the entire collected data corpus, as these collective limits define the operational range within which the model can be considered reliable. Neural networks excel at interpolation, providing accurate predictions for conditions represented within the span of the training data. However, they notoriously struggle with extrapolation; predictions for scenarios falling outside the minimum and maximum values observed during training (i.e., outside the conditions covered by these six datasets) become highly uncertain and potentially inaccurate. Therefore, understanding the boundaries defined by these datasets is paramount for deploying the resulting model safely and effectively.

2.5.1 Dataset_lateral_acc

The main statistical characteristics of the collected data, specifically recorded on the Continental test track in Veszprém, are summarized in Table 2.1. Analyzing these properties is essential, as this developed dataset forms the foundation for training models aimed at lateral acceleration prediction. The range and distribution of the steering angle indicate balanced

driving maneuvers because the interquartile range (Q1 to Q3) is relatively small, suggesting that most steering inputs were moderate. However, the minimum and maximum values show that the dataset includes both sharp turns and straight-line driving, ensuring a diverse representation of vehicle dynamics. The wheel speed values demonstrate consistency, but with a broad speed range because the median wheel speeds indicate that the dataset captures normal driving conditions, while the minimum speed and the maximum speed confirm that the dataset includes both standstill and high-speed scenarios. The small differences between the four wheel speeds suggest there was no wheel slip under standard conditions.

Table 2.1. Statistical properties of the preprocessed *Dataset_lateral_acc*.

	a_{long} [g]	a_{lat} [g]	δ [°]	v_{FL} [km/h]	v_{FR} [km/h]	v_{RR} [km/h]	v_{RL} [km/h]
Std	0.09	0.17	3.57	25.32	25.29	25.19	25.20
Min	−0.57	−0.75	−27.89	0.11	0.11	0.11	0.11
Q1(25%)	−0.05	−0.01	−0.14	34.20	34.23	33.92	33.96
Q2(50%)	−0.02	0.01	0.04	54.33	54.45	54.05	54.24
Q3(75%)	0.02	0.03	0.30	64.62	64.62	64.26	64.34
Max	0.32	0.63	32.98	135.28	135.23	134.26	134.46

2.5.2 Dataset_yaw_rate

This hybrid dataset was constructed by integrating real-world urban driving data with controlled test track experiments. The urban driving data was gathered in real traffic conditions within Veszprém, where the vehicle encountered a wide array of external factors, such as intersections, pedestrian crossings, and dynamic interactions with other road users. The combination of stop-and-go movements, moderate acceleration phases, and external disturbances ensured that the dataset accurately represented the challenges faced by vehicles navigating through dense urban environments. This part of the dataset also provides valuable insight into how the vehicle responded to unpredictable driving environments.

Alongside the *city driving* data, the test track data was collected in a controlled setting, where specific driving patterns and maneuvers could be repeatedly executed under consistent conditions. The test track data were collected from two distinct driving styles: *calm* and *aggressive driving* scenarios.

In the *calm driver* scenario, the test pilot executed driving maneuvers that closely mimicked natural city driving conditions but with significantly fewer standstill events. Unlike real urban traffic, where frequent stops due to traffic lights, congestion, and pedestrian crossings reduce the amount of continuous movement data collected, the *calm driving* scenario ensured a smoother flow of movement. As a result, a greater amount of useful data could be recorded in a given period compared to the *city driving* scenario. The driving style was

characterized by gradual accelerations and decelerations, smooth cornering, and controlled steering inputs, making it ideal for capturing stable vehicle dynamics under predictable driving conditions. This approach maximized the efficiency of data collection while preserving the characteristics of real-world urban driving.

In contrast, the *aggressive driver* scenario was designed to introduce higher dynamics into the dataset, ensuring that the model being developed can also learn from more extreme vehicle behaviors. The key characteristic of this scenario was the significantly higher gradient of acceleration and deceleration. The test pilot executed sharper throttle inputs, sudden braking events, and rapid steering maneuvers, pushing the vehicle through aggressive cornering and acceleration phases that far exceeded the smooth transitions seen in the *calm driving* scenario. This dataset segment was critical in capturing high-dynamic yaw rate variations, which are essential for training models that need to perform robustly under extreme driving conditions.

For creating this dataset, more than 4.5 hours of raw data were recorded within a speed range of 0 to 50 $\mathrm{km/h}$. The combination of these two sources ensured that the dataset captured both structured and naturally occurring variations in vehicle dynamics, making it suitable for both training and validation purposes. The collected dataset was used for the development and validation of an LSTM model for yaw rate prediction.

After the data cleaning phase, the available data for each driving scenario was refined to ensure high-quality input for model development. Specifically, the final version of the dataset included 0.60 hours of data for the *calm driving* scenario, 1.55 hours for the *aggressive driving* scenario, and 1.82 hours for the *city driving* scenario.

The comparison of statistical properties across the three driving styles (called as *combined driving*)—*calm* (Table 2.2), *aggressive* (Table 2.3), and *city driving* (Table 2.4)—reveals distinct characteristics in vehicle dynamics.

Table 2.2. Statistical properties of the *calm driver* segment from *Dataset_yaw_rate*.

	a_{long} [g]	a_{lat} [g]	$\dot{\Phi}$ [$^\circ/s$]	δ [$^\circ$]	v_{FL} [km/h]	v_{FR} [km/h]	v_{RR} [km/h]	v_{RL} [km/h]
Mean	−0.01	0.01	1.992	0.717	30.83	30.97	30.81	30.67
Std	0.06	0.20	12.722	5.096	10.16	10.12	10.12	10.16
Min	−0.49	−0.68	−36.625	−28.861	0.11	0.11	0.11	0.11
Q1 (25%)	−0.04	−0.08	−4.186	−1.470	25.10	25.57	25.39	24.96
Q2 (50%)	−0.01	0.00	0.343	0.114	31.80	32.27	32.08	31.64
Q3 (75%)	0.02	0.13	9.664	3.398	38.01	37.97	37.84	37.87
Max	0.30	0.61	36.871	18.811	62.52	63.00	62.90	62.35

Longitudinal acceleration (a_{long}) varies significantly between the scenarios. The *calm* and *city driving* styles exhibit smoother acceleration and braking patterns, while the *aggressive driving* scenario shows stronger and more frequent changes in speed. The*aggressive*

Table 2.3. Statistical properties of the *aggressive driver* segment from *Dataset_yaw_rate*.

	a_{long} [g]	a_{lat} [g]	$\dot{\Phi}$ [$^\circ/s$]	δ [$^\circ$]	v_{FL} [km/h]	v_{FR} [km/h]	v_{RR} [km/h]	v_{RL} [km/h]
Mean	−0.01	0.00	1.096	0.351	36.28	36.36	36.15	36.06
Std	0.13	0.32	15.145	5.331	9.71	9.65	9.67	9.73
Min	−0.85	−1.03	−69.358	−33.477	0.11	0.11	0.11	0.11
Q1 (25%)	−0.06	−0.20	−8.145	−2.619	33.06	33.03	32.80	32.82
Q2 (50%)	−0.01	0.00	0.177	0.049	38.17	38.19	37.99	37.96
Q3 (75%)	0.05	0.22	10.090	3.133	42.57	42.56	42.39	42.39
Max	0.51	0.92	71.260	33.346	60.09	60.07	59.70	59.91

Table 2.4. Statistical properties of the *city driver* segment from *Dataset_yaw_rate*.

	a_{long} [g]	a_{lat} [g]	$\dot{\Phi}$ [$^\circ/s$]	δ [$^\circ$]	v_{FL} [km/h]	v_{FR} [km/h]	v_{RR} [km/h]	v_{RL} [km/h]
Mean	−0.01	0.01	0.025	−0.035	29.62	29.56	29.45	29.51
Std	0.06	0.07	5.820	4.080	13.14	13.12	13.12	13.14
Min	−0.37	−0.46	−35.513	−31.111	0.11	0.11	0.11	0.11
Q1 (25%)	−0.02	−0.01	−0.812	−0.363	20.51	20.68	20.56	20.40
Q2 (50%)	−0.01	0.00	−0.029	−0.021	32.53	32.46	32.38	32.42
Q3 (75%)	0.02	0.02	0.549	0.191	40.04	39.96	39.87	39.94
Max	0.31	0.46	35.255	33.187	56.40	56.26	56.63	56.67

driver scenario also has the highest variability in acceleration, indicating a more dynamic and less predictable driving style.

Lateral acceleration (a_{lat}) follows a similar trend to longitudinal acceleration, with the *aggressive driving* scenario showing the greatest variability. This is consistent with sharper turns and more abrupt lane changes, while the *calm* and *city driving* styles demonstrate smoother lateral movements. The aggressive scenario reaches the most extreme values, reflecting the high-intensity maneuvers performed during the test.

Considering the values of the yaw rate ($\dot{\Phi}$), the *aggressive driving* scenario exhibits the highest variability, characterized by more pronounced and frequent directional changes. The *calm driver* scenario shows moderate variations, while the *city driver* scenario remains the most stable, as expected in urban traffic conditions.

Steering angle of front axle (δ) also varies significantly across the three styles. The *aggressive driving* scenario shows the most dynamic and abrupt steering changes, while the calm and *city driving* styles exhibit more controlled and predictable movements. The aggressive driver scenario includes sharper turns and more significant deviations in steering input.

In terms of wheel speed (v_{FL}, v_{FR}, v_{RR}, v_{RL}), the *aggressive driving* scenario maintains the highest average speeds, reflecting a more performance-oriented driving style. The calm driver scenario follows with moderate speeds, while the city driver scenario, constrained

by urban traffic conditions, shows the lowest overall speeds and the highest frequency of stop-and-go movements.

Overall, the dataset effectively captures the distinctions between the three driving styles. The aggressive scenario is marked by rapid changes in speed, sharper turns, and higher variability in vehicle dynamics. The calm driver scenario presents a more stable driving pattern, while the city driver scenario reflects the constraints of urban driving, with frequent stops and controlled maneuvering. These differences confirm the suitability of the dataset for training and validating predictive models for vehicle dynamics, particularly in yaw rate prediction.

2.5.3 Dataset_yaw_rate_ext

The extended yaw rate dataset was developed to enhance the diversity and representativeness of driving scenarios by incorporating additional measurement sessions for both calm and *aggressive driving* styles, while retaining the original *city driving* measurement from the *Dataset_yaw_rate*. This dataset expansion was crucial in ensuring a broader spectrum of vehicle dynamics, ultimately leading to improved model generalization for yaw rate prediction. The collection methodology remained identical to that employed in the *Dataset_yaw_rate*, ensuring consistency in data acquisition and comparability across different driving conditions. The primary purpose of constructing the extended yaw rate dataset is to establish a sufficient volume of data to determine the necessary amount required for training a neural network-based dynamic vehicle model effectively. The extended dataset includes 3.23 hours of *calm driving*, 2.60 hours of *aggressive driving*, and 1.72 hours of *city driving* data.

By extending the dataset, I aimed to systematically analyze how much driving data is needed to achieve reliable and accurate predictions of vehicle yaw rate using LSTM networks. Additionally, the extended calm driver scenario was utilized for forecasting longitudinal acceleration, providing valuable insights into vehicle dynamics beyond yaw rate prediction. This ensures that the dataset supports multiple predictive modeling tasks, enhancing its applicability in vehicle dynamics.

The analysis of the *calm* (Table 2.5) and *aggressive* (Table 2.6) driving datasets reveals significant differences in driving dynamics. The *calm driving* scenario is characterized by smooth and gradual acceleration, lower lateral forces, and minimal yaw rate variations, reflecting a stable and controlled driving style. In contrast, the *aggressive driving* scenario shows much higher variability in acceleration and yaw rate, with more extreme maneuvers, sharper turns, and rapid directional changes. The increased yaw rate fluctuations in *aggressive driving* highlight the intensity of steering inputs compared to the more predictable behavior observed in *calm driving*. Based on these characteristics, it can be stated that the

Table 2.5. Statistical properties of the *calm driver* segment from *Dataset_yaw_rate_ext*.

	a_{long} [g]	a_{lat} [g]	$\dot{\Phi}$ [°/s]	δ [°]	v_{FL} [km/h]	v_{FR} [km/h]	v_{RR} [km/h]	v_{RL} [km/h]
Mean	−0.03	0.01	0.491	1.493	36.53	36.66	36.33	36.45
Std	0.05	0.21	3.879	10.927	9.86	9.73	9.86	9.72
Min	−0.49	−0.73	−33.149	−36.625	0.11	0.11	0.11	0.11
Q1(25%)	−0.03	−0.14	−1.915	−6.781	31.25	31.55	31.05	31.31
Q2(50%)	−0.01	0.00	0.049	0.172	37.12	37.14	36.93	36.93
Q3(75%)	0.00	0.17	2.321	8.497	42.66	42.79	42.45	42.57
Max	0.35	0.62	30.953	42.911	62.52	63.00	62.35	62.90

Table 2.6. Statistical properties of the *aggressive driver* segment from *Dataset_yaw_rate_ext*.

	a_{long} [g]	a_{lat} [g]	$\dot{\Phi}$ [°/s]	δ [°]	v_{FL} [km/h]	v_{FR} [km/h]	v_{RR} [km/h]	v_{RL} [km/h]
Mean	−0.03	0.01	1.376	0.417	36.16	36.28	35.88	36.00
Std	0.13	0.32	15.935	5.343	8.88	8.81	8.91	8.84
Min	−0.85	−0.95	−64.562	−33.308	0.11	0.11	0.11	0.11
Q1(25%)	−0.08	−0.20	−8.689	−2.558	32.11	32.28	31.81	31.98
Q2(50%)	−0.02	0.00	0.372	0.107	37.35	37.41	37.08	37.14
Q3(75%)	0.04	0.23	11.397	3.224	42.09	42.07	41.86	41.86
Max	0.50	0.95	68.011	33.245	58.64	58.07	58.51	57.60

extended dataset has similar properties to the *Dataset_yaw_rate*, ensuring consistency in the data distribution and maintaining the representativeness of different driving styles.

2.5.4 Dataset_yaw_rate_sens

To comprehensively evaluate the generalization capability and robustness of the yaw rate prediction model, additional data collection was carried out beyond the base dataset. The extended dataset was specifically designed to capture the effects of key parameters influencing vehicle dynamics, such as tire pressure variations, changes in passenger load, and differences in vehicle types. These additions enabled the execution of targeted sensitivity analyses, allowing for a systematic assessment of the model's performance under conditions not present during training.

The dynamic behavior of a vehicle is significantly impacted by the tire pressure of the vehicle. My primary focus was not on the scenario of continuously decreasing tire pressure but rather on assessing how the neural network-based vehicle model responds to an extreme scenario where the tire pressure is significantly less than normal. To investigate the effect of tire pressure on the model, this pressure was reduced to 1.5 bar for each wheel separately. The selection of 1.5 bar as the reduced tire pressure level was intentional, as it represents a significant deviation from the original 2.3 bar, making its effects perceptible to both the

driver and passengers. Given that tire pressure directly influences vehicle dynamics by altering grip, rolling resistance, and slip angles, it was hypothesized that such a reduction would impact the accuracy of yaw rate predictions. To systematically evaluate this effect, the model's performance was analyzed under both nominal and reduced tire pressure conditions, assessing its ability to generalize beyond the training domain. For the evaluation, data were gathered for *aggressive*, *calm*, and *city* driver scenarios with reduced tire pressures. The aim was to evaluate the performance of the model, which was trained on data where all wheels had a tire pressure of 2.3 bar in situations where the pressure of one wheel was extremely low.

The weight of the vehicle is also a crucial parameter influencing its dynamic behaviour. To simulate the effect of an additional passenger, sandbags were used, with each sandbag weighing 20 kg. One passenger was simulated by placing five sandbags on a seat. Measurement data were collected for all three driving scenarios by placing five sandbags separately on the front passenger seat, the rear passenger seat opposite the driver's side, and the rear seat on the driver's side. Additionally, a comprehensive weight configuration was examined, involving the placement of sandbags on all three mentioned passenger seats. The driver's seat was, of course, occupied during all tests. The objective was to assess the performance of the model trained with data collected with only the driver present, in scenarios where additional passengers are also in the vehicle. A visualization of these different passenger configurations can be seen in Figure 2.5.

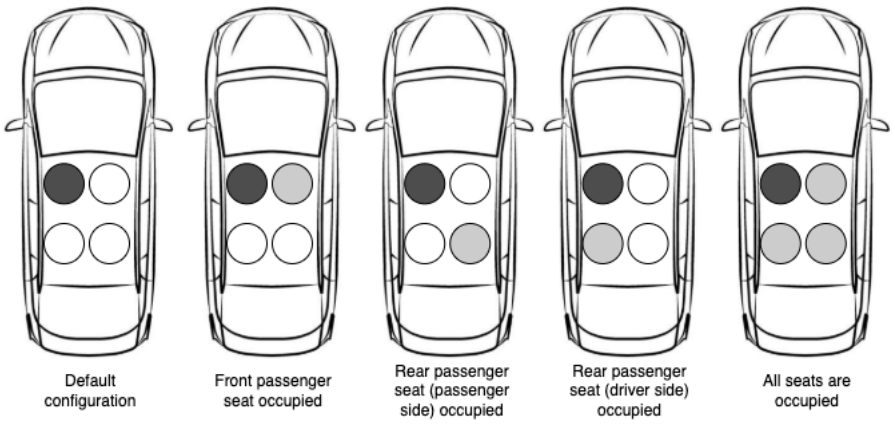

Figure 2.5. Visualization of the different passenger configuration.

Finally, the sensitivity analysis evaluated the performance of the model by applying it to different vehicle types. For this purpose, three other vehicles of varying sizes and drivetrains were utilized. The types of vehicles used for collecting supplementary data were as follows. *Vehicle A* represents a significantly smaller hatchback, while *Vehicle B* is another SUV, slightly larger than the *Vehicle Original*. *Vehicle C* is a substantial 7-seater SUV. It is important to note that both the *Vehicle Original* and *Vehicle A* were equipped exclusively with internal combustion engines, whereas *Vehicle B* and *Vehicle C* were hybrids, featuring

both internal combustion engines and electric drivetrains. Data were collected for each vehicle and for all three driving scenarios. The objective was to evaluate how a model trained on a combustion-engine mid-size SUV performs when applied to other vehicle types and sizes with different drivetrains.

Due to the large number of tables, the statistical properties of the datasets used for the sensitivity analysis are provided in the Appendix. Specifically, the statistical summaries for the tire pressure sensitivity analysis are presented in Tables from 5.22 to 5.33. The statistical properties of the datasets related to varying passenger loads can be found in Tables from 5.10 to 5.21. Finally, the statistical details of the vehicle body variation studies, which evaluate the model's performance across different vehicle types and sizes, are summarized in Tables from 5.1 to 5.9. These tables provide a comprehensive overview of the datasets used throughout the sensitivity analysis.

It is important to highlight that some of the collected data includes measurements where the vehicle speed exceeded 50 $\mathrm{km/h}$. These instances were intentionally included to evaluate how the developed model performs when exposed to driving conditions that extend beyond the typical speed range observed during training. This allowed for an additional assessment of the model's generalization capability, particularly in scenarios involving higher speeds, where vehicle dynamics may differ significantly.

2.5.5 Dataset_roll_rate

This dataset contains vehicle dynamics data collected under off-road conditions. The data collection took place in Brimley, MI (USA) covering a total of 300 minutes of driving. Measurements captured vehicle dynamics at speeds between 0 and 30 $\mathrm{km/h}$ across various terrain conditions, including gravel, mud, and uneven surfaces. The data collection process was designed to simulate real-world off-road driving scenarios, incorporating sudden elevation changes, sharp turns, and varying traction levels to challenge vehicle stability and control systems.

Table 2.7 captures the complex dynamics of off-road driving, where varying terrain significantly influences vehicle stability. Longitudinal and lateral accelerations fluctuate, reflecting the impact of uneven surfaces, sudden elevation changes, and changing traction conditions. The roll rate shows considerable variability, indicating strong vehicle body movements caused by rough terrain and rapid wheel articulation. The yaw rate also exhibits high deviations, suggesting frequent directional adjustments required to navigate obstacles and maintain control. Steering inputs vary widely, pointing to the necessity of continuous driver corrections in response to unpredictable road conditions. Wheel speed fluctuations further highlight the effects of surface irregularities, where traction loss and sudden grip changes influence vehicle movement. The dataset effectively represents real-world off-road

dynamics, making it essential for developing predictive models for roll stability. Based on this dataset, an LSTM neural network model was developed that utilizes both current and past data to predict future yaw rate values, enabling more accurate roll stability estimation under challenging off-road conditions.

Table 2.7. Statistical properties of the *Dataset_roll_rate*.

	a_{long} [g]	a_{lat} [g]	$\dot{\Phi}$ [$^\circ/s$]	$\dot{\Psi}$ [$^\circ/s$]	δ [$^\circ$]	v_{FL} [km/h]	v_{FR} [km/h]	v_{RR} [km/h]	v_{RL} [km/h]
Mean	0.00	0.00	1.126	−0.281	0.309	13.49	13.60	13.51	13.57
Std	0.08	0.16	11.079	7.446	9.101	6.03	6.04	6.04	6.03
Min	−0.60	−0.80	−52.979	−87.493	−32.82	0.11	0.11	0.11	0.11
Q1(25%)	−0.04	−0.10	−5.581	−4.393	−4.87	8.97	9.07	8.99	9.06
Q2(50%)	0.01	0.00	0.325	−0.297	0.06	12.73	12.84	12.75	12.82
Q3(75%)	0.04	0.10	7.957	3.865	5.49	17.18	17.28	17.21	17.25
Max	0.61	0.94	57.895	88.191	32.93	41.36	42.16	41.59	43.30

2.6 Summary of datasets

As presented, six distinct datasets were established to support the training, validation, and testing of various neural network models. The creation of these datasets was an iterative process, evolving in parallel with the objectives of PhD study and model development. Initially, datasets were generated for general vehicle dynamics prediction, while later datasets were designed for specific tasks such as sensitivity analysis or handling off-road conditions. This process inevitably led to some overlaps between datasets; however, each served a targeted purpose aligned with the progression of the work. A summary of the datasets, their application, and the corresponding sections where they are detailed is provided in Table 2.8.

This structure allowed the models to be trained and tested not only under controlled scenarios but also in real-world conditions, ensuring that each dataset contributed uniquely to achieving robust and generalizable predictive models.

2.7 Related publications

P1 János Kontos, László Bódis and Ágnes Vathy-Fogarassy (2025). Experimental Sensor Data from Vehicles for Dynamic Vehicle Models [Dataset]. figshare. `https://doi.org/10.6084/m9.figshare.28078274.v1`

Table 2.8. Summary of the developed datasets and their relationship to the models

Dataset Name	**Purpose / Model Developed**	**Dataset Description**	**Section**
Dataset_lateral_acc	Feedforward ANN (Artificial Neural Network) development for lateral acceleration prediction	Standard test track data covering diverse driving maneuvers up to highway conditions	2.5.1
Dataset_yaw_rate	LSTM model for yaw rate prediction	Dataset with different driving scenarios (*city*, *calm*, *aggressive driving*)	2.5.2
Dataset_yaw_rate_ext	Extended LSTM yaw rate model and longitudinal acceleration prediction	Extended driving scenarios to study model generalization and data volume effect	2.5.3
Dataset_yaw_rate_sens	Sensitivity analysis of yaw rate LSTM model (tire pressure, passenger load, vehicle variation)	Focused tests to assess model robustness in unseen conditions	2.5.4
Dataset_roll_rate	LSTM model for roll rate and yaw rate prediction under off-road conditions	Off-road driving data, capturing extreme roll behavior	2.5.5

Chapter 3

Neural Network-Based Prediction of Vehicle Accelerations

3.1 Introduction

The role of longitudinal and lateral acceleration in vehicle dynamics has gained increasing significance in recent years, particularly as automotive safety and automation technologies advance. Longitudinal acceleration, which governs a vehicle's forward and backward motion, is fundamental for functions such as traction control, adaptive cruise control, and collision detection. It serves as a critical parameter for evaluating vehicle stability and optimizing energy efficiency in electric vehicles [33]. Similarly, lateral acceleration, which describes the sideward movement of a vehicle, plays an essential role in stability control systems, particularly in cornering maneuvers where maintaining traction is crucial. Modern vehicles use IMU to gather real-time data on longitudinal and lateral acceleration, ensuring precise control inputs for safety-critical functions [34].

Recent advancements in artificial intelligence have enabled the development of predictive models that enhance the reliability of acceleration measurements. Among these, neural network-based models have demonstrated superior performance, particularly in forecasting acceleration values [35]. LSTM networks are particularly well-suited for time-series forecasting because they effectively capture long-range dependencies in vehicle motion. The advantage of LSTM networks lies in their ability to leverage both past and current acceleration data, yaw rate, wheel speed, and steering input to generate highly accurate acceleration predictions [36]. This is particularly beneficial in scenarios where traditional sensor outputs may be compromised due to road conditions or transient mechanical variations.

In parallel, feedforward neural networks have also been successfully employed in acceleration prediction tasks. While less computationally demanding than LSTM networks,

they remain effective for applications where real-time processing is required with minimal latency. In lateral acceleration estimation, for instance, feedforward neural networks have been trained using wheel speed, longitudinal acceleration, and steering angle data, achieving prediction accuracies that rival more complex models while maintaining lower hardware requirements [37].

The adoption of these advanced neural network models enhances vehicle safety by improving the plausibility monitoring of acceleration sensors. Predictive models enable real-time validation of sensor data, ensuring that any discrepancies due to sensor degradation or external disturbances are promptly identified. Moreover, integrating predictive analytics into the vehicle's electronic control systems allows for proactive adjustments, enhancing overall stability and safety under dynamic driving conditions.

This section of the PhD thesis will focus on the development and application of artificial neural networks for estimating and predicting vehicle acceleration parameters, presenting a feedforward neural network for estimating the current values of lateral acceleration and an LSTM-based neural network for forecasting the future values of longitudinal acceleration. The developed feedforward neural network, designed with minimal computational requirements, can be integrated not only into ECUs but also directly onto sensors, enhancing their functionality without additional hardware. The lateral acceleration prediction model is applicable in both city and highway driving scenarios, ensuring accurate estimations across diverse road conditions. The LSTM-based model, leveraging past and current sensor data, aims to predict longitudinal acceleration with high accuracy, ensuring proactive responses in safety-critical vehicle functions such as braking and stability control. This model is specifically optimized for city driving, where precise longitudinal acceleration predictions are crucial for smooth traffic flow and enhanced vehicle safety. A thorough literature review will contextualize the research within existing methodologies, highlighting the novelty and advantages of the proposed models. The predictive power of the developed longitudinal and lateral acceleration models is compared to other state-of-the-art models from the literature to evaluate their accuracy, computational efficiency, and overall applicability in real-world automotive scenarios. Finally, the results will be presented and analyzed, demonstrating the effectiveness and potential applications of these neural network models in modern automotive systems.

3.2 Theoretical Background

With the increasing number of vehicles on the roads, the frequency of traffic accidents has risen significantly. This has prompted car manufacturers to place greater emphasis on developing safety-critical systems for vehicles. ADAS and autonomous driving technologies have emerged as crucial components of these efforts, heavily relying on the accurate predic-

tion of both lateral and longitudinal accelerations [38]. These accelerations are fundamental to ensuring optimal vehicle performance and safety, as they serve as inputs to numerous control systems.

Lateral acceleration refers to the sideways motion of a vehicle, perpendicular to its longitudinal acceleration, which captures forward or backward movement. Together, these accelerations are measured by IMUs, which also include yaw rate sensors. The accurate placement of the IMU near the vehicle's center of mass is critical for reliable sensor output. Lateral acceleration plays a key role in safety-critical systems such as ESC and ACC. Additionally, it is used to derive lateral velocity, an input for determining the side-slip angle, which measures the deviation between the direction a wheel is pointing and the actual direction of travel. This metric is particularly important during cornering maneuvers [39]. Similarly, longitudinal acceleration is a critical descriptor of vehicle dynamics, representing the rate of change of longitudinal velocity. This metric is influenced by various external factors, including road gradient, vehicle load, wind resistance, and body dynamics such as pitching during braking. Longitudinal acceleration, alongside lateral acceleration, is essential for calculating trajectories and ensuring precise path tracking, particularly in the context of autonomous driving systems [40].

The literature on the prediction of vehicle accelerations predominantly divides into two methodological categories: model-based approaches and neural network-based approaches. Model-based methods leverage physical or semi-empirical models to calculate outputs. For instance, Rezaeian et al. [41] developed an estimator that calculates vehicle velocity in both lateral and longitudinal directions by utilizing sensor signals such as yaw rate, roll rate, and wheel speeds. However, the high number of required sensors and the inclusion of rarely used signals, such as pitch rate, limit the practical applicability of this approach in modern vehicles. Zhao et al. [42] introduced a nonlinear observer that employs the Dugoff tire model to estimate lateral and longitudinal velocities. While effective in certain scenarios, this model performs poorly during aggressive steering and does not account for vehicle roll [43]. Building on model-based frameworks, researchers have also developed methods for side-slip angle estimation, a key variable from which lateral velocity can be derived. Li et al. [44] combined kinematic and model-based approaches, using a Kalman filter to enhance transient-stage estimation. These methods, while valuable, often rely on numerous vehicle-specific parameters, making their implementation complex and computationally demanding.

In contrast, neural network-based methods offer a more adaptable framework for acceleration prediction, with the capacity to model nonlinear relationships in the data. Recent works have focused on using neural networks to predict both lateral and longitudinal accelerations, side-slip angle, and other crucial variables for vehicle dynamics. One of the most extensive articles on using artificial neural networks for modeling the nonlinear vehi-

cle dynamic was published by Rutherford et al. [45]. In this study, a basic hyperparameter tuning method was introduced for multi-layer feed-forward networks and for NARX (Nonlinear AutoRegressive with eXogenous) networks. Their key finding is the effectiveness of NARX in making future predictions for the side-slip angle. This insight underscores the potential of neural networks, especially NARX, in generating reliable forecasts for critical vehicle states. Chindamo et al. [46] also developed a neural network-based model for side-slip angle prediction. In their work, vehicle speed, lateral and longitudinal accelerations, yaw rate, and steering wheel angle served as the network inputs. Although their model was trained and tested using simulated data, the authors acknowledged that measuring side-slip angle accurately in real-world settings is challenging. Consequently, fitting such models to experimental data can become quite complex, emphasizing a common limitation in side-slip estimation research.

Another example is Zhang et al. [47], who proposed a self-adaptive neural network structure for predicting the lateral acceleration of a tilting passenger car (in the context of train carriages). Their multi-step prediction reliably forecast the next five steps, but the drawback was the relatively low sampling rate (1 Hz) of the dataset used. Furthermore, the underlying physics of tilting train carriages differs significantly from that of conventional road vehicles, limiting the direct applicability of the model in automotive scenarios. Kong et al. [48] presented an LSTM-based [49] approach for predicting vehicle lateral velocity. They demonstrated that the LSTM network can reliably forecast future values of the output using twelve inputs, including steering wheel angle, throttle opening, engine speed, gear, wheel speeds, longitudinal acceleration, lateral acceleration, yaw rate, and longitudinal speed. While effective, this method's limitation lies in its reliance on a large number of sensors and in the substantial hardware resources required for running the LSTM-based model.

Beyond these studies, Napolitano Dell' Annunziata et al. [50] developed a neural network to predict longitudinal velocity using inputs such as lateral and longitudinal acceleration, yaw rate, and steering angle. Although the approach demonstrated significant predictive power, it did not include a forecasting functionality to predict multiple future time steps. Zou et al. [51] introduced a sophisticated model combining a MHMM (Finite Mixture of Hidden Markov Models) with LSTM and GRU (Gated Recurrent Unit) networks to account for driver-specific variations. Their model utilized MHMM to categorize driving behaviors and trained separate neural networks for distinct driver groups, thus yielding enhanced accuracy in acceleration prediction tasks. Other neural network-based studies have specifically addressed the prediction of both lateral and longitudinal accelerations. Ono et al. [52] developed an LSTM model for forecasting vehicle accelerations and compared its performance to that of a traditional ARIMA (Autoregressive Integrated Moving Average) model. Historical acceleration data served as inputs, and hyperparameter optimization

was conducted to fine-tune the model's structure. The LSTM model demonstrated superior performance, particularly in emergency scenarios where accurate acceleration prediction is vital.

Despite these advancements, neural network-based methods face challenges related to computational demands and the need for extensive datasets, which are essential for capturing the wide variety of real-world driving conditions. Nevertheless, they offer significant flexibility and the ability to adapt to varying driving conditions, making them increasingly valuable in modern vehicle dynamics research. Recent advancements—ranging from the use of NARX networks for side-slip angle forecasting [45] to LSTM/GRU-based architectures tailored to different driving behaviors [48, 51]—show that integrating traditional vehicle dynamics knowledge with machine learning can lead to robust, real-time acceleration prediction. These hybrid or integrative approaches represent a promising research direction for next-generation automotive systems, combining the interpretability of physics-based models with the adaptability of neural networks.

3.3 Methods

This part of the thesis details the design and development of the feedforward and LSTM neural networks, covering the specific LSTM neuron structure and the performance metrics used for the networks' assessment. The developed feedforward neural network was established to estimate current values of lateral acceleration, suitable even for sensor-level integration due to its extremely low resource consumption. In contrast, the LSTM network was developed to predict future values of longitudinal acceleration by leveraging past and current sensor signals, enabling proactive vehicle control applications. Important to note, the training, validation, testing, and hyperparameter tuning of both networks were performed using Python 3.9 with Keras [53]. Training was accelerated using an NVIDIA A4000 GPU (Graphics Processing Unit) with 16 GB of memory, while the hyperparameter tuning process utilized a system equipped with a 36-core Intel 8th generation CPU (Central Processing Unit) and 36 GB of memory.

3.3.1 Used Datasets

In black-box modeling approaches, such as the neural networks developed in this thesis, the underlying data is paramount, as it dictates the model's learned behavior, predictive capabilities, and ultimately, its reliability. For the feedforward network predicting lateral acceleration, the *Dataset_lateral_acc* dataset was utilized (see Section 2.5.1), as it was specifically dedicated to this problem. In contrast, for the prediction of longitudinal acceleration, the *Dataset_yaw_rate_sens* dataset (see Section 2.5.3) was used, focusing on

the *calm driver* scenario. The *calm driver* scenario was selected because the longitudinal acceleration forecasting model was developed specifically for city conditions, and among the available datasets, the calm dataset provides the most relevant representation of such driving, making it the most suitable choice for this application.

3.3.2 Designing and Developing the Feed Forward Neural Network for Lateral Acceleration Prediction

In this chapter, the development of a feedforward neural network for estimating the vehicle's lateral acceleration is presented. The model was designed to provide accurate predictions while minimizing computational requirements, making it suitable for integration into resource-limited automotive control units or even directly into the sensors. Next, the network architecture, input selection, training process, and hyperparameter tuning are described, along with the techniques applied to prevent overfitting and ensure consistent performance. Beyond direct estimation, the developed model offers significant utility in practical applications: it can be employed for plausibility checking, allowing for a comparison between its predicted lateral acceleration and values measured by physical sensors to detect potential discrepancies or sensor faults. Furthermore, it can function effectively as a virtual sensor, inferring lateral acceleration solely from the input of other existing sensors (such as steering angle of the front, wheel speeds, longitudinal acceleration), thereby providing this crucial state variable even in the absence of a dedicated physical accelerometer or offering a redundant estimation channel.

The input-output structure of the developed neural network can be seen in Figure 3.1. The inputs of the neural network are the wheel speeds for each wheel, the longitudinal acceleration, and the steering angle of the front axle. The output is the lateral acceleration. The yaw rate is excluded from the inputs because, in many practical cases—especially in simpler or low-cost vehicles—yaw rate sensors may not be available. Excluding it ensures that the model remains applicable and usable across a wider range of vehicles, especially in markets of developing countries.

The adjustable parameters of the neural network (e.g., structural properties, settings of the learning algorithm) are called hyperparameters. Since the predictive power of the network is significantly influenced by the choice of hyperparameter values, special attention was given to finding the appropriate hyperparameter settings.

The number of hidden layers and the number of neurons placed in them are the most crucial topological information that significantly impacts the prediction accuracy. If the number of neurons is too low, the power of prediction is not sufficient; on the other hand, if the number of neurons is too high, the resources needed to train and use the network increase dramatically, and the network may be overfitted. To keep the neural network as

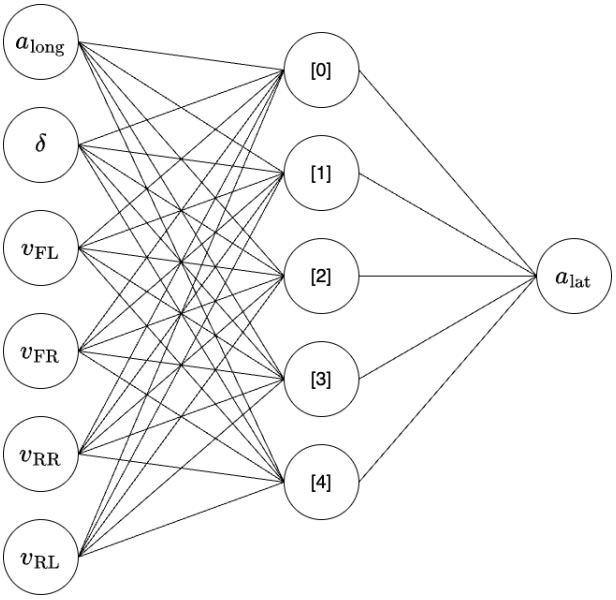

Figure 3.1. The inputs and the output of the feedforward neural network for lateral acceleration prediction. The inputs are the wheel speed for each wheel (v_{FL} , v_{FR}, v_{RR}, v_{RL}), the steering angle of the front axle (δ), the longitudinal acceleration (a_{long}). The lateral acceleration (a_{lat}) is the output of the model.

compact as possible and minimize computational resource requirements, a simpler network structure was preferred, while ensuring that the model provided sufficiently accurate results.

The transfer function of neurons and the normalization of the input values are in strong connection to each other. Normalization of the network's input can speed up the network's training and help to avoid the local minima. In the output layer, a linear transfer function was used to calculate the predicted values.

Since several studies have shown that the Adam optimizer [54] is computationally efficient, has low memory requirements, and works well with large datasets, this optimizer was chosen for use in this study. The weights of the network were initialized with random numbers following a normal distribution. The loss function minimized during training was the mean squared error.

The learning rate of the optimizer algorithm can control how quickly the neural network adapts to the problem. If the learning rate is too small, the training process may take too long or become trapped in local minima; however, if the learning rate is too high, the learning may become unstable, and the results might be sub-optimal. To assist the Adam optimizer in finding optimal solutions, the learning rate was also tuned according to best practice methods.

To avoid the overfitting of the network, different strategies were applied. On one hand, L1 regularization were applied for the sum of the weights to keep the values of the weights as small as possible to reduce the required training resources and minimize the risk of running into local minima. Additionally, dropout regularization was tested by inserting

a virtual dropout layer into the network. Finally, the early stopping technique was applied during neural network training to halt the iterative learning process at the optimal step, identified by monitoring performance on a validation set. The patience parameter for early stopping was set to six, based on practical experience.

3.3.3 Developing the Structure of the LSTM Neural Network for Forecasting Longitudinal Acceleration

This chapter details the development of an LSTM neural network specifically designed for predicting future longitudinal acceleration values in vehicles. The primary goal is to create a computationally efficient model suitable for integration into embedded systems, such as brake control ECUs. Accurate forecasting of longitudinal acceleration offers significant advantages: it can enhance the plausibility checking of sensor signals and, crucially, enable proactive vehicle stability control. By predicting the potential effects of interventions like targeted wheel braking or steering adjustments, the system can preemptively select the most effective action to maintain or restore stability. The following sections cover the fundamentals of the LSTM neuron structure employed, the overall network architecture, the optimization process used to tune the model, and the metrics used for performance evaluation.

The utilization of the Long Short-Term Memory network is often the most suitable choice for predicting time-series data. This is due to its specialized design that effectively captures and utilizes temporal dependencies over long periods, a key aspect in time-series forecasting.

The most important part of LSTM networks is the LSTM cell. The LSTM cell is a recurrent neural network unit that allows the model to remember information for extended periods. The basic structure of an LSTM cell consists of three main components: input gate (i), forget gate (f) and output gate (o). With these components, the LSTM cell combines the previous hidden state (h_{t-1}) (short-term memory of the network) with the new input (x_t) and updates the cell state (C), which represents the long-term memory of the network. The structure of the LSTM cell can be seen in Figure 3.2.

The forget gate decides which part of the cell state should be kept or forgotten for the current computation phase. It computes a weighted sum over the previous state and current input and applies a sigmoid activation function. This allows the model to forget information that is no longer relevant or useful. In our case, this means that the forget gate determines which historical information is no longer needed and/or is confusing for future yaw rate determination. The computation of the forget gate is given by Equation (3.1).

$$f_t = \sigma(W_f \cdot [h_{t-1}, x_t] + b_f) \tag{3.1}$$

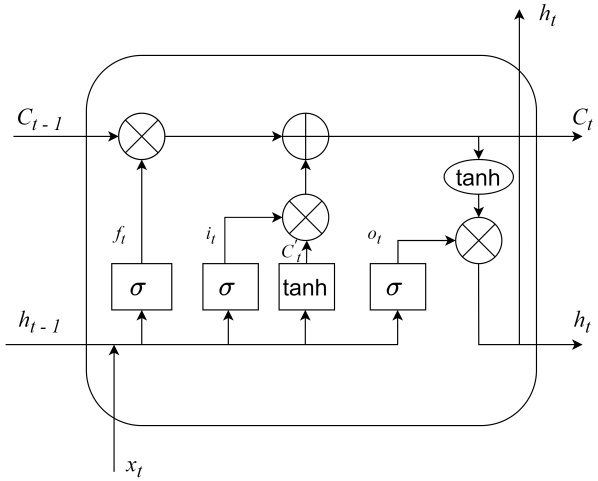

Figure 3.2. The structure of the used LSTM cell. Square notations containing σ and $tanh$ indicate sigma and tanh-activated neural networks, and circles with '+' and '$\times$' notations yield the pointwise vector addition (+) and multiplication ($\times$).

where σ denotes the sigmoid activation function, and W_f and b_f are the weight matrix and the bias used.

The input gate determines which values from the current data will be used in the current iteration and helps control what information is added to the cell state. The computation of the input gate is described by Equations (3.2) and (3.3).

$$i_t = \sigma(W_i \cdot [h_{t-1}, x_t] + b_i) \tag{3.2}$$

$$C'_t = tanh(W_C \cdot [h_{t-1}, x_t] + b_C) \tag{3.3}$$

where σ denotes the sigmoid and $tanh$ the tanh activation functions, W_i and W_C are weight matrices, and b_i and b_C are biases. The C' is the new candidate cell state. Following this, the cell memory (C) is updated at each iteration with information from the input and forget gates as follows:

$$C_t = f_t * C_{t-1} + i_t * C'_t \tag{3.4}$$

The output gate controls the new value of the hidden state (h_t), which goes back into the recurrent unit for the next time step. Thus, the output gate helps determine which parts of the short-term memory should be used at each step to produce meaningful results. The hidden states of the units in the last LSTM layer serve as the networks' output. The computation of the output gate is given by Equations (3.5) and (3.6).

$$o_t = \sigma(W_o \cdot [h_{t-1}, x_t] + b_o) \tag{3.5}$$

$$h_t = o_t * tanh(C_t) \tag{3.6}$$

where W_o and b_o are the applied weight matrix and the bias.

The general architecture of the developed LSTM-based neural network for forecasting longitudinal acceleration was developed is illustrated in Figure 3.3. The network is configured to receive both past and current values of each wheel's speeds (v_{FL} , v_{FR}, v_{RR} , v_{RL}), along with the longitudinal and lateral accelerations (a_{long}, a_{lat}), the steering angle of the front axle (δ), and the yaw rate ($\dot{\Phi}$), as its inputs. Its primary function is to output the predicted future values of the longitudinal acceleration in the time interval from $t + 1$ to $t + n_{\text{lookfuture}}$.

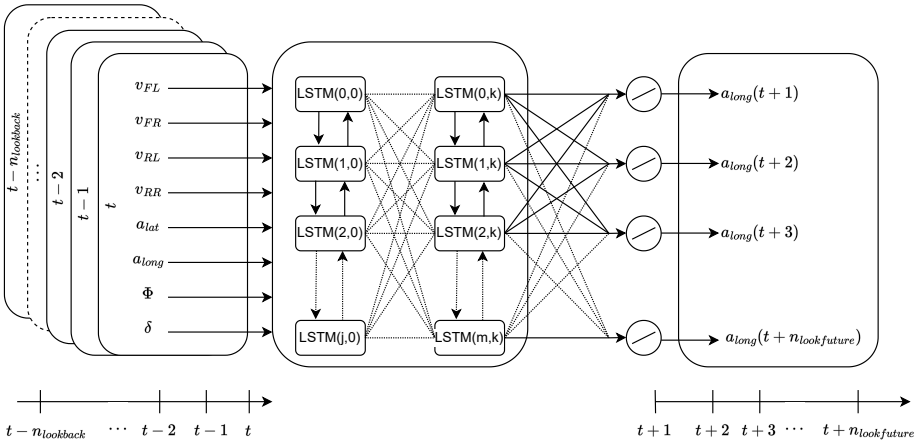

Figure 3.3. The general architecture of the LSTM network developed. In the diagram,v_{FL} , v_{FR} , v_{RR} , and v_{RL} denote the speeds of the front left, front right, rear left, and rear right wheels, respectively. a_{lat},and a_{long} represent the lateral and longitudinal accelerations. δ indicates the steering angle of the front axle, while $\dot{\Phi}$ corresponds to the vehicle's yaw rate. $n_{\text{look\_back}}$ describes the width of the discrete time window used as input for the prediction, while $n_{\text{look\_future}}$ represents the number of future timestamps for which the network predicts the longitudinal acceleration. LSTM(m,k) represents the m-th LSTM cell in the k-th hidden layer of the network.

Two key parameters are in this model: the $n_{\text{look\_back}}$ parameter, specifying the number of past discrete timestamps to be considered, and the $n_{\text{look\_future}}$ parameter, determining the number of future timestamps over which I intend to predict the value of longitudinal acceleration. If the $n_{\text{look\_back}}$ value is set too high, there is a risk that the neural network might process irrelevant information for future predictions, leading to increased resource usage. Conversely, if the $n_{\text{look\_back}}$ value is too low, it might result in insufficient data being available for accurately predicting future outcomes. If the $n_{\text{look\_future}}$ parameter is set too low, it may not fully leverage the developed method's capacity. Conversely, if it is set too high, the correlation between the input data and future predictions may become tenuous.

Hyperparameter tuning was essential to optimize the LSTM network's predictive accuracy while adhering to the strict computational constraints of the target ECU environment. Using a hybrid search strategy [55], key parameters including network topology (number

of hidden layers and neurons), activation functions (σ_g, σ_c), learning rate, and batch size were systematically evaluated. Additionally, it determined the optimal size of the time look back and look future window. This was done to ensure that the network accurately predicts future longitudinal acceleration values while keeping computational complexity low. The Adam optimizer [56] was employed with mean squared error as the loss function due to its proven efficiency. To prevent overfitting and select the optimal training iteration, regularization techniques including L1 regularization, dropout, and early stopping (patience set to 6 based on validation performance) were considered. This process identified a highly efficient configuration that balanced predictive power with minimal resource requirements, ultimately not requiring dropout or explicit L1 penalties in the final optimal model.

3.3.4 Evaluating the Predictive Capacity of the Network

For measuring the performance of the developed networks, the following performance metrics were calculated: mean squared error (MSE), root mean squared error ($RMSE$), mean absolute error (MAE) and $R\hat{}2$ score. The calculation of the error measures is given by Equations (3.7)–(3.10).

$$MSE = \frac{1}{k}\sum_{i=1}^{k}(y_i - \hat{y_i})^2 \tag{3.7}$$

$$RMSE = \sqrt{\frac{1}{k}\sum_{i=1}^{k}(y_i - \hat{y_i})^2} \tag{3.8}$$

$$MAE = \frac{1}{k}\sum_{i=1}^{k}|y_i - \hat{y_i}| \tag{3.9}$$

$$R^2 = 1 - \frac{\sum_{i=1}^{k}(y_i - \hat{y_i})^2}{\sum_{i=1}^{k}(y_i - \overline{y_i})^2} \tag{3.10}$$

where k denotes the number of samples, y is the actual measured sensor value (the target), $\overline{y}$ is the mean of these target values, and $\hat{y}$ is the value predicted by the developed neural network model. The target values (y) were determined from the recorded datasets based on the values of the examined sensor.

3.3.5 Outcome of Hyperparameter Tuning

For both lateral and longitudinal acceleration prediction, neural networks were developed and extensively optimized with the aim of achieving high predictive accuracy and low computational complexity, suitable for applications in hardware-constrained environments such as automotive control units.

3.3.5.1 Optimized Hyperparameters of the Lateral Acceleration Prediction Model

The applied parameter space during the random search phase for the feedforward network for lateral acceleration prediction is presented in Table 3.1.

Table 3.1. Hyperparameters explored during the random search phase (feedforward network for lateral acceleration prediction).The sigmoid function is defined as $sigmoid(x) = 1/(1 + e^{-x})$, and the hard sigmoid function is specified as follows: 0 if $x < -2.5$, 1 if $x > 2.5$, $0.2x + 0.5$ if $-2.5 \leq x \leq 2.5$.

Hyperparameter	**Explored Values**
Number of hidden layers	1, 2, 3, 4
Number of neurons	1, 2, 3, 4, 5, 6, 7, 8, 9, 10
Batch size	10, 50, 100, 200
Learning rate	0.0001, 0.001, 0.01
Mode of weight initialization	normal random, uniform random
Transfer function	relu, tanh, sigmoid, linear, hard sigmoid
Weight constraint	1, 2, 3, 4, 5
Dropout rate	0, 0.1, 0.2, 0.3, 0.4

Subsequently, a grid search was conducted within a reduced hyperparameter space, focusing on neurons, batch size, and dropout rate (Table 3.2). The final optimized configuration featured one hidden layer with five neurons, utilizing a hyperbolic tangent activation function, and one output neuron with a linear activation function.

Table 3.2. Reduced hyperparameter space for grid search (feedforward network for lateral acceleration). The optimal configuration is highlighted in bold.

Hyperparameter	**Explored Values**
Number of neurons	4, **5**, 6
Batch size	5, **10**, 15
Learning rate	**0.001**
Mode of weight initialization	**normal random**
Transfer function	**tanh**
Weight constraint	**2**
Dropout rate	**0**, 0.05

3.3.5.2 Optimized Hyperparameters of the Longitudinal Acceleration Forecasting Model

For longitudinal acceleration forecasting, an LSTM neural network was developed, particularly suitable for capturing temporal dependencies inherent in dynamic vehicle behavior. To comply with safety standards, predictions were limited to a maximum of 100 ms ahead (10

timesteps), comparable to deterministic models such as the single-track model [57]. Hyperparameters of the LSTM network were optimized using the same hybrid search strategy.

The optimized LSTM configuration includs a single hidden layer with five neurons, normal random weight initialization, hyperbolic tangent activation for gates, and sigmoid recurrent activation, with no dropout regularization. The hyperparameter search space and optimal values are presented in Table 3.3.

Table 3.3. Hyperparameters explored during LSTM network tuning (longitudinal acceleration). Selected optimal values are highlighted in bold. The sigmoid function is defined as $sigmoid(x) = 1/(1 + e^{-x})$, and the hard sigmoid function is specified as follows: 0 if $x < -2.5$, 1 if $x > 2.5$, $0.2x + 0.5$ if $-2.5 \leq x \leq 2.5$.

Hyperparameter	**Explored Values**
Number of hidden layers	**1**, 2
Number of LSTM neurons per layer	1, 2, 3, 4, **5**, 6, 7, 8, 9, 10
Batch size	32, 64, 128, 256, **512**, 1024, 2048
Learning rate	0.0001, **0.001**, 0.01
Mode of weight initialization	**normal random**, uniform random
LSTM activation function (σ_g)	**tanh**, sigmoid, hard sigmoid
Recurrent activation function (σ_c)	tanh, **sigmoid**, hard sigmoid
Dropout rate	**0**, 0.1, 0.2, 0.3
$n_{\text{look\_back}}$	5, **10**, 15, 20, 25

3.4 Results

This chapter presents the performance evaluation and validation of the two neural network models developed in this study. First, the feedforward network's ability to estimate current lateral acceleration is assessed by comparing its output against measured data across training, validation, and test sets, using scatter plots and standard metrics (R^2, MSE, MAE, $RMSE$). Subsequently, the LSTM network's capability to forecast future longitudinal acceleration is evaluated on the unseen test set across prediction horizons up to 100 ms. This analysis is illustrated via time-series comparisons and quantified by performance metrics for each forecast step, demonstrating the effectiveness of both models for their respective tasks.

3.4.1 Performance Evaluation of the Lateral Acceleration Prediction Neural Network

The performance of the developed neural network was evaluated by comparing the measured and predicted lateral acceleration values. The three scatter plots in Figures 3.4, 3.5 and 3.6 illustrate the relationship between measured and calculated lateral accelerations for

the training, validation, and test sets, respectively. Each graph demonstrates a strong linear correlation, as indicated by the alignment of data points along the fitted linear equation. The training set (Figure 3.4) shows the densest clustering around the linear fit, suggesting that the neural network has effectively learned the relationship between inputs and outputs. The validation set (Figure 3.5) maintains a high level of accuracy, indicating that the model generalizes well beyond the training data. The test set (Figure 3.6) also exhibits strong predictive performance, although minor deviations from the linear trend suggest slight variations in real-world conditions. Overall, these results confirm that the developed neural network reliably estimates lateral acceleration across different datasets, demonstrating its robustness and generalizability. A strong linear relationship between the measured and predicted values is evident. The high correlation coefficients $R = 0.9922$, $R = 0.9962$, and $R = 0.9912$ for training, validation, and test sets, respectively—further confirm the network's predictive performance.

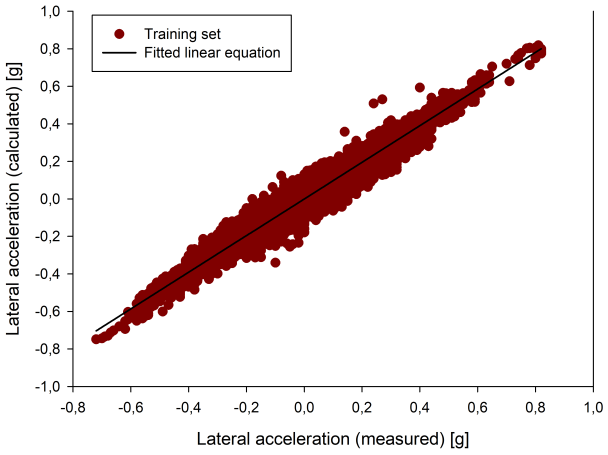

Figure 3.4. Scatter plot visualization of measured and calculated lateral accelerations for the training set.

The summary of R^2, MSE, MAE and $RMSE$ values of the network is provided in Table 3.4. The table presents the overall performance metrics of the optimized neural network for predicting lateral acceleration, evaluated across the training, validation, and test datasets. The high R^2 values (above 0.97 for all datasets) indicate a strong correlation between the predicted and measured values, confirming the model's accuracy. The MSE remains low across all datasets, suggesting minimal prediction errors, with the validation set showing slightly higher MSE, likely due to unseen data variations. The MAE is particularly low for the test set at 0.0172, demonstrating the model's precise performance even on independent data. These results confirm the robustness and reliability of the neural network, making it well-suited for accurate lateral acceleration prediction.

To further illustrate the prediction power of the developed neural network, a 20-second long comparison between the measured and calculated lateral acceleration is presented in

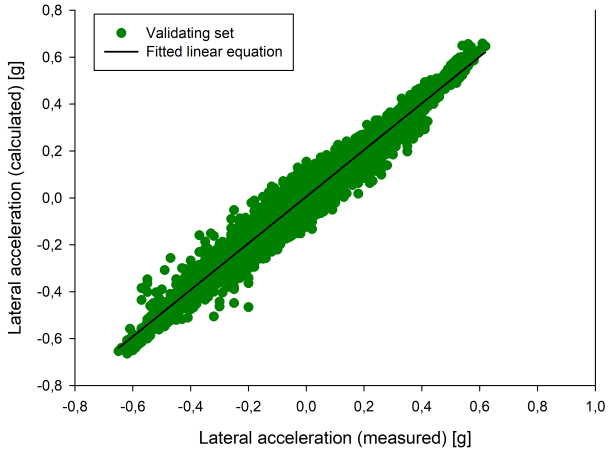

Figure 3.5. Scatter plot visualization of measured and calculated lateral accelerations for the validation set.

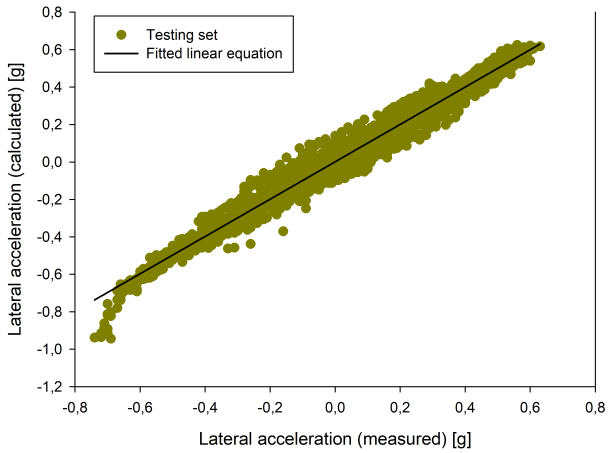

Figure 3.6. Scatter plot visualization of measured and calculated lateral accelerations for the test set.

Table 3.4. Overall metrics of the optimized neural network

Dataset	R^2	MSE [g^2]	MAE [g]	$RMSE$ [g]
Training	0.9778	5.6493E-4	0.1034	0.0238
Validation	0.9811	9.2150E-4	0.0215	0.0304
Test	0.9788	6.4984E-4	0.0172	0.0255

Figure 3.7. The two curves exhibit a strong alignment, indicating that the model accurately captures the variations in lateral acceleration over time. Minor discrepancies are noticeable, particularly in the highly dynamic regions, where sudden changes in acceleration introduce small deviations between the measured and estimated values. These differences may be attributed to sensor noise, external disturbances, or limitations in the network's ability to fully generalize to all driving conditions. Nonetheless, the MAE of the test set (0.0172 g) remains close to the sensor's resolution (0.01 g), confirming the network's reliability even in challenging conditions. Despite small variations, the overall fit remains strong, reinforcing the effectiveness of the neural network in predicting lateral acceleration with high precision for vehicle dynamics analysis and predictive applications.

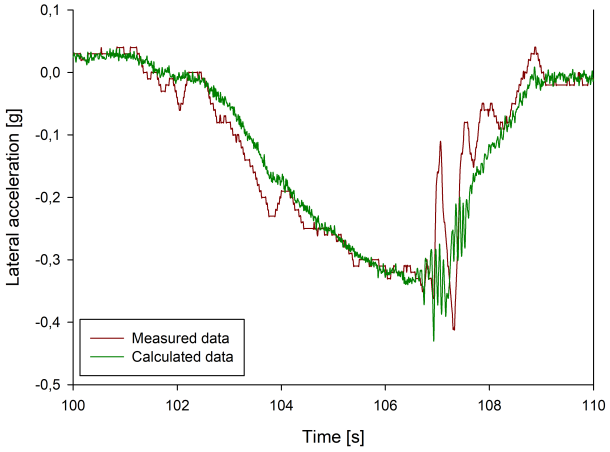

Figure 3.7. Measured vs. calculated lateral acceleration for the testing set.

3.4.2 Performance Evaluation of the Longitudinal Acceleration Forecasting Model

To evaluate the predictive capacity of the developed network, the predicted and observed longitudinal acceleration values were compared on the test set. The test set is an entirely distinct dataset and was not used for training or validating the network. Figure 3.8 shows the measured and predicted longitudinal acceleration values for 10 ms and 100 ms prediction horizons, demonstrating the high accuracy of the forecasting model as the predicted values closely follow the measured ones. The deviations in highly dynamic sections suggest that rapid acceleration changes and potential external influences, such as road conditions or aerodynamic effects, impact prediction accuracy.

To illustrate the context of the driving scenario, Figure 3.9 presents the speeds of all four wheels alongside the steering angle of the front axle. Initially, the vehicle's speed is approximately 30 $\mathrm{km/h}$, within which phases of acceleration and deceleration are observ-

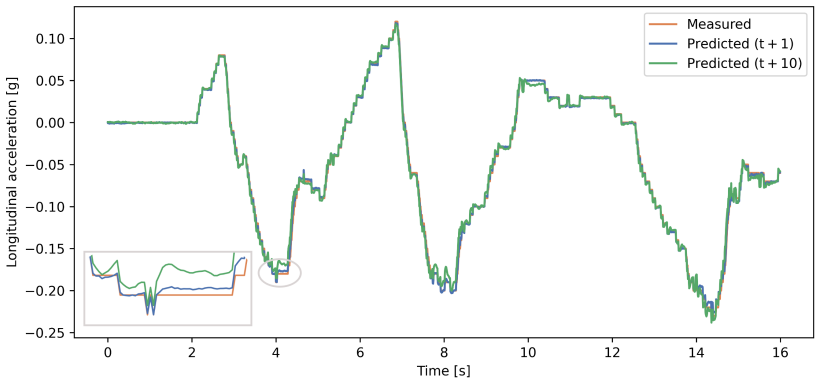

Figure 3.8. The longitudinal acceleration values forecasted for time frames of 10 ms and 100 ms into the future, denoted as $Predicted\ (t+1)$ and $Predicted\ (t+10)$ respectively, alongside the observed signal, represented as $Measured$.

able. The wheel speeds of all four wheels and the steering angle of the front axle, revealing how variations in wheel speed correlate with acceleration changes and how steering movements influence the vehicle's motion.

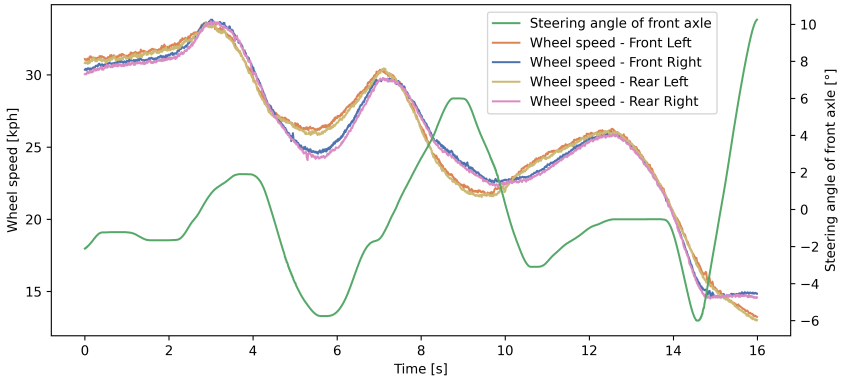

Figure 3.9. The wheel speeds and the steering angle of the front axle in the scenario shown in Figure 3.8.

Together, these figures validate the predictive model's reliability and offer an in-depth understanding of the interactions between acceleration, wheel speeds, and steering behavior in dynamic driving scenarios. The errors in the predicted longitudinal acceleration values for the entire prediction time interval, determined by the $n_{\text{look\_future}}$ parameter (from 10 ms to 100 ms in increments of 10 ms), are presented in Table 3.5. The results indicate that as the prediction horizon increases, the accuracy of the model slightly decreases, as reflected in the gradual decline of the R^2 value and the increase in MAE, MSE, and $RMSE$. Despite this trend, the predictions remain highly reliable, with an R^2 value above 0.97 even for the most extended prediction time frame, demonstrating the strong performance of the developed model.

Table 3.5. Error metrics for predicted longitudinal acceleration values over different prediction intervals ($n_{\text{look\_future}}$ from 10 ms to 100 ms).

	R^2	$MAE\,[g]$	$MSE\,[g^2]$	$RMSE\,[g]$
$a_{long}(t+1)$	0.9989	1.13E-03	3.22E-06	1.79E-03
$a_{long}(t+2)$	0.9967	1.66E-03	9.57E-06	3.09E-03
$a_{long}(t+3)$	0.9947	2.12E-03	1.52E-05	3.90E-03
$a_{long}(t+4)$	0.9923	2.65E-03	2.20E-05	4.69E-03
$a_{long}(t+5)$	0.9898	3.13E-03	2.91E-05	5.40E-03
$a_{long}(t+6)$	0.9869	3.63E-03	3.73E-05	6.11E-03
$a_{long}(t+7)$	0.9839	4.08E-03	4.59E-05	6.78E-03
$a_{long}(t+8)$	0.9805	4.52E-03	5.54E-05	7.44E-03
$a_{long}(t+9)$	0.9768	4.92E-03	6.54E-05	8.09E-03
$a_{long}(t+10)$	0.9729	5.30E-03	7.61E-05	8.73E-03

3.5 Discussion

This part of the PhD thesis details the development of neural network-based approaches for predicting both longitudinal and lateral vehicle acceleration. The accurate forecasting of these accelerations is crucial for enhancing various vehicle dynamics applications, including stability control, sensor plausibility monitoring, and predictive safety mechanisms. Both models were developed leveraging extensive experimental data for training, validation, and testing. Hyperparameter optimization for both networks was conducted using a hybrid approach. Specifically for the lateral acceleration prediction model, inputs comprised wheel speeds, the steering wheel angle, and longitudinal acceleration. The tuning process identified an optimal configuration featuring a single hidden layer with five neurons utilizing hyperbolic tangent activation functions. To improve efficiency, a weight sum constraint was applied, and the Adam optimizer algorithm with a learning rate of 0.001 was employed. Notably, the tuning results indicated that dropout regularization was unnecessary for this lateral acceleration model, contributing to a more streamlined and computationally efficient final design.

A comparison with existing studies further highlights the effectiveness of the proposed lateral acceleration model. For instance the model was developed by Jagelčák et al. estimates lateral acceleration based on vehicle speed and turning radius derived from GNSS (Global Navigation Satellite System) and INS (Inertial Navigation System) sensor data, leveraging precise trajectory measurements. It achieved an $RMSE$ of 0.187 $\mathrm{m/s^2}$ at speeds below 50 $\mathrm{km/h}$ and improved accuracy of 0.141 $\mathrm{m/s^2}$ at speeds above 50 $\mathrm{km/h}$, demonstrating better performance at higher velocities typical of highway conditions [58]. The developed model achieved an $RMSE$ of 0.2502 $\mathrm{m/s^2}$ on the test set, demonstrating performance within the same order of magnitude, while crucially relying only on sensors al-

ready present in the vehicle without needing external signal dependencies. This highlights the developed lateral acceleration model's practical advantage, offering comparable results through a more cost-effective and robust solution that leverages existing vehicle infrastructure and avoids the need for continuous GNSS/INS availability.

Unlike existing studies that employ complex architectures with a large number of neurons and multiple hidden layers, our model achieves high accuracy with a lightweight architecture, making it ideal for embedded systems. The overall predictive performance of our model is confirmed by the high correlation between measured and predicted lateral acceleration values. The network's ability to generalize well across independent test sets reinforces its applicability for plausibility monitoring and predictive safety systems. Future work will focus on extending the dataset to include different vehicle geometries and driving conditions, ensuring broader applicability and robustness of the predictive model.

For longitudinal acceleration prediction, an LSTM-based neural network model was developed, demonstrating its capability to accurately forecast acceleration values with a 0.1-second prediction horizon. The importance of longitudinal acceleration in vehicular dynamics necessitates precise predictions, and the observed results confirm the effectiveness of the model. A comparison with existing studies highlights the superior accuracy and efficiency of the proposed approach. For instance, the study by Zou et al. explored LSTM and GRU models for longitudinal acceleration forecasting, achieving MSE, $RMSE$, and MAE values of 2.36×10^{-3}, 4.86×10^{-2}, and 6.04×10^{-3}, respectively, with the GRU model slightly outperforming the LSTM variant [51]. However, their model required 128 LSTM neurons and 180 GRU neurons, whereas our model achieves significantly higher accuracy using only five LSTM neurons, demonstrating a much lower computational requirement.

Similarly, Ono et al. proposed LSTM and ARIMA-based models for predicting longitudinal acceleration, achieving an $RMSE$ of 0.0442 and a maximum absolute error of 0.2980 for moderate driving conditions. However, their model configuration consisted of 200 LSTM neurons and two hidden layers, significantly increasing computational demands [52]. In contrast, our model delivers higher accuracy while maintaining minimal resource consumption, making it well-suited for embedded applications.

The resulting LSTM network, designed for longitudinal acceleration prediction, contains 780 parameters and requires approximately 309 operations per prediction. In contrast, the feedforward network developed for lateral acceleration prediction contains significantly fewer parameters (36 parameters) and demands only 74 operations per prediction. Although the LSTM model requires more computational resources due to its recurrent architecture, it effectively captures temporal dynamics inherent to longitudinal acceleration, making it suitable for integration into electric brake systems. Conversely, the simpler feedforward architecture, with its minimal computational demand, can be integrated directly into sensor

clusters, facilitating rapid and efficient lateral acceleration prediction. Both optimized neural networks thus complement each other, providing robust and computationally efficient acceleration prediction for automotive systems.

3.6 Summary

In this part of my thesis, neural network-based predictive models were developed for both longitudinal and lateral acceleration, demonstrating their capability to enhance vehicle dynamics applications. The lateral acceleration model, designed with a lightweight architecture, effectively predicts acceleration values using wheel speeds, steering angle, and longitudinal acceleration, making it suitable for plausibility monitoring and vehicle stability control. The longitudinal acceleration model, based on an LSTM network, provides accurate short-term forecasts with minimal computational requirements, ensuring efficient real-time implementation. Both models achieve high accuracy while maintaining low complexity, allowing integration into embedded systems without reliance on vehicle-specific parameters. These findings contribute to the advancement of data-driven vehicle dynamics modeling, with potential applications in predictive control, stability enhancement, and safety-critical systems in modern and autonomous vehicles.

3.7 Related theses

Thesis 1.1

I developed and optimized a resource-efficient feedforward neural network with a single hidden layer comprising five neurons, capable of accurately predicting lateral acceleration of vehicles based on standard vehicle sensor signals. The network was trained, validated, and tested exclusively using experimental data. The model utilizes inputs: wheel speeds, the steering angle of the front axle, and longitudinal acceleration. Achieving an R^2 exceeding 0.97 and a Mean Absolute Error (MAE) for the test set of 0.0172 g, the developed model demonstrates high accuracy. Due to its minimal computational demands, it is highly suitable for direct integration into vehicle sensors or the electronic brake system, functioning as a reliable virtual sensor.

Thesis 1.2

I developed and optimized a resource-efficient Long Short-Term Memory (LSTM) neural network that predicts future longitudinal acceleration values up to 100 milliseconds ahead with high accuracy by processing the historical sensor signals. The model achieves an R^2

value above 0.97 and a MAE of 5.30×10^{-3} g, even when predicting 100 ms into the future. Despite containing only a single hidden layer with five LSTM neurons, the network significantly outperforms existing approaches that rely on much larger architectures and considerably higher computational requirements. The model's development relied exclusively on experimental data, which was used throughout the training, validation, and testing phases to ensure its reliability under real-world conditions.

Related publications

P2 János Kontos, Balázs Kránicz and Ágnes Vathy-Fogarassy (2022). Neural network-based prediction for lateral acceleration of vehicles. *2022 IEEE 2nd Conference on Information Technology and Data Science (CITDS)*, 153–158. Debrecen, Hungary. https://doi.org/10.1109/CITDS54976.2022.9914270

P3 János Kontos, László Bódis, Ágnes Vathy-Fogarassy (2024). Forecasting longitudinal acceleration in urban vehicles. In I. Maglogiannis, L. Iliadis, J. Macintyre, M. Avlonitis, & A. Papaleonidas (Eds.), *Artificial intelligence applications and innovations* (Q3), (Vol. 713, pp. 85-98). Springer. https://doi.org/10.1007/978-3-031-63219-8_7

P4 János Kontos, Ágnes Vathy-Fogarassy and Balázs Kránicz (2021). Phase plane-based approaches for event detection and plausibility check of vehicle dynamics. *2021 IEEE 25th International Conference on Intelligent Engineering Systems (INES)*, 31–36. Budapest, Hungary. https://doi.org/10.1109/INES52918.2021.9512897

Chapter 4

LSTM-Based Forecasting and Sensitivity Analysis of Yaw and Roll Rates in Automotive Systems

4.1 Introduction

Yaw rate and roll rate are two fundamental parameters in vehicle dynamics that play a crucial role in stability control and safety systems. The yaw rate represents the rotational velocity of the vehicle around its vertical axis, while the roll rate describes the angular velocity about its longitudinal axis. Both are measured in degrees per second and are critical for assessing vehicle behavior during maneuvers such as cornering, braking, and sudden directional changes.

Modern vehicles rely on ESC and ARP systems to ensure stability and prevent dangerous situations such as skidding or rollovers. The effectiveness of these systems depends on the accurate measurement and prediction of yaw and roll rates. Traditional model-based estimation methods require detailed vehicle-specific parameters and extensive calibration, making them complex and resource-intensive. In contrast, data-driven approaches, particularly neural network-based methods, offer a more flexible and adaptable solution by learning from experimental data without relying on predefined physical models.

Unlike traditional model-based approaches that rely on predefined physical parameters, the prediction of yaw rate and roll rate using artificial neural networks has received comparatively less attention. In particular, LSTM networks provide a novel approach to forecasting these critical vehicle dynamics parameters by learning directly from sensor data without requiring extensive vehicle-specific calibration. The developed LSTM-based model utilizes historical and real-time signals, such as wheel speeds, accelerations, steering angles, and

inertial measurements, to accurately predict future yaw and roll rates. While yaw rate prediction is essential for ESC to maintain directional stability, roll rate prediction is a key component of ARP systems, which detect and prevent rollover incidents. Additionally, roll rate prediction is particularly critical in off-road conditions, where vehicles operate on uneven terrain and experience extreme body roll. Unlike paved roads, off-road environments introduce dynamic and unpredictable forces that significantly affect vehicle stability. The ability to accurately forecast roll rate under such conditions enables preemptive stability control interventions, reducing rollover risks and improving safety in off-road applications. This is a unique approach, as traditional methods struggle to generalize across varying terrains and vehicle configurations. Off-road environments introduce dynamic and unpredictable forces that significantly affect vehicle stability. The ability to accurately forecast roll rate under such conditions enables preemptive stability control interventions, reducing rollover risks and improving safety in off-road applications. Off-road roll rate prediction using physical or semi-empirical methods is extremely challenging due to the complexity of terrain interactions and varying vehicle dynamics. My method is capable not only of predicting the actual roll rate in off-road conditions but also of providing future predictions, allowing for proactive stability adjustments and enhanced vehicle safety.

A critical aspect of deploying such predictive models in real-world applications is understanding their sensitivity to various influencing factors. Sensitivity analysis provides insights into how changes in vehicle conditions, such as weight distribution, tire pressure, and passenger load, affect prediction accuracy. Studies have shown that while tire pressure variations have a minor effect, changes in vehicle weight distribution significantly impact both yaw and roll rate predictions. Ensuring the robustness of these models across different driving scenarios and vehicle configurations is essential for their reliability in safety-critical applications.

This part of the PhD study focused on the development of LSTM-based neural networks for predicting yaw rate and roll rate, introducing a novel data-driven approach in vehicle dynamics. Unlike traditional model-based methods, the proposed networks utilize past and current sensor signals, including wheel speeds, accelerations, and steering angles, to enhance predictive accuracy. A literature review examines existing yaw rate and roll rate prediction methodologies, though no prior research explores the optimal data quantity or sensitivity analysis for these variables. The network design, hyperparameter tuning, and dataset utilization are detailed, followed by an evaluation of predictive performance. The impact of different hyperparameter configurations on yaw rate and roll rate predictions is assessed to ensure optimal efficiency and accuracy. Additionally, the prediction results are compared with both real-world measurements and other available methods from the literature, demonstrating the superiority of the proposed approach. The study also identifies the minimum dataset size required for effective yaw rate and roll rate forecasting, balancing

computational efficiency with predictive power. Lastly, a sensitivity analysis evaluates how variations in tire pressure, passenger distribution, and vehicle architecture influence yaw rate predictions, ensuring the model's robustness for practical automotive applications.

4.2 Theoretical background

This chapter reviews the key literature on predicting vehicle dynamic parameters, with a focus on yaw rate, roll rate, and the use of ANN in safety-critical automotive applications. Yaw rate is a crucial vehicle dynamic parameter, influenced by road-tire friction [59]. It is measured along with longitudinal and lateral acceleration using an IMU near the center of mass of the vehicle [60]. Proper monitoring and verification of the IMU's mounting position are essential to ensure accurate data acquisition [61]. Research shows a latency between steering input and resultant yaw rate, ranging from 50 $\mathrm{ms}$to 200 ms, depending on maneuvering and road conditions [62].

Yaw rate prediction plays a crucial role in autonomous driving by enabling precise vehicle state estimation, which is essential for trajectory planning and stability control. Accurate forecasting of yaw rate allows autonomous systems to make real-time adjustments in steering and braking, enhancing safety during dynamic maneuvers. Furthermore, yaw rate prediction is vital in trajectory prediction for autonomous driving, as it helps in anticipating the vehicle's future position and orientation [63]. This capability is particularly important for collision avoidance, lane-keeping, and path-following algorithms, ensuring smooth and efficient navigation even in complex driving environments. The integration of artificial neural networks in yaw rate estimation improves the adaptability of self-driving vehicles to changing road conditions, contributing to more reliable and robust autonomous navigation [64].

In vehicle dynamics, the roll rate, or roll angular velocity, is a crucial metric that quantifies the angular velocity of a vehicle's body around its longitudinal axis during maneuvers like cornering, lane changes, or uneven terrain navigation, reflecting the vehicle's roll stiffness and suspension system effectiveness in mitigating body roll [65]. While numerous articles focus on predicting the value of roll angle, there is a paucity of research addressing the prediction of roll rate. It is noteworthy that roll rate can be determined by differentiating the roll angle with respect to time. However, employing direct sensors to measure rotational rates can provide more accurate and reliable roll rate data. Conversely, calculating the roll rate from roll angle measurements may introduce inaccuracies, especially when faced with noisy data or low sampling frequencies.

In the literature, additional GPS-related (Global Positioning System) sensors are often integrated alongside the internal sensor cluster to enhance measurement accuracy of roll angle and roll rate [66, 67]. However, these high-precision systems typically incur higher

costs compared to other types of sensors. Furthermore, using lower-quality sensors can result in measurement errors, consequently affecting the accuracy of the vehicle's perceived attitude.

Vehicle state estimation, including sideslip angle, vehicle velocity, roll, and yaw rate, is extensively studied, with significant literature and reviews [68, 69, 70]. Roll and pitch rates, like yaw rate, relate to different dimensions of vehicle movement, such as tilting during turns and elevation changes during acceleration and braking. There is substantial research on predicting these dynamic attributes [71, 72]. ANNs are widely used to regulate yaw rates, primarily as control algorithms rather than estimation methods [73, 74, 75].

The literature on yaw rate prediction can be categorized into three clusters: data-driven estimators like ANNs, dynamic model-based solutions using filtering techniques or observers, and computer vision-based approaches. ANNs are adaptable and can learn from data without precise mathematical models, making them ideal for dynamic or uncertain environments. Kalman filters, however, require accurate system models and well-defined noise statistics but can handle non-linear behaviors with adaptive versions [76].

Extensive research explores ANN-based strategies in automotive safety mechanisms [77, 78]. The yaw rate is critical for various ANN-oriented models for estimating vehicle state [79, 80]. The early significant contributions of Karri and Butler highlight advances in input parameter selection, network architecture, and optimization for ANN-based yaw angle prediction [81]. Hermansdorfer et al. developed a comprehensive ANN framework for simulating vehicle dynamics, using inputs, like velocities, yaw rate, acceleration, steering angle, torque, and braking pressure. Despite its comprehensiveness, it does not predict future states [82].

González et al. [83] devised a deep learning-based approach for predicting vehicle roll and sideslip angles. Their method employs inputs such as longitudinal and lateral acceleration, roll rate, yaw rate, steering angle, and longitudinal speed. The output from their network, which consists of five hidden layers with a total of 450 neurons, predicts the vehicle's roll and sideslip angles. The architecture of their network necessitates substantial hardware and software resources. Boada et al. [84] utilized data primarily from on-board vehicle sensors to support their methodology. The inputs to their approach include lateral and longitudinal accelerations, as well as yaw and roll rates. These inputs are processed through a neural network that consists of a single hidden layer with 15 neurons tasked with estimating a "pseudo-roll angle." This estimated angle is subsequently employed in an H1 filtering-based observer. This observer is designed to determine the vehicle's actual roll angle, accounting for both uncertainties and external disturbances in its calculations.

Dynamic model-based solutions face limitations due to the need for extensive vehicle-specific parameters. Novara et al. introduced a Set Membership filter design for yaw rate prediction, notable for its direct data identification without an additional model [85].

Sum et al. proposed an estimation framework for autonomous vehicles with an innovative tire model and adaptive estimation using a square-root cubature Kalman Filter, validated through simulation [86]. Moussa et al. explored an EKF for estimating lateral velocity and yaw rate, incorporating a nonlinear tire model for improved precision [87]. Baffet et al. presented a two-block EKF (Extended Kalman Filter) approach for estimating dynamic parameters using standard sensors [88]. Zhang et al. developed an EH∞KF (Extended H-infinity Kalman Filter) for vehicle dynamics estimation, validated through simulation [89]. Shi et al. proposed a linear Kalman filter using magnetic angular rate and gravity sensors to mitigate magnetic disturbances [90].

Ding and Massel [91] introduced one of the seminal works in this field, focusing on the estimation of vehicle roll angle. This estimation process is facilitated by a state space model, which integrates various sensor inputs, including lateral acceleration, yaw rate, and vehicle velocity, along with fundamental vehicle dynamics parameters such as mass, gravity, and suspension properties. To enhance the accuracy of these estimations and assess estimation errors, an observer design was employed. This framework also offers a confidence interval, serving as an indicator of the reliability associated with the estimated roll angles.

Zhao and Liu [92] pioneered a method for estimating roll angle specifically tailored for four-wheel independent drive electric vehicles. Their approach utilizes a comprehensive set of inputs, including wheel angular velocity, longitudinal and lateral acceleration, yaw rate, roll rate, wheel steering angles, and wheel torques. They developed a direct observer to estimate the vehicle's roll angle, subsequently leveraging the established relationship associated with roll angle. Yun et al. [93] introduced an estimation-based approach for predicting roll rate by leveraging the vehicle's longitudinal velocity and yaw rate through transfer function estimation. The model parameters were determined using simulation data; however, its predictive capability was inadequately demonstrated when applied to experimental data. A notable limitation of this method lies in its reliance on a restricted range of driving scenarios during both parameter identification and testing phases. Nam et al. [94] devised a methodology for estimating roll and sideslip angles, employing a combination of RLS (Recursive Least Squares) and Kalman Filter techniques. The primary input for their methods is the lateral tire forces obtained using multi-sensing hub units affixed to each tire. Additional inputs include lateral acceleration, vehicle longitudinal velocity, roll rate, and yaw rate.

Interest in computer vision for yaw rate detection is increasing. This technique can forecast the yaw rate without additional sensors, using existing vehicle cameras. However, it does not inherently predict future yaw rates. Huang et al. introduced the yaw angle estimation network, a deep learning framework using a monocular camera for yaw angle estimation, which requires more hardware resources than typical electronic brake systems [95]. Cunliang et al. developed an adaptive neural network control based on YOLOv5

(You Only Look Once) for steering angle prediction, trained on real road images. Although showing a strong correlation between steering angle and yaw, it requires high hardware resources [96].

Based on the literature review, it can be stated that only roll rate estimation models are available, which can predict the current value of roll rate without the capability for future prediction. Additionally, the existing literature lacks studies that specifically address the determining the optimal volume of training data and sensitivity analysis of dynamic vehicle models, particularly in relation to yaw rate prediction methods. This gap underscores the novelty and significance of this part of my PhD thesis.

4.3 Used Datasets

The development and evaluation of the LSTM-based neural network models for yaw rate and roll rate prediction required multiple datasets, each serving a distinct purpose. The selection of datasets was based on specific objectives, including model training, determining the optimal amount of training data, and conducting sensitivity analysis. This chapter provides an overview of the datasets used and their respective roles in different phases of model development.

For the initial training of the yaw rate prediction model, the *Dataset_yaw_rate dataset* (see Section 2.5.2) was used. However, the results obtained using this dataset are not included in this part of the PhD work, as it primarily served as an early-stage reference for model experimentation. Instead, all reported findings are based on training conducted with the extended *Dataset_yaw_rate_ext* dataset (see Section 2.5.3 dataset), which was specifically curated to enhance model accuracy and generalization. This dataset provided a more refined and diverse set of driving conditions, ensuring that the final model was trained on a dataset representative of real-world scenarios. This dataset is also called as *baseline dataset*.

For the recognition of the optimal amount of training data *Dataset_yaw_rate_ext* dataset was also utilized. By systematically analyzing how the model performed when trained on datasets of varying sizes, I was able to determine the minimum required data volume needed for effective yaw rate prediction for non-safety relevant usecases.

For the sensitivity analysis, which examined how external factors such as tire pressure, passenger distribution, and vehicle architecture influenced model performance, a separate dataset, *Dataset_yaw_rate_sens* (see Section 2.5.4), was used. This dataset was specifically collected to include variations in vehicle conditions, allowing for a comprehensive evaluation of how these factors affect yaw rate predictions.

The roll rate prediction model was exclusively trained on off-road driving conditions using the *Dataset_roll_rate* (see Section 2.5.5) dataset. Unlike yaw rate prediction, which involved data from a mix of driving scenarios, the roll rate model was designed specifically

for off-road applications, where vehicle stability is highly sensitive to rough terrain and uneven surfaces. This dataset provided high-resolution roll rate measurements collected under diverse off-road conditions, capturing the dynamic and often unpredictable forces acting on the vehicle.

By using only off-road data for training, the roll rate model was optimized for challenging environments where traditional estimation methods struggle. This focus on off-road conditions ensures that the model is highly specialized for applications such as active rollover prevention, stability control, and vehicle safety systems operating in extreme terrains.

4.4 Forecasting Yaw Rate with LSTM Neural Network

This chapter focuses on developing an LSTM neural network to accurately forecast vehicle yaw rate, utilizing mandatory sensor signals common across various vehicle platforms. The subsequent sections detail the model's architecture, the hyperparameter tuning process optimized for deployment on resource-constrained ECUs, and an evaluation of its performance, confirming its suitability for safety-critical applications.

4.4.1 Designing the Structure of Yaw Rate Forecasting LSTM Model

The main objective of this part of my PhD thesis is to develop a neural network model capable of confidently forecasting future values of the vehicle's yaw rate. The available signals inside the vehicle are highly dependent on the producer of the vehicle. The ECUs built into the vehicle can have various architectures for communication, influencing the availability and accessibility of different sensor signals. Due to these variations, I focused on the selection of mandatory signals required for the brake system, ensuring that the model remains applicable across different vehicle platforms. The proposed neural network utilizes past and current data on the longitudinal and lateral acceleration (a_{long}, a_{lat}), yaw rate ($\dot{\Phi}$), steering angle for the front axis (δ), and wheel speeds (v) as its inputs.

Given its ability to effectively capture and leverage long-term temporal dependencies, which is crucial for time-series prediction, the long short-term memory network emerged as the preferred choice. This decision was further supported by the need to account for the dynamics and inertia inherent in vehicular motion, leading me to pursue the development of an LSTM-based network. A detailed description of the LSTM neuron used can be found in Section 3.3.3.

To develop an optimal neural network with low computational complexity and high accuracy, I undertook an extensive hyperparameter tuning process. The hyperparameters of the network were tuned using the hybrid search method described in [55], considering the fact that the model would be integrated into an electric control unit with limited hardware resources. The prediction interval for the LSTM network was set at 20 following timestamps, allowing the network to predict yaw rate values up to 200 ms ahead, according to the literature and safety considerations [62, 77]. Parameter optimization used the Adam optimizer [97], monitoring the MSE as the loss function. Early stopping was applied with a patience value of 5 to prevent overfitting. The final model consists of only one hidden layer with 5 LSTM units and does not contain dropout or L1 regularization. The input to the network comprises the past and current values of the input variables, while the output predicts the future values of the yaw rate. The structure of the developed model can be seen in Figure 4.1. This network configuration, along with its parameters and hyperparameters, will be referred to as the base LSTM network structure.

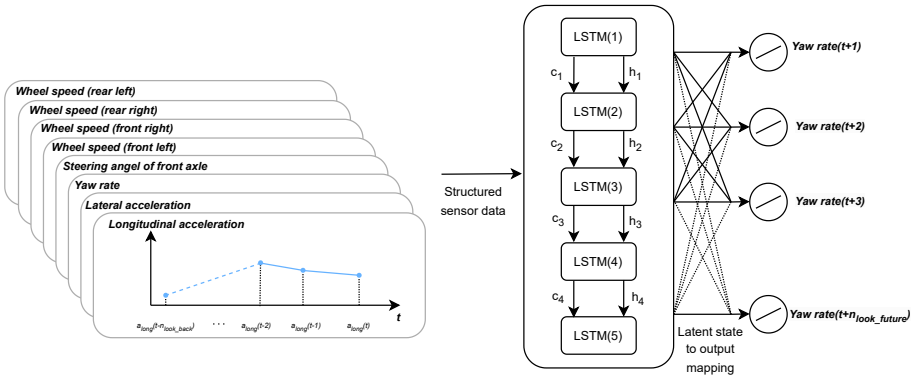

Figure 4.1. The structure of the developed neural network. Structured sensor data, including wheel speeds, steering angle, yaw rate, and accelerations, serve as inputs. The LSTM layers process these inputs over time, maintaining the cell state (c_t) and hidden state (h_t) to capture temporal dependencies. The final latent representations are mapped to the output layer, predicting future yaw rate values at multiple time steps.

4.4.2 Hyperparameter Tuning For the Yaw Rate Prediction Model

The details of the hyperparameter tuning process, including the explored parameter space and the optimal values selected for training the yaw rate prediction model, are summarized in Table 4.1. This table presents the key hyperparameters that were systematically adjusted to achieve the best balance between predictive accuracy, computational efficiency, and model generalization. The tuning process involved iterative experimentation with different configurations, evaluating their impact on model performance using validation data,

and selecting the most effective settings to enhance stability and reliability in yaw rate forecasting. This optimized network configuration, along with its tuned parameters and hyperparameters, will be referred to as the *base LSTM network structure* throughout the remainder of the thesis.

Table 4.1. The parameter space used for hyperparameter tuning. The bold values refer to the results of the process. The sigmoid function is defined as $sigmoid(x) = 1/(1 + e^{-x})$, and the hard sigmoid function is specified as follows: 0 if $x < -2.5$, 1 if $x > 2.5$, $0.2x + 0.5$ if $-2.5 \leq x \leq 2.5$.

Hyperparameter	**Values**
Number of hidden layers	**1**, 2, 3, 4
Number of LSTM neurons per layer	1, 2, 3, 4, **5**, 6, 7, 8, 9, 10
Batch size	32, 64, 128, 256, **512**, 1024, 2048
Learning rate	0.0001, **0.001**, 0.01
Mode of weight initialization	**normal random**, uniform random
LSTM activation function	**tanh**, sigmoid, hard sigmoid
Recurrent activation function	tanh, **sigmoid**, hard sigmoid
Dropout rate	**0**, 0.1, 0.2, 0.3
$n_{\text{look\_back}}$	10, 20 , **30**, 40, 50

4.4.3 Results for Yaw Rate Forecasting

Training and testing the developed LSTM network structure using the *baseline dataset* was crucial in establishing a performance benchmark, allowing us to assess how well the model performed under standard conditions.

Figure 4.2 illustrates the steering angle of the front axle, as well as the lateral and longitudinal acceleration, during a 40 s varied slalom maneuver selected from the test set. The vehicle, starting at an average speed of 40 $\mathrm{km/h}$, eventually reached a standstill. The comparison between the forecast and measured yaw rate values over this interval is shown in Figure 4.3, highlighting the accuracy of the proposed LSTM model's 0.2 s forecast. The mathematical relationship between these signals depends on the vehicle model used. Simplified models, such as the bicycle model, rely on only a few parameters, making them computationally efficient but less precise for complex dynamics. More advanced models, such as the four-wheel vehicle model, incorporate slip angles and load transfer, improving the accuracy at the cost of increased complexity. Unlike these physics-based approaches, our LSTM model learns the underlying relationships directly from the data, capturing both linear and nonlinear dependencies without requiring explicit equations. Neural network models excel in this regard: they achieve highly precise predictions without needing vehicle-dependent parameters as input, making them ideal for real-time vehicle control applications.

Table 4.2 presents the detailed performance metrics of the developed network across the three different driving scenarios and the combined one. Optimal fits were observed for both

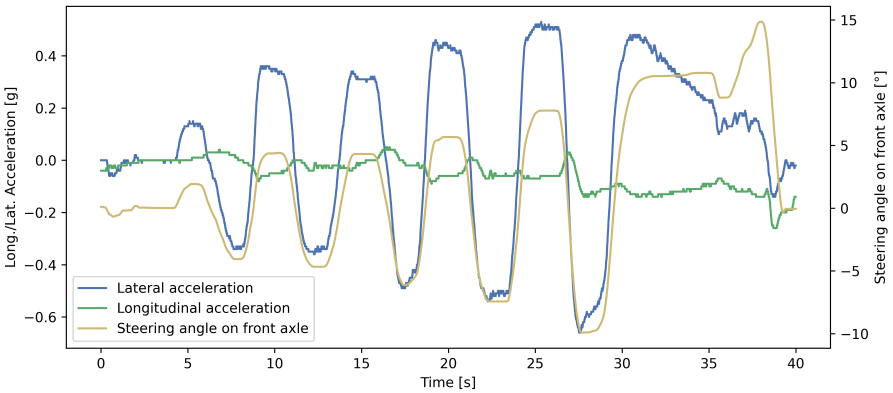

Figure 4.2. The longitudinal and lateral acceleration, along with the steering angle of the front axle, for a 40-s-long period selected from the test dataset.

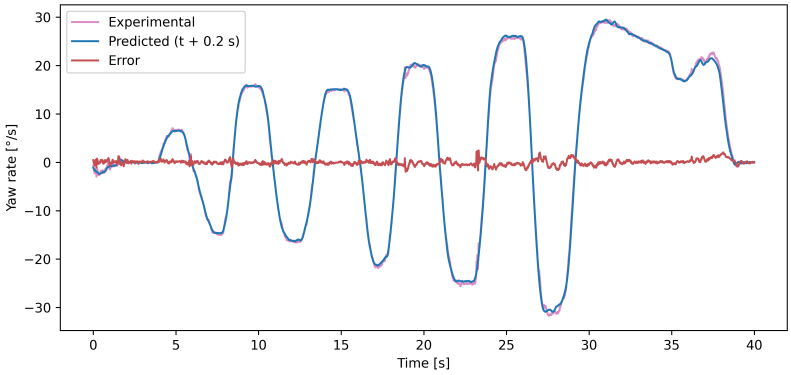

Figure 4.3. Forecasted and observed yaw rate values for the period presented in Figure 4.2. The error was calculated as the signed difference between the experimentally derived and computationally predicted yaw rates.

the training and validation sets, as expected, demonstrating their homogeneity. In the test dataset, the R^2 values were high for all driving scenarios, with the best results seen in the *calm driver* scenario ($R^2 = 0.9989$), and the lowest value ($R^2 = 0.9938$) observed in the *city driving* scenario. Regarding the model's mean absolute error, the values range between 0.268 $^\circ/\mathrm{s}$ and 0.375 $^\circ/\mathrm{s}$ for the test set, but when considering the training, validation, and test errors together, the MAE value does not exceed 0.470 $^\circ/\mathrm{s}$ in any scenario. Based on the calculated metrics for the test set, it can be concluded that the model's output is suitable for use in safety-critical functionality, as its error consistently remained within the mandatory threshold of 3 $^\circ/\mathrm{s}$ MAE, which is required to meet the safety standard (ASIL B – Automotive Safety Integrity Level) [57]. This ASIL B classification corresponds to the same safety level that is mandated for a non-redundant sensor, thus ensuring that the model's output is compliant with the industry's safety requirements for such configurations.

Table 4.2. Error metrics of the proposed model on the *baseline* dataset.

	$combined$	$calm$	$aggressive$	$city$
		Training set		
Length [min]	328.4	139.2	112.0	77.2
R^2 [1]	0.9980	0.9989	0.9977	0.9955
MAE [$^\circ/\mathrm{s}$]	0.338	0.262	0.470	0.285
MSE [$(^\circ/\mathrm{s})^2$]	0.294	0.125	0.598	0.155
$RMSE$ [$^\circ/\mathrm{s}$]	0.542	0.354	0.773	0.394
		Validating set		
Length [min]	36.6	15.5	12.5	8.6
R^2 [1]	0.9980	0.9989	0.9977	0.9955
MAE [$^\circ/\mathrm{s}$]	0.338	0.262	0.469	0.286
MSE [$(^\circ/\mathrm{s})^2$]	0.291	0.126	0.590	0.157
$RMSE$ [$^\circ/\mathrm{s}$]	0.540	0.354	0.768	0.397
		Test set		
Length [min]	92.1	39.0	31.6	21.5
R^2 [1]	0.9984	0.9989	0.9985	0.9938
MAE [$^\circ/\mathrm{s}$]	0.316	0.268	0.375	0.316
MSE [$(^\circ/\mathrm{s})^2$]	0.210	0.134	0.288	0.231
$RMSE$ [$^\circ/\mathrm{s}$]	0.458	0.366	0.537	0.481

4.5 Determining Optimal Volume of Training Data and Assessing Sensitivity of the Yaw Rate Forecasting Model

This section outlines the methodology used to assess the practical applicability of the proposed yaw rate forecasting model and presents the findings from these evaluations. The first part focuses on determining the necessary volume of data required to effectively train the neural network model. Following this, sensitivity analyses were conducted to understand how factors like tire pressure and passenger load influence the model's performance. Lastly, this section investigated the model's ability to generalize its predictions when applied to entirely different vehicle types than the one it was initially trained on.

4.5.1 Methodology of Analyses for Yaw Rate Forecasting Model

The practical applicability of the neural network model was assessed from four key perspectives. First, the necessary data volume for effective training was determined. Next, the impact of the tire pressure and the number of passengers on the model performance was evaluated. Lastly, the applicability of the model to entirely different vehicles was explored.

4.5.1.1 Methodology to Determine the Required Amount of Data to Train the Proposed Model

During the development process, a critical question emerged regarding how much data users need to effectively train the model on their own data. To determine the required data volume for the training of a well-performing model, the following method was employed. A random starting point was selected ten times within each driving scenario subset from the *baseline dataset*. Starting from each starting point, datasets of various durations (1, 2, 3, 5, 10, 15, 20, 25, ... 60 min) were extracted. These selected datasets were then used to train the *base LSTM network structure*. During the training processes, 10% of the training chunks was randomly selected for validation purposes.

4.5.1.2 Methodology of Sensitivity Analyses

To evaluate the yaw rate prediction model's robustness and generalization, a sensitivity analysis was conducted using additional data collected under conditions not present during training. This involved testing the base LSTM model's performance with markedly reduced tire pressure (1.5 bar on one wheel), simulated passenger loads using sandbags, and application to different vehicle types—including a smaller hatchback and larger SUVs with

varying drivetrains. The goal was to systematically assess how these variations in tire pressure, weight distribution, and vehicle characteristics affect the model's prediction accuracy relative to its performance on the original training data.

4.5.2 Determination of the Optimal Volume of Data to Train the Proposed Model for Yaw Rate Forecasting

One possible step in implementing the proposed model involves adapting the LSTM structure to a specific vehicle type by training it with data collected from that vehicle. Therefore, an important question arises: What kind and amount of data need to be collected from the target vehicle to properly train the neural model, and how does the size of the training dataset affect the performance of the proposed LSTM network? To answer the questions the *baseline* dataset was used as a training dataset and the research method introduced in Subsection 4.5.1.1 was applied.

The results are presented in Figure 4.4, showing the relationship between the predictive capability of the neural network and the volume of data used for training the network for different driving scenarios. The figures present the mean squared errors of the network on the test datasets. As shown, the best performance is achieved by using a dataset containing various driving styles (*combined dataset*); however, maneuvers characterized by high dynamics, such as those of an *aggressive driver*, should be prioritized during data collection. In general, satisfactory results can be achieved by collecting 10-15 minutes of highly diverse driving data, beyond which further improvements become difficult to attain. For comfort-related functions, this amount of data is sufficient to train an effective and practical neural network for vehicle dynamics predictions. However, in the context of safety-critical systems, the prevailing strategy is to utilize the maximum amount of data possible to ensure the highest level of accuracy and reliability.

4.5.3 Sensitivity Analyses for the Yaw Rate Forecasting Model

To facilitate model comparison and evaluation, several additional error metrics are introduced. In each case, the model performance is compared to that of the LSTM network trained on the *baseline data* (see Section 4.3). The analysis focuses on deviations in the following metrics: R^2, MAE, MSE, and $RMSE$. These deviations are defined by Equations (4.1)–(4.4).

$$\Delta R^2_{d,g} = R^2_{d,g} - R^2_{d,\text{baseline}} \tag{4.1}$$

$$\Delta MAE_{d,g} = MAE_{d,g} - MAE_{d,\text{baseline}} \tag{4.2}$$

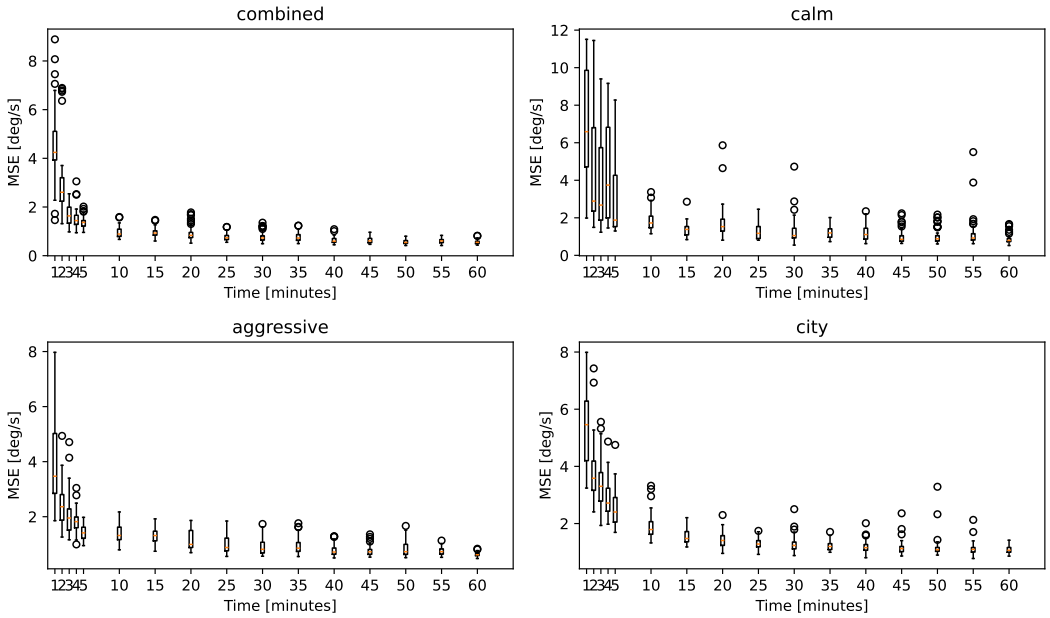

Figure 4.4. Box plot representation showing the relationship between the amount of data used for training the neural network and the accuracy of the fine-tuned network in different driving scenarios. Whiskers stretch from the edges of the box to the most distant data points that fall within 1.5 times the IQR (Inter-quartile Range).

$$\Delta MSE_{d,g} = MSE_{d,g} - MSE_{d,\text{baseline}} \tag{4.3}$$

$$\Delta RMSE_{d,g} = RMSE_{d,g} - RMSE_{d,\text{baseline}} \tag{4.4}$$

where d denotes the distinct driving scenarios, including *aggressive*, *calm*, *city*, and *combined* driving scenarios, and g corresponds to the particular analysis condition, such as variations in tire pressure, passenger load, or vehicle type.

During the sensitivity analyses, several evaluations were conducted. Table 4.3 presents the results concerning the impact of reduced tire pressure. The most pronounced effect was observed under the aggressive driving condition. From the perspective of tire dynamics, the front wheels are most affected due to their function as the steered axle. Additionally, the weight distribution in SUV-type vehicles typically favors the front axle, further contributing to this effect. Regarding the MAE, the maximum deviation remains below 0.5 $^\circ/$s, with the largest observed change (ΔMAE) being 0.4179 for the case of reduced pressure in the front left tire.

In Table 4.4, the impact of the number and positions of passengers on the prediction of the vehicle's yaw rate is presented for various passenger configurations (with the driver's seat always occupied). In most cases, the greatest effects were observed in the *aggressive driving* scenario, while the lowest deviation in the error metrics occurred in the *calm driving*

Table 4.3. The impact of reduced tire pressure (1.5 bar) on the model performance relative to the performance of the *base model* (2.3 bar on each tire).

	$combined$	$calm$	$aggressive$	$city$
		Reduced p_{FL}		
Length [min]	50.0	10.2	9.3	30.5
ΔR^2 [1]	−0.0042	0.0002	−0.0054	0.0005
ΔMAE [°/s]	0.1231	−0.0064	0.4179	−0.0104
ΔMSE [(°/s)^2]	0.3946	−0.0244	2.0328	−0.0648
$\Delta RMSE$ [°/s]	0.3195	−0.0350	0.9868	−0.0729
		Reduced p_{FR}		
Length [min]	50.9	10.7	10.1	30.1
ΔR^2 [1]	−0.0013	0.0004	−0.0020	−0.0011
ΔMAE [°/s]	0.0559	0.0063	0.3238	−0.0113
ΔMSE [(°/s)^2]	0.1851	−0.0030	1.1919	−0.0829
$\Delta RMSE$ [°/s]	0.1705	−0.0042	0.6799	−0.0957
		Reduced p_{RL}		
Length [min]	50.6	10.4	10.0	30.2
ΔR^2 [1]	−0.0003	0.0004	−0.0002	−0.0005
ΔMAE [°/s]	0.0614	0.0257	0.1532	0.0394
ΔMSE [(°/s)^2]	0.1003	−0.0016	0.5172	−0.0305
$\Delta RMSE$ [°/s]	0.0989	−0.0021	0.3607	−0.0328
		Reduced p_{RR}		
Length [min]	55.0	11.1	11.0	32.9
ΔR^2 [1]	0.0001	0.0005	0.0005	0.0003
ΔMAE [°/s]	0.0431	−0.0128	0.1432	0.0257
ΔMSE [(°/s)^2]	0.0362	−0.0311	0.2596	−0.0348
$\Delta RMSE$ [°/s]	0.0380	−0.0452	0.2034	−0.0377

scenario. The smallest changes compared to the original metrics were seen when the driver and passenger were neither on the same side nor in the same row, followed by configurations where they were either on the same side or in the same row. The largest deviation was observed when all seats, except the middle rear one, were unoccupied. Even in that case, the maximum MAE remained below 0.5 $^\circ/\mathrm{s}$ (0.4215 $^\circ/\mathrm{s}$). In other scenarios, when only one additional person was seated in the car, the maximum MAE deviation did not exceed 0.13 $^\circ/\mathrm{s}$.

Table 4.4. The impact of number and positions of passengers on the model performance relative to the performance of the *base model*.

	combined	*calm*	*aggressive*	*city*
Front passenger seat occupied				
Length [min]	51.4	10.3	9.9	31.2
ΔR^2 [1]	−0.0015	−0.0007	−0.0003	−0.0033
ΔMAE [$^\circ/\mathrm{s}$]	0.1091	0.0258	0.1173	0.1321
ΔMSE [$(^\circ/\mathrm{s})^2$]	0.1368	0.1203	0.3126	0.0674
$\Delta RMSE$ [$^\circ/\mathrm{s}$]	0.1308	0.1382	0.2383	0.0656
Rear passenger seat (passenger side) occupied				
Length [min]	50.9	10.7	10.1	30.1
ΔR^2 [1]	−0.0006	0.0003	0.0003	−0.0021
ΔMAE [$^\circ/\mathrm{s}$]	0.0516	0.0142	0.1027	0.0448
ΔMSE [$(^\circ/\mathrm{s})^2$]	0.1120	−0.0151	0.2418	0.0928
$\Delta RMSE$ [$^\circ/\mathrm{s}$]	0.1093	−0.0212	0.1912	0.0884
Rear passenger seat (driver side) occupied				
Length [min]	50.2	10.7	10.4	29.1
ΔR^2 [1]	−0.0011	0.0004	−0.0008	−0.0008
ΔMAE [$^\circ/\mathrm{s}$]	0.0572	0.0177	0.1253	0.0437
ΔMSE [$(^\circ/\mathrm{s})^2$]	0.1532	−0.0079	0.5165	0.0611
$\Delta RMSE$ [$^\circ/\mathrm{s}$]	0.1445	−0.0110	0.3603	0.0598
All seats are occupied, except the rear middle one				
Length [min]	52.5	10.4	10.6	31.5
ΔR^2 [1]	−0.0025	−0.0006	−0.0029	−0.0030
ΔMAE [$^\circ/\mathrm{s}$]	0.1533	0.1137	0.4215	0.0734
ΔMSE [$(^\circ/\mathrm{s})^2$]	0.3768	0.2400	1.4528	0.0418
$\Delta RMSE$ [$^\circ/\mathrm{s}$]	0.3080	0.2454	0.7828	0.0416

In the final phase, I investigated whether a model trained on a specific vehicle type could be applied to other types of vehicles. In other words, the difference in the model's error was examined when applied to a different vehicle compared to the error measured on the vehicle used for training. The results are summarized in Table 4.5. Except for *Vehicle A*, the greatest impact is observed in the *aggressive driving* scenario, followed by the *calm driving* scenario. From a vehicle perspective, the largest differences are noted for the biggest

vehicle, *Vehicle C*, followed by *Vehicle B* and *Vehicle A*. The smallest effect is seen in the combustion engine vehicle, *Vehicle A*, while a considerably larger difference is observed for the hybrid vehicle, *Vehicle B*, despite its size being comparable to the original vehicle. The purely electric *Vehicle C* also demonstrates a notable impact. This table suggests that, rather than the overall weight of the vehicle, the weight distribution plays a more critical role and should be taken into account when applying the model across different vehicle types. To draw more reliable conclusions, a broader range of vehicle types must be analyzed. Additionally, it should be noted that even in these experiments, the MAE deviation from the reference values remained below 0.5 $^\circ/\mathrm{s}$.

Table 4.5. The impact of the entire vehicle body on the model performance relative to the performance of the *base model*.

	combined	*calm*	*aggressive*	*city*
		Vehicle A		
Length [min]	77.3	20.8	21.7	34.8
ΔR^2 [1]	−0.0008	−0.0005	−0.0003	−0.0033
ΔMAE [$^\circ$/s]	0.0718	0.0954	0.0436	0.0668
ΔMSE [($^\circ$/s)^2]	0.2103	0.2123	0.3756	0.0809
$\Delta RMSE$ [$^\circ$/s]	0.1902	0.2223	0.2780	0.0778
		Vehicle B		
Length [min]	75.1	21.3	22.0	31.8
ΔR^2 [1]	−0.0010	−0.0008	−0.0010	−0.0015
ΔMAE [$^\circ$/s]	0.1792	0.1960	0.3545	0.0375
ΔMSE [($^\circ$/s)^2]	0.3614	0.2845	0.9115	0.0066
$\Delta RMSE$ [$^\circ$/s]	0.2979	0.2808	0.5586	0.0068
		Vehicle C		
Length [min]	57.0	11.3	10.2	35.5
ΔR^2 [1]	−0.0045	−0.0016	−0.0057	−0.0005
ΔMAE [$^\circ$/s]	0.1247	0.0749	0.4396	0.0486
ΔMSE [($^\circ$/s)^2]	0.3215	0.1148	1.5206	0.0247
$\Delta RMSE$ [$^\circ$/s]	0.2710	0.1327	0.8082	0.0250

To further validate the results of the sensitivity analyses, a statistical test was performed to determine whether the differencwoes between the measured and predicted yaw rates are significantly affected by changes in specific vehicle conditions. A paired t-test was applied to compare the residuals (differences between the actual and predicted yaw rates) between the *baseline* test set and test sets corresponding to three types of perturbations: reduced tire pressure, different passenger load, and variations in vehicle body type.

The tests were performed pairwise within identical driving scenarios (e.g., *calm* with *calm*, *aggressive* with *aggressive*) to ensure that the comparisons reflect the effect of the condition being tested, rather than differences in driving behavior. For each case, the null

hypothesis (H_0) assumed no significant difference between the residual distributions of the baseline and perturbed conditions. The alternative hypothesis (H_1) assumed that the condition introduces a statistically significant change in the residuals.

The results of the paired t-tests showed that all p-values exceeded the standard significance threshold ($\alpha = 0.05$), indicating that the null hypothesis could not be rejected for any configuration. This suggests that, despite observable numerical deviations in error metrics (see Tables 4.3–4.5), these differences are not statistically significant.

Overall, the test confirms that the LSTM model maintains a consistent prediction error distribution across variations in tire pressure, passenger load, and vehicle type. This reinforces the conclusion that the model is robust and generalizable within the tested operating conditions.

4.6 LSTM-Based Forecast of Vehicle Roll Rates During Off-Road Conditions

This section details the development of an LSTM neural network designed to predict future vehicle roll rates specifically for off-road conditions. The discussion will cover the model's architecture, the extensive hyperparameter tuning process undertaken, and an evaluation of its predictive performance using independent test data.

4.6.1 Architecture of the LSTM Model for Roll Rate Forecasting

The objective was to develop an LSTM neural network model by which future values of a vehicle's roll rate in off-road conditions could be forecasted. The conceptual framework for the proposed neural network is depicted in Figure 4.5. This architecture was designed to assimilate both historical and contemporary data from wheel speeds, measurements of longitudinal and lateral accelerations, the steering angle at the front axle, the yaw rate, and the roll rate. The output of the network is the predicted roll rate over a future time span ranging from t_{i+1} to $t_{i+n_{\text{look\_future}}}$. The structure of the LSTM network is detailed in Section 3.3.3.

The developed model incorporates two critical parameters: $n_{\text{look\_back}}$, which specifies the number of past discrete time points to consider, and $n_{\text{look\_future}}$, which determines the number of future time points over which the model predicts the roll rate. Setting $n_{\text{look\_back}}$ too high may lead to the neural network processing unnecessary information, thereby increasing computational demands and prediction error. Conversely, a low $n_{\text{look\_back}}$ may result in insufficiently precise predictions. Similarly, an excessively low $n_{\text{look\_future}}$ could

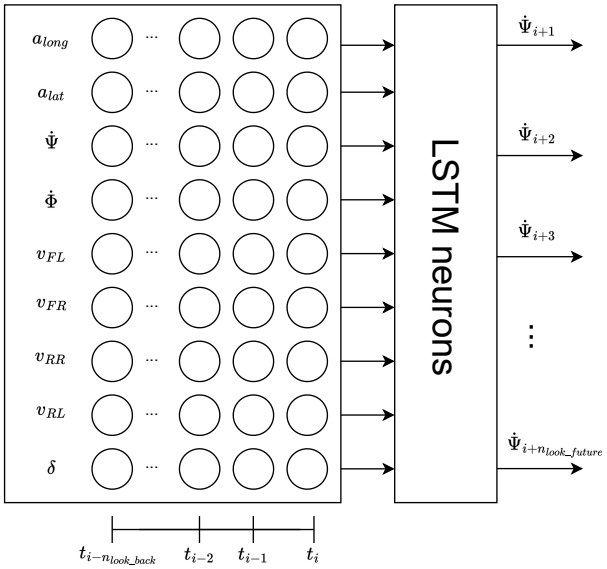

Figure 4.5. The schematic illustration of the LSTM network architecture presented herein details the input and output variables employed. Specifically, v_{FL}, v_{FR}, v_{RL}, and v_{RR} represent the velocities of the front left, front right, rear left, and rear right wheels, respectively. The terms a_{lat} and a_{long} denote lateral and longitudinal accelerations, respectively. The variable δ denotes the steering angle at the front axle, while $\dot{\Psi}$ and $\dot{\Phi}$ indicate the roll and yaw rates of the vehicle, respectively. The parameter $n_{\text{look\_back}}$ defines the span of the discrete time window utilized for inputting data into the model, and $n_{\text{look\_future}}$ denotes the extent of future time intervals over which the network forecasts the vehicle's roll rate.

underutilize the capabilities of the developed model, while a very high $n_{\text{look\_future}}$ might weaken the correlation between input data and the predicted outcomes.

4.6.2 Hyperparameter Tuning for the Roll Rate Forecasting Model

Optimization of parameters and hyperparameters was a pivotal aspect of the work. This phase aimed to establish the optimal architecture for the network, including the appropriate number of LSTM neurons and hidden layers within the LSTM network. It also involved identifying the most effective hyperparameter settings for the learning process and determining the ideal length of the time lookback window to ensure precise predictions of future roll rate values with minimized computational complexity. A detailed description of the hyperparameter tuning process can be found in Section 3.3.2. The hyperparameter tuning process for the roll rate prediction model is detailed in Table 4.6, which outlines the explored parameter space and the final optimal configuration selected. This optimal setup features 1 hidden layer with 7 LSTM neurons, a batch size of 512, a learning rate of 0.001, and normal random weight initialization. Additionally, it utilizes tanh and sigmoid activation functions, no dropout (0 rate), and sequence lengths of 4 for both $n_{\text{look\_back}}$ and $n_{\text{look\_future}}$. This meticulous tuning resulted in a configuration that ensures the model's robustness for

roll rate prediction while keeping resource consumption low, which is particularly critical for maintaining stability and preventing rollovers in off-road conditions.

Table 4.6. The parameter space established for tuning the parameters/hyperparameters, with the tuning outcomes emphasized in bold. The sigmoid function is described by $sigmoid(x) = 1/(1 + e^{(-x)})$. Additionally, the hard sigmoid function was delineated as follows: it assumes a value of 0 for $x < -2.5$, a value of 1 for $x > 2.5$, and $0.2x + 0.5$ for $-2.5 <= x <= 2.5$.

Parameter/Hyperparameter	Values
Number of hidden layers	**1**, 2
Number of LSTM neurons per layer	1, 2, 3, 4, 5, 6, **7**, 8, 9
Batch size	32, 64, 128, 256, **512**, 1024
Learning rate	0.0001, **0.001**, 0.01
Mode of weight initialization	**normal random**, uniform random
LSTM activation function (σ_g)	**tanh**, sigmoid, hard sigmoid
Recurrent activation function (σ_c)	tanh, **sigmoid**, hard sigmoid
Dropout rate	**0**, 0.1, 0.2, 0.3
$n_{\text{look\_back}}$	1, 2, 3, **4** 5, 6, 7, 8, 9, 10
$n_{\text{look\_future}}$	1, 2, 3, **4** 5, 6, 7, 8, 9, 10

4.6.3 Evaluation of Roll Rate Estimation Accuracy

To assess the predictive performance of the developed model, I compared the predicted roll rates with the observed values within the test dataset, which was entirely independent and was neither utilized for training nor validation. Figure 4.6 illustrates the predicted versus measured roll rates for a period of 40 milliseconds following the current time instant, depicted for a randomly chosen segment of the test dataset. As observed in the figure, the predicted and measured values of the roll rate are closely aligned, demonstrating substantial overlap during the prediction interval.

The deviations in the forecasted roll rate values for the time interval from 10 ms to 40 ms ahead (in 10 ms increments), are presented in Table 4.7. The data reveal a gradual decline in prediction accuracy for roll rate values as the forecast horizon extends. Nevertheless, the observed errors remain within the limits required to fulfill the ASIL B safety level, confirming the suitability of the model for safety-critical applications.

4.7 Discussion

This part details the practical performance and deployment considerations for the LSTM-based yaw and roll rate predictors are rigorously assessed, including a benchmark against current methods, determination of sufficient training data volumes, and a detailed sensitivity analysis concerning tire pressure, passenger distribution, and fundamental vehicle dynamics

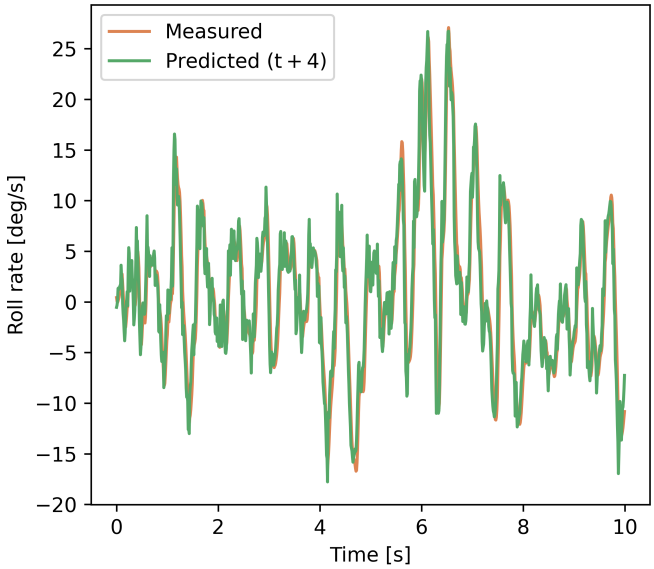

Figure 4.6. Measured and predicted roll rate values (0.04 seconds into the future) on the test dataset, on off-road conditions.

Table 4.7. Error metrics for the predicted roll rate values for different values of $n_{\text{look\_future}}$ parameter (ranging from 10 ms to 40 ms ahead, in 10 ms increments).

	$t+1$	$t+2$	$t+3$	$t+4$
R^2 [1]	0.9978	0.9948	0.9829	0.9593
MAE [°/s]	0.230	0.369	0.715	1.107
MSE [(°/s)^2]	0.129	0.306	1.002	2.339
$RMSE$ [°/s]	0.359	0.553	1.001	1.529

For the yaw rate forecasting model direct comparison with other models from the literature could not be performed, as no known methods predict future yaw rate values. Instead, comparison was made with models estimating or computing current yaw rate values based on other sensor signals. Since published models typically provide $RMSE$ for evaluation, the same metric was applied.

The EH∞KF filter proposed by Zhang et al. [89] utilized 20 seconds of simulated double-lane change data, achieving an $RMSE$ of 1.378 $^\circ/\mathrm{s}$ for current yaw rate values. This result is valid only for present yaw rate estimation and depends on several vehicle-specific parameters, increasing implementation complexity.

The neural network model by Hermansdorfer et al. [82] was tested on three driving scenarios, reporting an $RMSE$ of 1.604 $^\circ/\mathrm{s}$ on the Monteblanco dataset. However, the model required significant computational resources (150 GRU units), complicating its integration into embedded systems. Additionally, the absence of wheel speed data prevented direct comparison, and the model only estimated current yaw rate values.

In the "Set Membership" method [85], 211 seconds of experimental data and 5000 simulated single-track model data points were used. The M2 model from this work achieved the lowest $RMSE$ of 1.089 $^\circ/\mathrm{s}$ for yaw rate estimation.

Comparison of these results showed that the developed model achieved superior accuracy, with $RMSE$ values of 0.458 $^\circ/\mathrm{s}$, 0.366 $^\circ/\mathrm{s}$, 0.537 $^\circ/\mathrm{s}$, and 0.481 $^\circ/\mathrm{s}$ for the *combined*, *calm*, *aggressive*, and *city* datasets, respectively. These values are lower than the best results reported in the literature (1.089 $^\circ/\mathrm{s}$) for current yaw rate estimation. Although direct comparison is limited due to differences in prediction targets (future vs. current yaw rate), the developed model outperformed existing methods while requiring significantly fewer computational resources, emphasizing its efficiency for future yaw rate prediction.

Regarding the training dataset size, approximately 10-15 minutes of diverse driving data were found sufficient for non-safety-related applications. For safety-critical scenarios, all available data must be used to maximize model robustness and prediction accuracy.

The sensitivity analysis highlighted that tire pressure has a notable influence on yaw rate predictions, particularly on the front wheels, which are responsible for steering. The potential negative effects of reduced tire pressure are mitigated in modern vehicles equipped with tire pressure monitoring systems (TPMS).

Passenger number and seating position also affected predictions. The greatest impact occurred when passengers were seated on the same side or row as the driver, while the largest deviation was observed when the vehicle was fully loaded, altering the center of mass.

Additionally, the horizontal weight distribution influenced prediction accuracy. Electric and hybrid vehicles, due to large battery packs, tend to have a lower center of mass, improving stability but also changing dynamic behavior. This effect is less pronounced in

traditional internal combustion engine vehicles. For non-safety applications, a single model may be used across vehicle types, but for safety-critical functions, separate models are recommended for internal combustion engine and hybrid/electric variants to ensure accuracy.

Similarly, the developed LSTM-based model demonstrated effectiveness in predicting roll rate values in off-road conditions. Accurate short-term predictions over a horizon of 0.04 seconds were achieved, supporting roll rate plausibility checks and evaluation of ARP system interventions. Although this prediction horizon does not cover entire intervention events, it offers valuable insight into the immediate effects of control actions.

Direct comparison of roll rate prediction with literature results was also limited, as no known studies predict future roll rate values. Comparison was instead made against the best methods estimating current roll rate. Yun et al. [93] developed a model capable of predicting current roll rate values under normal road conditions, achieving an $RMSE$ of 0.7012 $^\circ/s$ during a lane change maneuver. However, future roll rate prediction was not performed, and the method was valid only for specific maneuvers on paved roads.

In contrast, the developed model achieved an $RMSE$ of 0.553 $^\circ/s$ across the entire test set when predicting 0.02 seconds into the future under off-road conditions. This result confirmed the model's ability to provide accurate short-term roll rate forecasts in challenging environments where vehicle stability is critical.

To fully realize this integration in real-world applications, however, it is essential to consider the operational lifecycle of the models beyond their initial development and validation. This is where the application of MLOps (Machine Learning Operations) becomes particularly important. MLOps methodologies provide a structured framework for managing the entire lifecycle of machine learning models, including development, deployment, continuous monitoring, automated updating, and validation, in a transparent and reproducible manner. This is especially critical in safety-critical automotive domains, where reliability and traceability are non-negotiable.

Furthermore, integrating AI-based models into safety-critical embedded vehicle systems must comply with rigorous engineering and validation frameworks such as the V-model, Automotive SPICE, ISO 26262, and emerging AI-specific standards like ISO/IEC 24029 and SOTIF. The V-model facilitates systematic requirement tracing and verification, while Automotive SPICE emphasizes traceable and requirements-driven development, including data set and model validation. According to ISO 26262, AI models must demonstrate behavior that is reliably verifiable and conform to required ASIL. Supporting this necessitates appropriate safety barriers such as redundancy, fault detection, and fallback mechanisms to ensure system integrity in the event of model malfunction.

It should be noted that the roll rate model was specifically developed and validated using data from a single vehicle type operating in off-road conditions within a speed range of 0 to 30 $\mathrm{km/h}$. To expand its applicability to other vehicle types or to normal road conditions,

additional training with new datasets representing those conditions would be required.

Overall, the developed LSTM-based models demonstrated superior prediction accuracy for both yaw and roll rates compared to existing estimation methods. Robustness was confirmed under varying conditions, including changes in tire pressure, passenger load, and vehicle architecture. These results indicate that the models are well-suited for integration into vehicle control systems, enhancing stability and safety in both on-road and off-road driving environments.

4.8 Summary

This part of my PhD thesis investigated the application of LSTM neural networks for the short-term prediction of vehicle yaw and roll rates, paying special attention not only to the evaluation of prediction accuracy but also to determining the optimal amount of training data and analyzing the model's sensitivity to various factors (such as tire pressure, load, and general vehicle dynamics), in the context of developing vehicle safety and automation

The performance of the improved LSTM model, designed to predict vehicle yaw rates up to 0.2 seconds into the future, was examined. The predictive accuracy of the model, the necessary amount of training data, and the sensitivity of yaw rate predictions to variables such as tire pressure, passenger load, and overall vehicle dynamics were evaluated.

The model was trained using more than 17.5 hours of experimental data collected across various driving scenarios, including *aggressive*, *calm*, and *city driving*.

The results confirmed that the LSTM-based neural network model was capable of accurately forecasting yaw rates under diverse conditions. The MAE remained below 0.5 $^\circ/\mathrm{s}$ in all investigated cases, which is well below the 3 $^\circ/\mathrm{s}$ threshold defined by the ASIL B safety standard [57]. These findings indicate that neural network-based vehicle dynamics models have the potential to be applied in both safety-critical and non-safety applications, contributing to improved vehicle performance and safety across a wide range of driving environments.

An LSTM neural network was developed to predict roll rate values under off-road conditions. The model was trained on approximately five hours of preprocessed data collected by test drivers at an off-road testing facility in Brimley, Michigan (USA).

The architecture of the model included a single hidden layer containing seven LSTM neurons. Nine vehicular signals served as inputs: longitudinal and lateral accelerations, yaw and roll rates, front axle steering angle, and the speeds of all four wheels. Data from the past 40 milliseconds were used by the model to predict the roll rate over the following 40 milliseconds. Accurate roll rate predictions were achieved with minimal computational demand, and no vehicle-specific parameters were required.

However, a key limitation for both models stems from the data collection constraints.

The experimental data used for development and validation were gathered within specific speed ranges: 0–50 $\mathrm{km/h}$ for the yaw rate model and 0–30 $\mathrm{km/h}$ for the off-road roll rate model. Therefore, the demonstrated applicability and performance of these models are currently validated only within these respective speed intervals and associated environments.

This approach demonstrated strong potential for enhancing safety features in both autonomous and conventional vehicles. By providing reliable roll rate forecasts under challenging off-road conditions, the model supports advanced vehicle stability functions and improves overall vehicle safety performance.

4.9 Related theses

Thesis 2.1

I have developed an LSTM neural network optimized for forecasting vehicle yaw rate up to $200\,\mathrm{ms}$ ahead. The model is designed for broad applicability, utilizing only standard sensor signals - longitudinal/lateral acceleration, yaw rate, steering angle of the front axle, and wheel speeds - which are commonly found in vehicle electronic brake systems, thereby eliminating the need for vehicle-specific parameters. The model, featuring a single hidden layer with 5 LSTM neurons, achieved exceptional performance on an independent test set: R^2 = 0.9984 , MAE = 0.316 $^\circ/s$, demonstrating high accuracy and efficiency for real-time deployment.

Thesis 2.2

I designed, trained, and validated a novel LSTM-based model for forecasting vehicle roll rate, specifically tailored for complex off-road driving conditions. After investigating various prediction horizons, I selected $40\,\mathrm{ms}$ ahead as an optimal timeframe. This choice balances declining prediction accuracy over longer horizons with the practical needs of safety-critical functions like ARP, providing valuable insight into immediate control effects while ensuring the model's output remains within ASIL B safety limits. The model, featuring a single hidden layer with 7 LSTM neurons, achieved R^2 = 0.9593, MAE = 1.107 $^\circ/\mathrm{s}$ on an independent test set, demonstrating robust performance for off-road applications.

Thesis 2.3

I conducted a sensitivity analysis that confirmed the yaw rate prediction model's robustness against operational variations. Tests involving reduced tire pressure and varying passenger loads had minimal impact on prediction accuracy, with maximum Mean Absolute Error

(MAE) deviations remaining below $0.5°/s$, even during aggressive driving where the effects were most noticeable. Furthermore, transferability tests across different vehicle types also yielded MAE deviations under $0.5°/s$, suggesting that vehicle weight distribution is more critical than overall mass, especially for hybrid and electric vehicles. Building on this demonstrated resilience, an investigation into training data volume established a practical guideline: based on the extensive experimental data collected for this study, 10-15 minutes of diverse, dynamic driving data provides sufficient accuracy for non-safety-critical applications. For safety-critical systems, however, the complete dataset is required to ensure maximum model robustness.

Related publications

P5 János Kontos, László Bódis, Ágnes Vathy-Fogarassy (2025). Sensitivity analysis of Long Short-Term Memory-based Neural Network Model for Vehicle Yaw Rate Prediction. *Sensors* (Q2, IF: 3.9), 25 (5), 1363. `https://doi.org/10.3390/s25051363`

P6 János Kontos, László Bódis, Ágnes Vathy-Fogarassy (2023). Prediction for Future Yaw Rate Values of Vehicles Using Long Short-Term Memory Network. *Sensors* (Q2, IF: 3.9), 23(12), 5670. `https://doi.org/10.3390/s23125670`

P7 János Kontos, László Bódis, Ágnes Vathy-Fogarassy (2024). Forecasting Roll Rate for Sensor Plausibility Check in Off-Road Vehicle Conditions. *2024 IEEE 3rd Conference on Information Technology and Data Science (CITDS)*, 1–6. Debrecen, Hungary. `10.1109/CITDS62610.2024.10791355`

Summary

This PhD dissertation addresses the critical issue of using neural network-based models for predicting key vehicle dynamics parameters in embedded automotive systems with limited computational resources. The focus lies in enhancing safety-critical functions like Electronic Stability Control , Anti-lock Braking Systems , and Active Rollover Protection.

Specialized neural network architectures capable of accurately predicting lateral and longitudinal acceleration, yaw rate, and roll rate are introduced. Standard vehicle sensor inputs, including wheel speeds, steering angle of front axle, and accelerations collected under controlled and off-road experimental conditions, are employed by the models.

For lateral acceleration estimation, a compact feedforward neural network was developed to efficiently function directly within sensors, acting as a virtual sensor. Additionally, Long Short-Term Memory networks were designed to forecast future values of longitudinal acceleration (0.1 s ahead), yaw rate (0.2 s ahead), and specifically roll rate for off-road scenarios (0.04 s ahead), applicable to brake control systems.

The proposed models significantly outperform existing literature solutions in terms of accuracy while maintaining lower computational demands. An optimal data amount study indicated that even minimal data, as little as 15 minutes, could effectively train models for non-safety-critical scenarios.

Sensitivity analyses of the yaw rate model confirmed robust performance despite variations in tire pressure, passenger load, and vehicle structural changes, underscoring compliance with stringent automotive safety standards. These models were rigorously validated using experimental datasets to ensure reliability and accuracy in real-world conditions. The adaptability of these models also makes them suitable for future integration into autonomous driving systems.

While the developments primarily target automotive applications, two scientific findings are more broadly applicable. First, even compact and well-optimized neural networks can achieve high predictive performance, challenging the assumption that complexity is necessary for accuracy. Second, the quality and representativeness of training data are often more critical than its quantity, especially in domains where data collection is constrained. These insights suggest that the neural network approaches presented here hold promise for other real-time, time-series prediction tasks beyond vehicle dynamics.

In conclusion, this research presents resource-efficient, high-accuracy neural network models applicable to modern vehicle dynamics control systems, contributing significantly to vehicle safety and stability enhancements.

Összefoglalás

Doktori disszertációm során a neurális hálózatokon alapuló járműdinamikai modellek alkalmazásával foglalkoztam biztonságkritikus járműrendszerekben. A kidolgozott modellek kulcsfontosságú járműdinamikai paraméterek pontos előrejelzésére alkalmasak, még korlátozott számítási kapacitással rendelkező beágyazott autóipari rendszerekben is, mint például az elektronikus fékvezérlő. Célom a biztonságkritikus járműfunkciók bemeneti jeleinek előrejelzésén és becslésén keresztül a rendszerek biztonsági szintjének növelése volt.

Speciális neurális hálózat-alapú modelleket fejlesztettem ki, amelyek képesek pontosan előre jelezni a jármű hosszirányú és oldalirányú gyorsulását, valamint a perdületi és dőlési szögsebességet. Ezek a modellek modern gépjárművekben elérhető szenzoradatokat használnak fel, mint például a kerekek sebessége, az első tengely kormányszöge, valamint a jármű perdületi és dőlési szögsebessége.

Az oldalirányú gyorsulás becslésére egy kisméretű előrecsatolt neurális hálózatot dolgoztam ki, amely virtuális szenzorként alkalmazható alacsony teljesítményű beágyazott rendszerekben. Emellett Long Short-Term Memory (LSTM) hálózatokat hoztam létre a hosszirányú gyorsulás (0,1 másodperc), a perdületi szögsebesség (0,2 másodperc) és terepi körülmények között a dőlési szögsebesség (0,04 másodperc) hatékony előrejelzésére. Valamennyi modell sikeresen integrálható elektronikus fékvezérlőkbe.

A kidolgozott modellek jelentősen meghaladják a szakirodalomban található ismert megoldások pontosságát, miközben alacsonyabb számítási kapacitást igényelnek. Vizsálataim alapján, bizonyos nem biztonságkritikus esetekben már 15 percnyi adat is elegendő lehet a modellek betanításához.

A perdületi szögsebesség modelljével végzett érzékenységi vizsgálatok igazolták, hogy a modell robusztus teljesítményt nyújt a gumiabroncsnyomás változásától, az utasok számától és elhelyezkedésétől, valamint nagyobb járműszerkezeti eltérésektől függetlenül, megfelelve az autóipari biztonsági szabványok legszigorúbb követelményeinek.

Bár a bemutatott ejlesztések elsősorban az autóipari alkalmazásokra irányulnak, két tudományos eredmény szélesebb körben is alkalmazható. Először is, még a kompakt és jól optimalizált neurális hálózatok is képesek jól használható előrejelzést adni, ami megkérdőjelezi azt a feltételezést, hogy nagy komplexitás szükséges a megfelelő pontossághoz. Másodszor, a tanítási adatok minősége gyakran kritikusabb, mint azok mennyisége, különösen olyan területeken, ahol az adatgyűjtés korlátozott.

Összességében kutatásomban erőforrás-hatékony, nagy pontosságú neurális hálózati modelleket hoztam létre, amelyek jelentősen hozzájárulnak a modern járműdinamikai szabályozórendszerek fejlesztéséhez, növelve a járművek biztonságát és stabilitását.

Appendices

Table 5.1. Statistical properties of the aggressive scenario for *Vehicle A* when assessing the influence of vehicle body on the performance of the developed model.

	a_{long} [g]	a_{lat} [g]	$\dot{\Phi}$ [°/s]	δ [°]	v_{FL} [km/h]	v_{FR} [km/h]	v_{RR} [km/h]	v_{RL} [km/h]
Mean	−0.01	0.06	2.681	0.64	38.48	38.72	38.13	38.4
Std	0.08	0.38	19.312	6.73	8.19	8.29	8.25	8.35
Min	−0.44	−0.91	−72.341	−34.51	0.11	0.11	0.11	0.11
Q1 (25%)	−0.04	−0.22	−9.639	−2.92	33.6	33.73	33.26	33.38
Q2 (50%)	0.0	0.01	0.898	0.23	39.66	39.57	39.35	39.28
Q3 (75%)	0.03	0.39	17.423	4.81	43.85	44.46	43.55	44.2
Max	0.34	0.94	68.657	33.96	66.55	66.11	66.18	65.61

Table 5.2. Statistical properties of the calm scenario for *Vehicle A* when assessing the influence of vehicle body on the performance of the developed model.

	a_{long} [g]	a_{lat} [g]	$\dot{\Phi}$ [°/s]	δ [°]	v_{FL} [km/h]	v_{FR} [km/h]	v_{RR} [km/h]	v_{RL} [km/h]
Mean	0.0	0.02	1.356	0.29	27.5	27.63	27.22	27.35
Std	0.05	0.2	14.807	8.08	9.37	9.48	9.44	9.56
Min	−0.24	−0.52	−41.127	−34.25	0.11	0.11	0.11	0.11
Q1 (25%)	−0.02	−0.14	−9.604	−3.41	20.49	20.73	20.17	20.48
Q2 (50%)	0.0	0.0	0.475	0.14	28.54	28.56	28.29	28.33
Q3 (75%)	0.02	0.19	12.81	4.6	34.72	35.1	34.49	34.9
Max	0.25	0.51	47.496	33.61	46.41	46.91	46.13	46.75

Table 5.3. Statistical properties of the city scenario for *Vehicle A* when assessing the influence of vehicle body on the performance of the developed model.

	a_{long} [g]	a_{lat} [g]	$\dot{\Phi}$ [°/s]	δ [°]	v_{FL} [km/h]	v_{FR} [km/h]	v_{RR} [km/h]	v_{RL} [km/h]
Mean	0.01	0.0	0.051	0.03	32.84	32.82	32.63	32.63
Std	0.06	0.07	5.891	5.02	16.17	16.15	16.13	16.11
Min	−0.66	−0.38	−29.449	−34.18	0.11	0.11	0.11	0.11
Q1 (25%)	−0.01	−0.01	−0.709	−0.24	20.89	21.01	20.65	20.83
Q2 (50%)	0.01	0.0	0.014	0.01	35.64	35.6	35.49	35.44
Q3 (75%)	0.04	0.02	0.515	0.16	45.25	45.19	45.02	44.98
Max	0.49	0.43	36.542	33.65	61.33	61.3	60.99	61.04

Table 5.4. Statistical properties of the aggressive scenario for *Vehicle B* when assessing the influence of vehicle body on the performance of the developed model.

	a_{long} [g]	a_{lat} [g]	$\dot{\Phi}$ [°/s]	δ [°]	v_{FL} [km/h]	v_{FR} [km/h]	v_{RR} [km/h]	v_{RL} [km/h]
Mean	−0.02	0.04	2.945	0.86	37.63	37.93	37.5	37.8
Std	0.05	0.44	22.091	7.23	8.35	8.43	8.41	8.48
Min	−0.23	−0.9	−51.148	−22.66	0.11	0.11	0.11	0.11
Q1 (25%)	−0.05	−0.33	−14.829	−4.49	33.14	33.1	33.03	32.95
Q2 (50%)	−0.02	0.04	3.544	0.99	38.4	38.5	38.3	38.38
Q3 (75%)	0.0	0.43	22.248	6.5	43.27	44.18	43.21	44.08
Max	0.37	0.89	53.825	21.55	57.93	56.89	58.02	56.84

Table 5.5. Statistical properties of the calm scenario for *Vehicle B* when assessing the influence of vehicle body on the performance of the developed model.

	a_{long} [g]	a_{lat} [g]	$\dot{\Phi}$ [°/s]	δ [°]	v_{FL} [km/h]	v_{FR} [km/h]	v_{RR} [km/h]	v_{RL} [km/h]
Mean	−0.01	0.01	1.662	0.52	28.25	28.43	28.09	28.27
Std	0.03	0.22	14.843	8.78	11.76	11.8	11.85	11.89
Min	−0.22	−0.44	−27.633	−33.45	0.11	0.11	0.11	0.11
Q1 (25%)	−0.03	−0.18	−12.79	−4.85	19.37	20.09	19.08	19.84
Q2 (50%)	0.0	0.02	3.744	1.28	30.41	30.26	30.31	30.14
Q3 (75%)	0.01	0.2	15.241	5.75	37.43	37.64	37.36	37.55
Max	0.12	0.4	30.891	33.21	50.12	49.88	50.2	49.88

Table 5.6. Statistical properties of the city scenario for *Vehicle B* when assessing the influence of vehicle body on the performance of the developed model.

	a_{long} [g]	a_{lat} [g]	$\dot{\Phi}$ [°/s]	δ [°]	v_{FL} [km/h]	v_{FR} [km/h]	v_{RR} [km/h]	v_{RL} [km/h]
Mean	0.0	0.0	0.113	−0.02	34.82	34.84	34.76	34.78
Std	0.05	0.06	5.62	4.01	13.88	13.84	13.89	13.85
Min	−0.25	−0.37	−30.459	−30.96	0.11	0.11	0.11	0.11
Q1 (25%)	−0.02	−0.02	−0.518	−0.2	26.75	26.94	26.73	26.86
Q2 (50%)	0.0	0.0	−0.046	0.0	37.07	37.13	37.03	37.09
Q3 (75%)	0.02	0.01	0.286	0.12	45.13	45.18	45.1	45.11
Max	0.24	0.35	41.164	33.96	55.76	56.23	55.82	56.47

Table 5.7. Statistical properties of the aggressive scenario for *Vehicle C* when assessing the influence of vehicle body on the performance of the developed model.

	a_{long} [g]	a_{lat} [g]	$\dot{\Phi}$ [°/s]	δ [°]	v_{FL} [km/h]	v_{FR} [km/h]	v_{RR} [km/h]	v_{RL} [km/h]
Mean	−0.02	0.0	1.194	0.3	37.81	37.93	37.71	37.79
Std	0.14	0.31	15.937	5.61	8.06	8.0	8.12	8.05
Min	−0.71	−0.81	−41.04	−25.72	0.12	0.12	0.12	0.12
Q1 (25%)	−0.07	−0.2	−8.913	−2.79	32.82	32.98	32.69	32.75
Q2 (50%)	−0.03	−0.01	0.307	0.05	38.71	38.47	38.61	38.33
Q3 (75%)	0.03	0.23	11.437	3.34	43.59	43.55	43.58	43.46
Max	0.46	0.85	42.395	15.83	53.95	53.8	54.34	54.28

Table 5.8. Statistical properties of the calm scenario for *Vehicle C* when assessing the influence of vehicle body on the performance of the developed model.

	a_{long} [g]	a_{lat} [g]	$\dot{\Phi}$ [°/s]	δ [°]	v_{FL} [km/h]	v_{FR} [km/h]	v_{RR} [km/h]	v_{RL} [km/h]
Mean	−0.02	0.0	1.615	0.55	36.49	18.43	36.41	36.54
Std	0.06	0.16	9.563	3.92	7.31	18.67	7.35	7.15
Min	−0.34	−0.46	−30.468	−25.93	0.12	0.0	0.12	0.12
Q1 (25%)	−0.04	−0.11	−4.908	−1.47	34.01	0.0	33.94	33.85
Q2 (50%)	−0.02	0.0	0.874	0.24	38.39	15.27	38.33	38.37
Q3 (75%)	0.0	0.12	7.082	2.05	41.06	37.89	41.01	41.11
Max	0.23	0.41	31.09	15.98	48.65	48.69	48.85	48.74

Table 5.9. Statistical properties of the city scenario for *Vehicle C* when assessing the influence of vehicle body on the performance of the developed model.

	a_{long} [g]	a_{lat} [g]	$\dot{\Phi}$ [°/s]	δ [°]	v_{FL} [km/h]	v_{FR} [km/h]	v_{RR} [km/h]	v_{RL} [km/h]
Mean	0.01	0.01	0.305	−0.21	30.15	30.2	30.1	30.14
Std	0.06	0.07	5.905	4.53	14.05	14.07	14.07	14.08
Min	−0.37	−0.35	−31.531	−34.51	0.12	0.12	0.12	0.12
Q1 (25%)	−0.02	−0.01	−0.745	−0.33	20.1	20.5	19.97	20.38
Q2 (50%)	0.0	0.01	0.009	0.03	32.28	32.35	32.25	32.31
Q3 (75%)	0.03	0.02	0.831	0.35	40.17	40.22	40.17	40.18
Max	0.4	0.53	33.316	25.14	56.56	56.68	56.77	56.84

Table 5.10. Statistical properties of the aggressive scenario with the front right passenger seat occupied when assessing the influence of passenger distribution on the performance of the developed model.

	a_{long} [g]	a_{lat} [g]	$\dot{\Phi}$ [°/s]	δ [°]	v_{FL} [km/h]	v_{FR} [km/h]	v_{RR} [km/h]	v_{RL} [km/h]
Mean	−0.02	0.03	1.671	0.36	39.93	40.04	39.6	39.77
Std	0.11	0.43	19.004	5.27	9.02	9.11	9.0	9.1
Min	−0.61	−0.89	−45.285	−15.71	0.11	0.11	0.11	0.11
Q1 (25%)	−0.08	−0.31	−12.661	−3.12	36.24	36.61	35.83	36.26
Q2 (50%)	−0.02	0.0	0.277	0.1	41.16	41.19	40.88	40.92
Q3 (75%)	0.03	0.41	17.372	4.18	45.47	45.69	45.16	45.43
Max	0.39	0.93	40.549	13.0	64.89	64.29	64.81	64.21

Table 5.11. Statistical properties of the calm scenario with the front right passenger seat occupied when assessing the influence of passenger distribution on the performance of the developed model.

	a_{long} [g]	a_{lat} [g]	$\dot{\Phi}$ [°/s]	δ [°]	v_{FL} [km/h]	v_{FR} [km/h]	v_{RR} [km/h]	v_{RL} [km/h]
Mean	−0.01	0.03	1.687	0.35	34.7	34.85	34.5	34.66
Std	0.05	0.21	12.246	5.29	10.88	10.87	10.92	10.93
Min	−0.26	−0.5	−41.167	−33.29	0.11	0.11	0.11	0.11
Q1 (25%)	−0.03	−0.16	−7.259	−1.86	28.63	29.17	28.43	28.96
Q2 (50%)	0.0	0.03	2.013	0.5	37.91	37.82	37.72	37.63
Q3 (75%)	0.02	0.2	10.119	2.48	43.02	43.23	42.86	43.08
Max	0.16	0.5	33.087	17.65	51.38	51.14	51.21	51.12

Table 5.12. Statistical properties of the city scenario with the front right passenger seat occupied when assessing the influence of passenger distribution on the performance of the developed model.

	a_{long} [g]	a_{lat} [g]	$\dot{\Phi}$ [°/s]	δ [°]	v_{FL} [km/h]	v_{FR} [km/h]	v_{RR} [km/h]	v_{RL} [km/h]
Mean	−0.01	0.0	0.255	0.04	44.1	44.11	43.86	43.85
Std	0.07	0.09	5.781	3.06	13.09	13.07	13.07	13.05
Min	−0.41	−0.56	−30.519	−33.2	0.11	0.11	0.11	0.11
Q1 (25%)	−0.04	−0.01	−0.706	−0.18	37.76	37.68	37.55	37.45
Q2 (50%)	0.0	0.0	0.126	0.03	49.19	49.2	48.92	48.94
Q3 (75%)	0.02	0.02	0.698	0.14	53.56	53.6	53.31	53.31
Max	0.35	0.62	30.819	32.79	59.92	59.85	59.78	59.67

Table 5.13. Statistical properties of the aggressive scenario with the rear left passenger seat occupied when assessing the influence of passenger distribution on the performance of the developed model.

	a_{long} [g]	a_{lat} [g]	$\dot{\Phi}$ [°/s]	δ [°]	v_{FL} [km/h]	v_{FR} [km/h]	v_{RR} [km/h]	v_{RL} [km/h]
Mean	−0.02	0.05	2.829	0.54	41.65	41.9	41.35	41.59
Std	0.1	0.41	18.943	5.72	7.9	7.89	7.99	7.99
Min	−0.47	−0.96	−66.149	−33.32	0.11	0.11	0.11	0.11
Q1 (25%)	−0.06	−0.33	−13.728	−3.27	39.61	39.61	39.3	39.3
Q2 (50%)	−0.01	0.04	2.7	0.56	43.59	43.87	43.32	43.54
Q3 (75%)	0.03	0.41	18.968	4.44	46.18	46.44	45.93	46.17
Max	0.45	0.88	59.948	28.95	59.47	59.3	59.23	59.32

Table 5.14. Statistical properties of the calm scenario with the rear left passenger seat occupied when assessing the influence of passenger distribution on the performance of the developed model.

	a_{long} [g]	a_{lat} [g]	$\dot{\Phi}$ [°/s]	δ [°]	v_{FL} [km/h]	v_{FR} [km/h]	v_{RR} [km/h]	v_{RL} [km/h]
Mean	−0.01	0.02	2.143	0.77	35.84	36.02	35.65	35.83
Std	0.05	0.24	13.523	4.8	8.72	8.51	8.79	8.55
Min	−0.28	−0.55	−29.504	−12.71	0.11	0.11	0.11	0.11
Q1 (25%)	−0.03	−0.2	−9.487	−2.36	32.37	32.3	32.23	32.1
Q2 (50%)	0.0	0.02	1.896	0.45	37.64	37.41	37.48	37.24
Q3 (75%)	0.02	0.24	13.105	3.07	41.77	42.16	41.63	42.0
Max	0.21	0.53	39.179	33.2	51.4	51.09	51.16	50.94

Table 5.15. Statistical properties of the city scenario with the rear left passenger seat occupied when assessing the influence of passenger distribution on the performance of the developed model.

	a_{long} [g]	a_{lat} [g]	$\dot{\Phi}$ [°/s]	δ [°]	v_{FL} [km/h]	v_{FR} [km/h]	v_{RR} [km/h]	v_{RL} [km/h]
Mean	0.0	0.0	0.22	0.01	30.88	30.89	30.71	30.7
Std	0.08	0.08	6.826	4.95	13.3	13.31	13.31	13.3
Min	−0.3	−0.47	−32.87	−32.84	0.11	0.11	0.11	0.11
Q1 (25%)	−0.04	−0.03	−1.004	−0.35	22.14	22.71	21.96	22.51
Q2 (50%)	0.0	0.0	0.017	0.0	32.51	32.49	32.36	32.32
Q3 (75%)	0.04	0.01	1.09	0.32	41.87	41.91	41.7	41.7
Max	0.31	0.41	41.336	33.11	55.5	55.41	55.23	55.35

Table 5.16. Statistical properties of the aggressive scenario with the rear right passenger seat occupied when assessing the influence of passenger distribution on the performance of the developed model.

	a_{long} [g]	a_{lat} [g]	$\dot{\Phi}$ [°/s]	δ [°]	v_{FL} [km/h]	v_{FR} [km/h]	v_{RR} [km/h]	v_{RL} [km/h]
Mean	−0.03	0.0	0.541	0.09	40.65	40.67	40.31	40.35
Std	0.09	0.43	21.197	6.51	8.79	8.77	8.89	8.85
Min	−0.4	−0.81	−55.524	−27.44	0.11	0.11	0.11	0.11
Q1 (25%)	−0.07	−0.38	−16.905	−4.26	35.85	35.85	35.54	35.6
Q2 (50%)	−0.02	0.0	0.39	0.1	43.21	43.08	42.94	42.85
Q3 (75%)	0.03	0.36	16.641	4.06	47.18	47.26	46.87	46.92
Max	0.26	0.81	57.578	25.67	57.17	57.1	57.1	56.9

Table 5.17. Statistical properties of the calm scenario with the rear right passenger seat occupied when assessing the influence of passenger distribution on the performance of the developed model.

	a_{long} [g]	a_{lat} [g]	$\dot{\Phi}$ [°/s]	δ [°]	v_{FL} [km/h]	v_{FR} [km/h]	v_{RR} [km/h]	v_{RL} [km/h]
Mean	0.0	0.01	1.098	0.31	36.3	36.38	36.13	36.22
Std	0.04	0.23	12.758	3.77	8.25	8.17	8.26	8.18
Min	−0.2	−0.53	−30.101	−10.36	0.11	0.11	0.11	0.11
Q1 (25%)	−0.02	−0.19	−8.594	−2.03	32.02	32.03	31.85	31.87
Q2 (50%)	0.0	0.0	0.521	0.14	36.58	36.63	36.39	36.5
Q3 (75%)	0.01	0.22	12.026	2.98	42.21	42.31	42.06	42.16
Max	0.22	0.46	29.309	12.27	52.7	51.63	52.53	51.47

Table 5.18. Statistical properties of the city scenario with the rear right passenger seat occupied when assessing the influence of passenger distribution on the performance of the developed model.

	a_{long} [g]	a_{lat} [g]	$\dot{\Phi}$ [°/s]	δ [°]	v_{FL} [km/h]	v_{FR} [km/h]	v_{RR} [km/h]	v_{RL} [km/h]
Mean	0.0	0.0	0.252	0.07	34.14	34.16	33.95	33.95
Std	0.09	0.08	6.728	5.2	14.75	14.78	14.75	14.77
Min	−0.52	−0.45	−38.913	−33.19	0.11	0.11	0.11	0.11
Q1 (25%)	−0.03	−0.02	−0.804	−0.21	25.3	25.3	25.13	25.1
Q2 (50%)	0.0	0.0	0.112	0.04	36.51	36.51	36.34	36.34
Q3 (75%)	0.04	0.02	1.133	0.33	46.38	46.4	46.2	46.2
Max	0.36	0.45	33.353	32.13	59.36	59.36	59.23	59.14

Table 5.19. Statistical properties of the aggressive scenario with all passenger seats occupied when assessing the influence of passenger distribution on the performance of the developed model.

	a_{long} [g]	a_{lat} [g]	$\dot{\Phi}$ [°/s]	δ [°]	v_{FL} [km/h]	v_{FR} [km/h]	v_{RR} [km/h]	v_{RL} [km/h]
Mean	0.0	0.04	2.671	0.79	35.37	35.63	35.05	35.3
Std	0.15	0.39	20.759	7.11	10.08	10.04	10.17	10.1
Min	−0.55	−0.85	−65.94	−33.33	0.11	0.11	0.11	0.11
Q1 (25%)	−0.08	−0.25	−10.848	−2.8	30.71	30.62	30.35	30.28
Q2 (50%)	0.0	0.03	1.968	0.5	37.22	37.65	36.95	37.38
Q3 (75%)	0.1	0.36	17.194	4.08	42.79	42.79	42.56	42.49
Max	0.44	0.86	69.896	33.03	55.67	56.14	55.69	56.02

Table 5.20. Statistical properties of the calm scenario with all passenger seats occupied when assessing the influence of passenger distribution on the performance of the developed model.

	a_{long} [g]	a_{lat} [g]	$\dot{\Phi}$ [°/s]	δ [°]	v_{FL} [km/h]	v_{FR} [km/h]	v_{RR} [km/h]	v_{RL} [km/h]
Mean	0.02	0.04	2.635	0.67	35.54	35.8	35.36	35.61
Std	0.06	0.26	14.321	4.61	7.76	7.72	7.81	7.75
Min	−0.28	−0.6	−41.058	−18.79	0.11	0.11	0.11	0.11
Q1 (25%)	−0.01	−0.14	−6.618	−1.61	31.84	32.1	31.64	31.9
Q2 (50%)	0.01	0.03	1.765	0.35	37.28	37.14	37.17	36.98
Q3 (75%)	0.05	0.26	12.269	2.82	40.98	41.04	40.87	40.89
Max	0.17	0.66	54.635	25.35	48.35	48.39	48.25	48.31

Table 5.21. Statistical properties of the city scenario with all passenger seats occupied when assessing the influence of passenger distribution on the performance of the developed model.

	a_{long} [g]	a_{lat} [g]	$\dot{\Phi}$ [°/s]	δ [°]	v_{FL} [km/h]	v_{FR} [km/h]	v_{RR} [km/h]	v_{RL} [km/h]
Mean	0.02	0.0	−0.009	0.01	38.91	38.92	38.76	38.76
Std	0.07	0.07	5.63	3.5	14.3	14.27	14.3	14.26
Min	−0.3	−0.39	−31.592	−30.45	0.11	0.11	0.11	0.11
Q1 (25%)	0.0	−0.01	−0.838	−0.25	31.17	31.14	31.03	31.01
Q2 (50%)	0.02	0.0	−0.154	−0.04	42.99	42.97	42.85	42.82
Q3 (75%)	0.05	0.01	0.349	0.08	49.92	49.92	49.77	49.75
Max	0.26	0.47	32.112	32.98	60.28	60.24	60.08	60.05

Table 5.22. Statistical properties of the agressive scenario with the front left tire pressure decreased to 1.5 bar when assessing the influence of tire pressure on the performance of the developed model.

	a_{long} [g]	a_{lat} [g]	$\dot{\Phi}$ [°/s]	δ [°]	v_{FL} [km/h]	v_{FR} [km/h]	v_{RR} [km/h]	v_{RL} [km/h]
Mean	−0.03	0.01	0.897	−0.05	34.58	34.6	34.19	34.25
Std	0.13	0.35	19.303	7.19	7.85	8.0	7.95	8.17
Min	−0.82	−1.05	−68.528	−32.75	0.11	0.11	0.11	0.11
Q1 (25%)	−0.07	−0.18	−7.822	−2.14	29.7	29.97	29.38	29.64
Q2 (50%)	−0.02	0.0	0.509	0.15	35.75	35.67	35.44	35.38
Q3 (75%)	0.02	0.23	11.797	3.14	40.55	40.54	40.17	40.27
Max	0.44	0.87	54.943	23.61	52.56	52.61	52.39	52.5

Table 5.23. Statistical properties of the calm scenario with the front left tire pressure decreased to 1.5 bar when assessing the influence of tire pressure on the performance of the developed model.

	a_{long} [g]	a_{lat} [g]	$\dot{\Phi}$ [°/s]	δ [°]	v_{FL} [km/h]	v_{FR} [km/h]	v_{RR} [km/h]	v_{RL} [km/h]
Mean	−0.01	0.02	2.077	0.71	34.5	34.62	34.25	34.42
Std	0.05	0.19	11.244	3.62	6.48	6.23	6.5	6.24
Min	−0.28	−0.53	−27.848	−8.58	0.11	0.11	0.11	0.11
Q1 (25%)	−0.03	−0.12	−5.414	−1.4	31.16	31.11	30.92	30.92
Q2 (50%)	−0.01	0.0	0.626	0.16	35.0	34.91	34.79	34.73
Q3 (75%)	0.01	0.14	7.678	1.93	39.02	38.88	38.79	38.7
Max	0.17	0.52	46.741	21.46	49.92	50.43	49.61	50.35

Table 5.24. Statistical properties of the city scenario with the front left tire pressure decreased to 1.5 bar when assessing the influence of tire pressure on the performance of the developed model.

	a_{long} [g]	a_{lat} [g]	$\dot{\Phi}$ [°/s]	δ [°]	v_{FL} [km/h]	v_{FR} [km/h]	v_{RR} [km/h]	v_{RL} [km/h]
Mean	0.0	−0.01	−0.053	−0.02	35.79	35.66	35.47	35.44
Std	0.07	0.07	5.714	2.95	13.25	13.22	13.18	13.19
Min	−0.39	−0.54	−41.178	−32.17	0.11	0.11	0.11	0.11
Q1 (25%)	−0.04	−0.02	−0.658	−0.18	27.89	27.74	27.6	27.52
Q2 (50%)	0.0	0.0	0.049	0.02	40.6	40.46	40.27	40.22
Q3 (75%)	0.03	0.01	0.704	0.19	45.72	45.61	45.35	45.37
Max	0.33	0.44	36.903	26.12	55.48	55.15	55.41	55.69

Table 5.25. Statistical properties of the agressive scenario with the front right tire pressure decreased to 1.5 bar when assessing the influence of tire pressure on the performance of the developed model.

	a_{long} [g]	a_{lat} [g]	$\dot{\Phi}$ [°/s]	δ [°]	v_{FL} [km/h]	v_{FR} [km/h]	v_{RR} [km/h]	v_{RL} [km/h]
Mean	−0.04	0.04	3.211	0.88	32.79	33.12	32.4	32.7
Std	0.14	0.36	21.285	8.3	7.86	7.87	8.02	8.02
Min	−0.57	−0.87	−63.503	−33.24	0.11	0.11	0.11	0.11
Q1 (25%)	−0.09	−0.17	−7.605	−2.03	27.72	27.83	27.4	27.35
Q2 (50%)	−0.02	0.01	1.496	0.39	32.94	33.64	32.59	33.3
Q3 (75%)	0.03	0.29	15.982	4.57	38.2	38.54	37.94	38.22
Max	0.42	0.88	67.919	33.17	53.36	53.12	53.25	52.79

Table 5.26. Statistical properties of the calm scenario with the front right tire pressure decreased to 1.5 bar when assessing the influence of tire pressure on the performance of the developed model.

	a_{long} [g]	a_{lat} [g]	$\dot{\Phi}$ [°/s]	δ [°]	v_{FL} [km/h]	v_{FR} [km/h]	v_{RR} [km/h]	v_{RL} [km/h]
Mean	−0.02	0.0	0.925	0.37	33.26	33.38	33.04	33.1
Std	0.06	0.23	14.199	4.94	7.63	7.53	7.67	7.55
Min	−0.32	−0.61	−49.055	−24.24	0.11	0.11	0.11	0.11
Q1 (25%)	−0.04	−0.15	−7.119	−1.98	28.93	28.75	28.67	28.48
Q2 (50%)	−0.01	0.0	0.194	0.08	34.07	34.11	33.88	33.86
Q3 (75%)	0.01	0.15	7.373	1.9	38.62	38.41	38.42	38.17
Max	0.19	0.64	46.441	24.01	48.84	48.06	48.58	47.87

Table 5.27. Statistical properties of the city scenario with the front right tire pressure decreased to 1.5 bar when assessing the influence of tire pressure on the performance of the developed model.

	a_{long} [g]	a_{lat} [g]	$\dot{\Phi}$ [°/s]	δ [°]	v_{FL} [km/h]	v_{FR} [km/h]	v_{RR} [km/h]	v_{RL} [km/h]
Mean	−0.01	0.0	0.173	0.08	33.98	34.09	33.75	33.77
Std	0.08	0.07	4.857	2.5	15.4	15.44	15.33	15.33
Min	−0.4	−0.46	−34.566	−19.26	0.11	0.11	0.11	0.11
Q1 (25%)	−0.04	−0.02	−0.586	−0.18	22.56	22.8	22.36	22.55
Q2 (50%)	0.0	0.0	0.017	0.0	38.42	38.54	38.19	38.2
Q3 (75%)	0.02	0.01	0.686	0.18	46.29	46.51	46.02	46.11
Max	0.37	0.45	37.786	27.83	57.58	58.49	58.38	58.66

Table 5.28. Statistical properties of the agressive scenario with the rear left tire pressure decreased to 1.5 bar when assessing the influence of tire pressure on the performance of the developed model.

	a_{long} [g]	a_{lat} [g]	$\dot{\Phi}$ [°/s]	δ [°]	v_{FL} [km/h]	v_{FR} [km/h]	v_{RR} [km/h]	v_{RL} [km/h]
Mean	−0.04	0.02	1.609	0.29	36.5	36.64	36.22	36.28
Std	0.1	0.43	22.37	7.21	8.16	8.18	8.25	8.26
Min	−0.61	−0.88	−58.355	−31.4	0.11	0.11	0.11	0.11
Q1 (25%)	−0.09	−0.31	−14.623	−3.98	32.93	33.14	32.67	32.76
Q2 (50%)	−0.03	0.01	1.107	0.29	37.64	37.61	37.4	37.17
Q3 (75%)	0.02	0.38	18.181	4.77	42.27	42.34	42.03	42.06
Max	0.31	0.91	55.232	23.06	52.56	53.54	52.7	53.56

Table 5.29. Statistical properties of the calm scenario with the rear left tire pressure decreased to 1.5 bar when assessing the influence of tire pressure on the performance of the developed model.

	a_{long} [g]	a_{lat} [g]	$\dot{\Phi}$ [°/s]	δ [°]	v_{FL} [km/h]	v_{FR} [km/h]	v_{RR} [km/h]	v_{RL} [km/h]
Mean	−0.02	0.0	0.487	0.03	33.24	33.27	33.09	33.05
Std	0.05	0.24	14.467	5.01	8.27	8.31	8.32	8.34
Min	−0.23	−0.49	−35.85	−18.51	0.11	0.11	0.11	0.11
Q1 (25%)	−0.04	−0.2	−10.779	−3.01	29.42	29.49	29.26	29.25
Q2 (50%)	−0.01	0.0	0.669	0.17	34.02	34.04	33.9	33.82
Q3 (75%)	0.01	0.21	11.157	2.9	38.61	38.36	38.54	38.18
Max	0.21	0.51	43.541	20.34	49.76	50.75	49.61	50.58

Table 5.30. Statistical properties of the city scenario with the rear left tire pressure decreased to 1.5 bar when assessing the influence of tire pressure on the performance of the developed model.

	a_{long} [g]	a_{lat} [g]	$\dot{\Phi}$ [°/s]	δ [°]	v_{FL} [km/h]	v_{FR} [km/h]	v_{RR} [km/h]	v_{RL} [km/h]
Mean	−0.01	−0.01	−0.231	−0.09	34.53	34.52	34.45	34.3
Std	0.08	0.07	5.798	3.1	15.48	15.46	15.49	15.41
Min	−0.45	−0.42	−36.98	−22.17	0.11	0.11	0.11	0.11
Q1 (25%)	−0.04	−0.03	−1.018	−0.35	24.47	24.84	24.35	24.59
Q2 (50%)	−0.01	0.0	−0.203	−0.06	38.99	38.97	38.92	38.73
Q3 (75%)	0.03	0.01	0.44	0.12	47.28	47.3	47.18	47.03
Max	0.35	0.42	32.993	22.58	59.01	59.03	59.03	58.81

Table 5.31. Statistical properties of the agressive scenario with the rear right tire pressure decreased to 1.5 bar when assessing the influence of tire pressure on the performance of the developed model.

	a_{long} [g]	a_{lat} [g]	$\dot{\Phi}$ [°/s]	δ [°]	v_{FL} [km/h]	v_{FR} [km/h]	v_{RR} [km/h]	v_{RL} [km/h]
Mean	−0.05	0.06	4.942	1.7	31.25	31.69	30.75	31.28
Std	0.22	0.4	23.881	8.43	9.43	9.36	9.52	9.45
Min	−0.86	−0.99	−60.129	−24.42	0.11	0.11	0.11	0.11
Q1 (25%)	−0.17	−0.14	−9.058	−2.7	25.37	26.15	24.66	25.6
Q2 (50%)	−0.03	0.02	1.173	0.41	32.41	33.14	31.92	32.72
Q3 (75%)	0.12	0.4	24.895	7.87	37.93	38.0	37.57	37.73
Max	0.38	0.83	60.295	29.03	53.59	53.63	53.66	53.58

Table 5.32. Statistical properties of the calm scenario with the rear right tire pressure decreased to 1.5 bar when assessing the influence of tire pressure on the performance of the developed model.

	a_{long} [g]	a_{lat} [g]	$\dot{\Phi}$ [°/s]	δ [°]	v_{FL} [km/h]	v_{FR} [km/h]	v_{RR} [km/h]	v_{RL} [km/h]
Mean	−0.01	0.05	3.214	0.96	33.38	33.68	33.14	33.51
Std	0.09	0.22	13.214	4.4	8.62	8.59	8.64	8.63
Min	−0.35	−0.66	−35.584	−12.56	0.11	0.11	0.11	0.11
Q1 (25%)	−0.06	−0.06	−3.355	−0.9	28.34	28.24	28.04	28.03
Q2 (50%)	0.0	0.04	2.114	0.56	34.12	34.58	33.91	34.41
Q3 (75%)	0.05	0.21	12.209	3.34	39.9	39.99	39.69	39.87
Max	0.2	0.53	44.779	20.13	50.7	50.96	50.5	51.01

Table 5.33. Statistical properties of the city scenario with the rear right tire pressure decreased to 1.5 bar when assessing the influence of tire pressure on the performance of the developed model.

	a_{long} [g]	a_{lat} [g]	$\dot{\Phi}$ [°/s]	δ [°]	v_{FL} [km/h]	v_{FR} [km/h]	v_{RR} [km/h]	v_{RL} [km/h]
Mean	0.0	0.0	0.156	−0.09	35.28	35.3	35.09	35.21
Std	0.07	0.08	6.068	3.35	15.24	15.25	15.21	15.26
Min	−0.31	−0.55	−36.125	−33.25	0.11	0.11	0.11	0.11
Q1 (25%)	−0.03	−0.02	−0.827	−0.26	25.13	25.57	24.89	25.38
Q2 (50%)	0.0	0.0	−0.046	−0.01	40.27	40.32	40.09	40.25
Q3 (75%)	0.03	0.01	0.804	0.22	47.52	47.64	47.3	47.56
Max	0.3	0.55	37.189	23.83	57.88	58.44	57.64	57.83

Bibliography

[1] P. V. Teixeira, D. Raposo, R. Lopes, and S. Sargento, "Deterministic and reliable software-defined vehicles: Key building blocks, challenges, and vision," 2025. [Online]. Available: https://arxiv.org/abs/2407.17287

[2] B. Frieske, S. Hasselwander, O. Deniz, S. Stieler, and S. Schumich, "Scenario-based analysis of electrification effects on value creation and employment structures for the automotive industry in the federal state of baden-wuerttemberg, germany," *World Electric Vehicle Journal*, vol. 15, no. 10, 2024. [Online]. Available: https://www.mdpi.com/2032-6653/15/10/480

[3] M. Yu, S. A. Evangelou, and D. Dini, "Advances in active suspension systems for road vehicles," *Engineering*, vol. 33, pp. 160–177, 2024. [Online]. Available: https://www.sciencedirect.com/science/article/pii/S2095809923003983

[4] D.-S. Yoon and S.-B. Choi, "Adaptive control for suspension system of in-wheel motor vehicle with magnetorheological damper," *Machines*, vol. 12, no. 7, 2024. [Online]. Available: https://www.mdpi.com/2075-1702/12/7/433

[5] I. Dridi, A. Hamza, and N. B. Yahia, "A new approach to controlling an active suspension system based on reinforcement learning," *Advances in Mechanical Engineering*, vol. 15, no. 6, p. 16878132231180480, 2023. [Online]. Available: https://doi.org/10.1177/16878132231180480

[6] A. E. Thomas, P. S. Bauer, M. Dam, V. Perraud, L. M. Wingen, and J. N. Smith, "Automotive braking is a source of highly charged aerosol particles," *Proceedings of the National Academy of Sciences of the United States of America*, vol. 121, 2024. [Online]. Available: https://api.semanticscholar.org/CorpusID:268362404

[7] C. Li, L. Zhang, S. Lian, and M. Liu, "Research on regenerative braking control of electric vehicles based on game theory optimization," *Science Progress*, vol. 107, 2024. [Online]. Available: https://api.semanticscholar.org/CorpusID:269612725

[8] P. Śliż and E. Wycinka, "Identification of factors that differentiate motor vehicles that have experienced wear or failure of brake system components during the warranty

service period," *Eksploatacja I Niezawodnosc-maintenance and Reliability*, vol. 23, pp. 430–442, 2021. [Online]. Available: https://api.semanticscholar.org/CorpusID:236334386

[9] D. Khorasani-Zavareh, S. Shoar, and S. Saadat, "Antilock braking system effectiveness in prevention of road traffic crashes in iran," *BMC Public Health*, vol. 13, pp. 439 – 439, 2013. [Online]. Available: https://api.semanticscholar.org/CorpusID:18523468

[10] A. Lie, C. Tingvall, M. Krafft, and A. Kullgren, "The effectiveness of esc (electronic stability control) in reducing real life crashes and injuries," 2005. [Online]. Available: https://api.semanticscholar.org/CorpusID:40433087

[11] J. Betancur, A. Castillo, E. Ramos *et al.*, "Diagnostic methodology for vehicles equipped with antilock braking system and electronic stability control," *Discovery Applied Science*, vol. 6, p. 452, 2024. [Online]. Available: https://doi.org/10.1007/s42452-024-06069-9

[12] V. Guarenghi, R. Pizzi, A. Depetris, and G. Pinto, "Analysis of road safety implementation strategies to support the easiest introduction of autonomous braking products for complex vehicle combinations," SAE International, Tech. Rep. 2024-36-0319, 2024. [Online]. Available: https://www.sae.org/publications/technical-papers/content/2024-36-0319/

[13] S. Guo, J. Guo, Y. Zhang, and J. Wu, "Tire-road friction estimation based on adaptive unscented kalman filter and burckhardt model under braking conditions," Huazhong University of Science and Technology, Tech. Rep. 2024-01-2331, 2024. [Online]. Available: https://doi.org/10.4271/2024-01-2331

[14] S. Di Cairano, C. Guardiola, A. A. Malikopoulos, and J. B. Siegel, "Future impact and challenges of automotive control," in *The Impact of Automatic Control Research on Industrial Innovation*, 2024, ch. 4, pp. 85–133. [Online]. Available: https://onlinelibrary.wiley.com/doi/abs/10.1002/9781119983644.ch4

[15] R. Rajamani, *Vehicle Dynamics and Control*, 2nd ed., ser. Mechanical Engineering Series. Springer, 2012. [Online]. Available: https://link.springer.com/book/10.1007/978-3-642-39440-9

[16] W. Zhang, J. Li, X. Wang, and H. Chen, "A review of longitudinal/lateral integrated control technology for in-wheel motor electric vehicles," *Proceedings of the Institution of Mechanical Engineers, Part D: Journal of Automobile Engineering*, 2025. [Online]. Available: https://doi.org/10.1177/09544070251316635

[17] P. Sinha, "Architectural design and reliability analysis of a fail-operational brake-by-wire system from iso 26262 perspectives," *Reliability Engineering & System Safety*, vol. 96, no. 10, pp. 1349–1359, 2011. [Online]. Available: https://www.sciencedirect.com/science/article/pii/S095183201100041X

[18] X. Jin, G. Yin, and N. Chen, "Advanced estimation techniques for vehicle system dynamic state: A survey," *Sensors*, vol. 19, no. 19, 2019. [Online]. Available: https://www.mdpi.com/1424-8220/19/19/4289

[19] M. Essa and T. Sayed, "Traffic conflict models to evaluate the safety of signalized intersections at the cycle level," *Transportation Research Part C: Emerging Technologies*, vol. 89, pp. 289–302, 2018. [Online]. Available: https://www.sciencedirect.com/science/article/pii/S0968090X18302249

[20] L. Cui, J. Hu, B. Park, and P. Bujanovic, "Development of a simulation platform for safety impact analysis considering vehicle dynamics, sensor errors, and communication latencies: Assessing cooperative adaptive cruise control under cyber attack," *Transportation Research Part C Emerging Technologies*, vol. 97, 12 2018.

[21] Y. Wang and P. Xie, "Ai-based finite-element simulation automation workflow applied to automotive electronics field," in *2024 25th International Conference on Electronic Packaging Technology (ICEPT)*, 2024, pp. 1–5.

[22] L. Yao, Q. Feng, D. Wan, L. Wu, K. Yang, J. Hou, B. Liu, and Q. Wan, "Experiment and finite element simulation of high strength steel adhesive joint reinforced by rivet for automotive applications," *Journal of Adhesion Science and Technology*, vol. 31, no. 14, pp. 1617–1625, 2017. [Online]. Available: https://doi.org/10.1080/01694243.2016.1266845

[23] Y. Zhuang, J. Zhang, and M. Tu, "Long-range sequence modeling with predictable sparse attention," pp. 234–243, 2022.

[24] H. G. Souto, "Charting new avenues in financial forecasting with timesnet: The impact of intraperiod and interperiod variations on realized volatility prediction," *Expert Systems with Applications*, vol. 255, p. 124851, 2024. [Online]. Available: https://consensus.app/papers/charting-new-avenues-in-financial-forecasting-with-souto/ffc1f493be91584c9453a9e0e7fdfc79/?utm_source=chatgpt

[25] C. Zhang, Y. Wang, Y. Fu, X. Qiao, M. S. Nazir, and T. Peng, "A novel dwtimesnet-based short-term multi-step wind power forecasting model using feature selection and auto-tuning methods," *Energy Conversion and Management*, 2024. [Online]. Available: https://consensus.app/

papers/a-novel-dwtimesnetbased-shortterm-multistep-wind-power-zhang-wang/e4891673518e530993424f22d12ca1e6/?utm_source=chatgpt

[26] L. Hou, S. Li, B. Yang, Z. Wang, and K. Nakano, "Structural transformer improves speed-accuracy trade-off in interactive trajectory prediction of multiple surrounding vehicles," *IEEE Transactions on Intelligent Transportation Systems*, vol. 23, pp. 24 778–24 790, 2022.

[27] J. Wang, J. Zhou, and D. Xu, "A real-time predictive energy management strategy of fuel cell/battery/ ultra-capacitor hybrid energy storage system in electric vehicle," *2020 Chinese Automation Congress (CAC)*, pp. 3951–3954, 2020.

[28] F. D. Keles, P. M. Wijewardena, and C. Hegde, "On the computational complexity of self-attention," pp. 597–619, 2022.

[29] E. A. Etukudoh, S. Sonko, K. I. Ibekwe, V. I. Ilojianya, and C. D. Daudu, "A comprehensive review of embedded systems in autonomous vehicles: Trends, challenges, and future directions," *World Journal of Advanced Research and Reviews*, 2024.

[30] A. Björklund, A. Henelius, E. Oikarinen, K. Kallonen, and K. Puolamäki, "Explaining any black box model using real data," *Frontiers in Computer Science*, vol. 5, 2023. [Online]. Available: https://www.frontiersin.org/articles/10.3389/fcomp.2023.1143904/full

[31] F. Jiménez, "Sensors for road vehicles of the future," *Sensors*, vol. 23, no. 1, 2023. [Online]. Available: https://www.mdpi.com/1424-8220/23/1/22

[32] X. Gong, L. Qian, W. Ge, and J. Yan, "Research on electronic brake force distribution and anti-lock brake of vehicle based on direct drive electro hydraulic actuator," *International Journal of Automotive Engineering*, vol. 11, no. 2, pp. 220–226, 2020.

[33] R. Attia, R. Orjuela, and M. Basset, "Combined longitudinal and lateral control for automated vehicle guidance," *Vehicle System Dynamics*, vol. 52, pp. 261 – 279, 2014.

[34] Y. Huang and Y. Chen, "Vehicle lateral stability control based on shiftable stability regions and dynamic margins," *IEEE Transactions on Vehicular Technology*, vol. 69, pp. 14 727–14 738, 2020.

[35] D. Xu, Z. Zhu, C. Liu, Y. Wang, S. xi Zhao, L. Zhang, H. Liang, H. Li, and K.-T. Cheng, "Reliability evaluation and analysis of fpga-based neural network acceleration system," *IEEE Transactions on Very Large Scale Integration (VLSI) Systems*, vol. 29, pp. 472–484, 2021.

[36] A. Isbitirici, L. Giarré, W. Xu, and P. Falcone, "Lstm-based virtual load sensor for heavy-duty vehicles," *Sensors (Basel, Switzerland)*, vol. 24, 2023.

[37] C. M. Nguyen, A. Nguyen, and S. Delprat, "Neural-network-based fuzzy observer with data-driven uncertainty identification for vehicle dynamics estimation under extreme driving conditions: Theory and experimental results," *IEEE Transactions on Vehicular Technology*, vol. 72, pp. 8686–8696, 2023.

[38] B. Paden, M. Čáp, S. Z. Yong, D. Yershov, and E. Frazzoli, "A survey of motion planning and control techniques for self-driving urban vehicles," *IEEE Transactions on Intelligent Vehicles*, vol. 1, no. 1, pp. 33–55, 2016.

[39] S. Azadi, R. Kazemi, and H. R. Nedamani, "Chapter 8 - directional stability analysis and integrated control of articulated heavy vehicles," in *Vehicle Dynamics and Control*, S. Azadi, R. Kazemi, and H. R. Nedamani, Eds. Elsevier, 2021, pp. 319–375.

[40] R. Rajamani, *Vehicle Dynamics and Control*, ser. Mechanical Engineering Series. Springer New York, NY, 2012.

[41] A. Rezaeian, A. Khajepour, W. Melek, S.-K. Chen, and N. Moshchuk, "Simultaneous vehicle real-time longitudinal and lateral velocity estimation," *IEEE Transactions on Vehicular Technology*, vol. 66, no. 3, pp. 1950–1962, 2017.

[42] L.-H. Zhao, Z.-Y. Liu, and H. Chen, "Design of a nonlinear observer for vehicle velocity estimation and experiments," *IEEE Transactions on Control Systems Technology*, vol. 19, no. 3, pp. 664–672, 2011.

[43] R. Rajamani, *Vehicle dynamics and control*. Springer Science & Business Media, 2011.

[44] X. Li, N. Xu, Q. Li, K. Guo, and J. Zhou, "A fusion methodology for sideslip angle estimation on the basis of kinematics-based and model-based approaches," *Proceedings of the Institution of Mechanical Engineers, Part D: Journal of Automobile Engineering*, vol. 234, no. 7, pp. 1930–1943, 2020.

[45] S. Rutherford and D. Cole, "Modelling nonlinear vehicle dynamics with neural networks," *International Journal of Vehicle Design - INT J VEH DES*, vol. 53, 07 2010.

[46] D. Chindamo and M. Gadola, "Estimation of vehicle side-slip angle using an artificial neural network," *MATEC Web of Conferences*, vol. 166, p. 02001, 2018. [Online]. Available: https://doi.org/10.1051/matecconf/201816602001

[47] J. Zhang, B. Zhang, and Z. Yang, "Investigation on lateral acceleration prediction of tilting passenger car based on neural networks," in *2010 Sixth International Conference on Natural Computation*, vol. 1, 2010, pp. 349–352.

[48] D. Kong, W. Wen, R. Zhao, Z. Lv, K. Liu, Y. Liu, and Z. Gao, "Vehicle lateral velocity estimation based on long short-term memory network," *World Electric Vehicle Journal*, vol. 13, no. 1, 2022. [Online]. Available: https://www.mdpi.com/2032-6653/13/1/1

[49] A. Graves, *Supervised Sequence Labelling with Recurrent Neural Networks*, ser. Studies in computational intelligence. Berlin: Springer, 2012. [Online]. Available: https://cds.cern.ch/record/1503877

[50] G. Napolitano Dell'Annunziata, V. M. Arricale, F. Farroni, A. Genovese, N. Pasquino, and G. Tranquillo, "Estimation of vehicle longitudinal velocity with artificial neural network," *Sensors*, vol. 22, no. 23, 2022. [Online]. Available: https://www.mdpi.com/1424-8220/22/23/9516

[51] Y. Zou, L. Ding, H. Zhang, T. Zhu, and L. Wu, "Vehicle acceleration prediction based on machine learning models and driving behavior analysis," *Applied Sciences*, vol. 12, no. 10, 2022. [Online]. Available: https://www.mdpi.com/2076-3417/12/10/5259

[52] T. Ono, R. Eto, and J. Yamakawa, "Forecasting vehicle accelerations using lstm," *Mechanical Engineering Journal*, vol. 8, 06 2021.

[53] A. Géron, *Hands-on machine learning with Scikit-Learn, Keras, and TensorFlow: Concepts, tools, and techniques to build intelligent systems*. " O'Reilly Media, Inc.", 2019.

[54] D. P. Kingma and J. Ba, "Adam: A method for stochastic optimization," 2014, cite arxiv:1412.6980Comment: Published as a conference paper at the 3rd International Conference for Learning Representations, San Diego, 2015. [Online]. Available: http://arxiv.org/abs/1412.6980

[55] J. Kontos, B. Kranicz, and A. Vathy-Fogarassy, "Neural network-based prediction for lateral acceleration of vehicles," in *2022 IEEE 2nd Conference on Information Technology and Data Science (CITDS)*, 2022, pp. 153–158.

[56] D. P. Kingma and J. Ba, "Adam: A method for stochastic optimization," in *Proceedings of the 3rd International Conference on Learning Representations (ICLR)*, 2015. [Online]. Available: https://arxiv.org/abs/1412.6980

[57] ISO 26262:2018, "Road vehicles – functional safety," International Organization for Standardization, Geneva, CH, Standard, 2018.

[58] J. Jagelčák, J. Gnap, O. Kuba, J. Frnda, and M. Kostrzewski, "Determination of turning radius and lateral acceleration of vehicle by gnss/ins sensor," *Sensors*, vol. 22, no. 6, 2022. [Online]. Available: https://www.mdpi.com/1424-8220/22/6/2298

[59] J. Matuško, I. Petrović, and N. Perić, "Neural network based tire/road friction force estimation," *Engineering Applications of Artificial Intelligence*, vol. 21, no. 3, pp. 442–456, 2008.

[60] M. Fazekas and P. Gáspár, "Wheel odometry model calibration with neural network-based weighting," *Engineering Applications of Artificial Intelligence*, vol. 134, p. 108631, 2024.

[61] X. Xia, L. Xiong, Y. Huang, Y. Lu, L. Gao, N. Xu, and Z. Yu, "Estimation on imu yaw misalignment by fusing information of automotive onboard sensors," *Mechanical Systems and Signal Processing*, vol. 162, p. 107993, 2022.

[62] H. Zhu, L. Li, M. Jin, H. Li, and J. Song, "Real-time yaw rate prediction based on a non-linear model and feedback compensation for vehicle dynamics control," *Proceedings of the Institution of Mechanical Engineers, Part D: Journal of Automobile Engineering*, vol. 227, no. 10, pp. 1431–1445, 2013.

[63] Y. Huang, J. Du, Z. Yang, Z. Zhou, L. Zhang, and H. Chen, "A survey on trajectory-prediction methods for autonomous driving," *IEEE Transactions on Intelligent Vehicles*, vol. 7, no. 3, pp. 652–674, 2022.

[64] Y. Wiseman, "Autonomous vehicles," in *Encyclopedia of Information Science and Technology, Fifth Edition*, M. Khosrow-Pour, Ed. IGI Global Scientific Publishing, 2021, pp. 1–11. [Online]. Available: https://doi.org/10.4018/978-1-7998-3479-3.ch001

[65] B. Lenzo, *Vehicle Dynamics: Fundamentals and Ultimate Trends*, ser. CISM International Centre for Mechanical Sciences. Springer International Publishing, 2021.

[66] L. S. Brown and D. M. Bevly, "Roll and bank estimation using gps/ins and suspension deflections," *Electronics*, vol. 4, no. 1, pp. 118–149, 2015. [Online]. Available: https://www.mdpi.com/2079-9292/4/1/118

[67] Y. Li, J. Zhang, T. Fei, N. Cui, and Y. Shang, "Single antenna gps carrier amplitude based rolling angle determination," in *Proceedings of 2014 IEEE Chinese Guidance, Navigation and Control Conference*, 2014, pp. 206–211.

[68] H. Guo, D. Cao, H. Chen, C. Lv, H. Wang, and S. Yang, "Vehicle dynamic state estimation: state of the art schemes and perspectives," *IEEE/CAA Journal of Automatica Sinica*, vol. 5, pp. 418–431, 2018.

[69] X. Jin, G. Yin, and N. Chen, "Advanced estimation techniques for vehicle system dynamic state: A survey," *Sensors*, vol. 19, no. 19, 2019.

[70] G. Xu, M. Chen, X. He, Y. Liu, J. Wu, and P. Diao, "Research on state-parameter estimation of unmanned tractor—a hybrid method of dekf and arbfnn," *Engineering Applications of Artificial Intelligence*, vol. 127, p. 107402, 2024.

[71] M. Kamal Mazhar, M. J. Khan, A. I. Bhatti, and N. Naseer, "A novel roll and pitch estimation approach for a ground vehicle stability improvement using a low cost imu," *Sensors*, vol. 20, no. 2, 2020.

[72] D. Selmanaj, M. Corno, G. Panzani, and S. M. Savaresi, "On vehicle pitch estimation via solid-state lidar," *IFAC-PapersOnLine*, vol. 53, no. 2, pp. 13 904–13 909, 2020, 21st IFAC World Congress.

[73] D. Fényes, T. Hegedus, B. Németh, and P. Gáspár, "Robust control design for autonomous vehicles using neural network-based model-matching approach," *Energies*, vol. 14, no. 21, 2021.

[74] R. Cespi, S. Di Gennaro, B. Castillo-Toledo, J. C. Romero-Aragon, and R. A. Ramírez-Mendoza, "Neural network inverse optimal control of ground vehicles," *Neural Processing Letters*, vol. 55, no. 8, pp. 10 287–10 313, Dec 2023.

[75] A. Wasala, D. Byrne, P. Miesbauer, J. O'Hanlon, P. Heraty, and P. Barry, "Trajectory based lateral control: A reinforcement learning case study," *Engineering Applications of Artificial Intelligence*, vol. 94, p. 103799, 2020.

[76] O. A. Stepanov, Y. A. Litvinenko, D. V. Antonov, and O. V. Zaitsev, "Adaptive algorithm for vessel roll prediction based on the bayesian approach," in *2022 30th Mediterranean Conference on Control and Automation (MED)*, 2022, pp. 713–718.

[77] R. Salay, R. Queiroz, and K. Czarnecki, "An analysis of iso 26262: Using machine learning safely in automotive software," *SAE Technical Paper*, 09 2017.

[78] K. Yurii and G. Liudmila, "Application of artificial neural networks in vehicles' design self-diagnostic systems for safety reasons," *Transportation Research Procedia*, vol. 20, pp. 283–287, 2017, 12th International Conference "Organization and Traffic Safety Management in large cities", SPbOTSIC-2016, 28-30 September 2016, St. Petersburg, Russia.

[79] D. Chindamo and M. Gadola, "Estimation of vehicle side-slip angle using an artificial neural network," *MATEC Web of Conferences*, vol. 166, p. 02001, 2018.

[80] N. Spielberg, M. Brown, N. Kapania, J. Kegelman, and J. Gerdes, "Neural network vehicle models for high-performance automated driving," *Science Robotics*, vol. 4, p. eaaw1975, 03 2019.

[81] V. Karri and D. Butler, "Using artificial neural networks to predict vehicle acceleration and yaw angles," in *Proceedings of the 9th International Conference on Neural Information Processing, 2002. ICONIP '02.*, vol. 4, 2002, pp. 1915–1919 vol.4.

[82] L. Hermansdorfer, R. Trauth, J. Betz, and M. Lienkamp, "End-to-end neural network for vehicle dynamics modeling," in *2020 6th IEEE Congress on Information Science and Technology (CiSt)*, 2020, pp. 407–412.

[83] L. P. González, S. S. Sánchez, J. Garcia-Guzman, M. J. L. Boada, and B. L. Boada, "Simultaneous estimation of vehicle roll and sideslip angles through a deep learning approach," *Sensors*, vol. 20, no. 13, 2020. [Online]. Available: https://www.mdpi.com/1424-8220/20/13/3679

[84] B. L. Boada, M. J. L. Boada, L. Vargas-Melendez, and V. Diaz, "A robust observer based on h∞ filtering with parameter uncertainties combined with neural networks for estimation of vehicle roll angle," *Mechanical Systems and Signal Processing*, vol. 99, pp. 611–623, 2018. [Online]. Available: https://www.sciencedirect.com/science/article/pii/S0888327017303631

[85] C. Novara, F. Ruiz, and M. Milanese, "Direct identification of optimal sm-lpv filters and application to vehicle yaw rate estimation," *IEEE Transactions on Control Systems Technology*, vol. 19, no. 1, pp. 5–17, 2011.

[86] X. Sun, Y. Wang, and W. Hu, "Estimation of longitudinal force, sideslip angle and yaw rate for four-wheel independent actuated autonomous vehicles based on pwa tire model," *Sensors*, vol. 22, no. 9, 2022.

[87] H. Ben Moussa and M. Bakhti, "Extended kalman filter based lateral velocity and yaw rate estimation for a vehicle with nonlinear tire model," in *Automatic Control and Emerging Technologies*, H. El Fadil and W. Zhang, Eds. Singapore: Springer Nature Singapore, 2024, pp. 618–629.

[88] G. Baffet, A. Charara, D. Lechner, and D. Thomas, "Experimental evaluation of observers for tire–road forces, sideslip angle and wheel cornering stiffness," *Vehicle System Dynamics*, vol. 46, no. 6, pp. 501–520, 2008.

[89] F. Zhang, Y. Wang, J. Hu, G. Yin, S. Chen, H. Zhang, and D. Zhou, "A novel comprehensive scheme for vehicle state estimation using dual extended h-infinity kalman filter," *Electronics*, vol. 10, no. 13, 2021.

[90] G. Shi, X. Li, and Z. Jiang, "An improved yaw estimation algorithm for land vehicles using marg sensors," *Sensors*, vol. 18, no. 10, 2018.

[91] E. Ding and T. Massel, "Estimation of vehicle roll angle," *IFAC Proceedings Volumes*, vol. 38, no. 1, pp. 122–127, 2005, 16th IFAC World Congress. [Online]. Available: https://www.sciencedirect.com/science/article/pii/S1474667016379204

[92] L. Zhao and Z. Liu, "Vehicle velocity and roll angle estimation with road and friction adaptation for four-wheel independent drive electric vehicle," *Mathematical Problems in Engineering*, vol. 2014, pp. 1–11, 2014. [Online]. Available: https://EconPapers.repec.org/RePEc:hin:jnlmpe:801628

[93] S. Yun, Y. Ahn, and K. Huh, "Development of vehicle roll rate estimator using transfer function estimation," *Transactions of the Korean Society of Automotive Engineers*, vol. 30, no. 1, pp. 1–7, 2022.

[94] K. Nam, S. Oh, H. Fujimoto, and Y. Hori, "Estimation of sideslip and roll angles of electric vehicles using lateral tire force sensors through rls and kalman filter approaches," *IEEE Transactions on Industrial Electronics*, vol. 60, no. 3, pp. 988–1000, 2013.

[95] W. Huang, W. Li, L. Tang, X. Zhu, and B. Zou, "A deep learning framework for accurate vehicle yaw angle estimation from a monocular camera based on part arrangement," *Sensors*, vol. 22, no. 20, 2022.

[96] C. Ye, Y. Wang, Y. Wang, and M. Tie, "Steering angle prediction yolov5-based end-to-end adaptive neural network control for autonomous vehicles," *Proceedings of the Institution of Mechanical Engineers, Part D: Journal of Automobile Engineering*, vol. 236, no. 9, pp. 1991–2011, 2022.

[97] D. P. Kingma and J. Ba, "Adam: A method for stochastic optimization," 2017.